

SEDIMENTATION AND TECTONICS OF LOWER CENOZOIC SEQUENCES  
FROM SOUTHEAST OF SHILLONG PLATEAU, INDIA: PROVENANCE  
HISTORY OF THE ASSAM-BENGAL SYSTEM, EASTERN HIMALAYAS

Except where reference is made to the work of others, the work described in this thesis is my own or was done in collaboration with my advisory committee. This thesis does not include proprietary or classified information.

---

Subhadip Mandal

Certificate of Approval:

---

Charles E. Savrda  
Professor  
Geology and Geography

---

Ashraf Uddin, Chair  
Associate Professor  
Geology and Geography

---

David T. King, Jr.  
Professor  
Geology and Geography

---

George T. Flowers  
Dean  
Graduate School

SEDIMENTATION AND TECTONICS OF LOWER CENOZOIC SEQUENCES  
FROM SOUTHEAST OF SHILLONG PLATEAU, INDIA: PROVENANCE  
HISTORY OF THE ASSAM-BENGAL SYSTEM, EASTERN HIMALAYAS

Subhadip Mandal

A Thesis

Submitted to

the Graduate faculty of

Auburn University

in Partial Fulfillment of the

Requirements for the

Degree of

Master of Science

Auburn, Alabama

December 18, 2009

SEDIMENTATION AND TECTONICS OF LOWER CENOZOIC SEQUENCES  
FROM SOUTHEAST OF SHILLONG PLATEAU, INDIA: PROVENANCE  
HISTORY OF THE ASSAM-BENGAL SYSTEM, EASTERN HIMALAYAS

Subhadip Mandal

Permission is granted to Auburn University to make copies of this thesis at its discretion, upon the request of individuals or institutions and at their expense. The author reserves all publication rights.

---

Signature of Author

---

Date of Graduation

## VITA

Subhadip Mandal, son of Baidyanath Mandal and Amita Mandal, was born in January 21, 1981, at Birbhum, West Bengal, India. He completed his schooling from Nalhati H.P High School in 1998. He received his Bachelor of Science degree in geology (honors) from T.D. B College, Raniganj, affiliated under the University of Burdwan in 2001. Afterwards, he completed the Master of Science degree in Geology at the University of Calcutta, India, in 2003. He joined the Graduate School at Auburn University to pursue another Master of Science degree from the Department of Geology and Geography in Fall 2007.

## THESIS ABSTRACT

### SEDIMENTATION AND TECTONICS OF LOWER CENOZOIC SEQUENCES FROM SOUTHEAST OF SHILLONG PLATEAU, INDIA: PROVENANCE HISTORY OF THE ASSAM-BENGAL SYSTEM, EASTERN HIMALAYAS

Subhadip Mandal

Master of Science, December 18, 2009  
(Master of Science, University of Calcutta, India, 2003)  
(Bachelor of Science, University of Burdwan, India, 2001)

155 Typed Pages

Directed by Ashraf Uddin

The present study area is located along the southeastern part of the Shillong Plateau in the eastern and southeastern part of the Meghalaya State and in the lower (southern) part of Assam State, northeast India. A continuous Eocene to Miocene sequence is exposed along the Jowai-Badarpur Road (NH-44). The study area is at the junction between Assam and Bengal basins. Detrital history from this area provides data pertaining to uplift and erosional history of the hinterland areas (i.e., Himalayas, Indo-Burma Ranges and Shillong Plateau).

Lower Cenozoic units from the study area bear signatures of the both orogenic belts and stable craton. Lower Eocene Tura and Sylhet sandstones are quartzose (Q<sub>98</sub>F<sub>2</sub>L<sub>0</sub>), which points to the Indian Craton as a potential source area. Sandstones from the late Eocene Kopili Formation are quartzolitic (Q<sub>73</sub>F<sub>4</sub>L<sub>23</sub>). Younger Oligocene and

Miocene sandstones are also quartzolithic, rich in unstable grains, suggesting derivation from adjacent orogenic belts.

Eocene sandstones are rich in opaque and ultra-stable heavy minerals (e.g., zircon, rutile, and tourmaline). Concentrations of unstable heavy minerals (e.g., amphibole, chrome-spinel, and serpentine) increase in Oligocene and Miocene strata. Progressively lower maturity indices of heavy mineral assemblages in up-section suggest that the orogenic fronts are getting closer.

Mineral chemistry of detrital tourmaline grains suggests that derivation from metapelites with a subordinate Li-poor granitoid source. The majority of the detrital tourmalines belong to the schorl-dravite series. Low Al, low Fe, and high Mg-bearing chrome spinels suggest derivation from Alpine-type peridotites, likely from the Indo-Burma Ranges (Naga ophiolites) to the east of the study area. Detrital garnet chemistry suggests a broad P-T range for source rock terranes.

Mudrock geochemical data suggest that the majority of the sediments were derived from recycled orogenic sources. Based on the chemical index of alteration, the intensity of weathering in the source area was moderate to high. Future research project in the area should explain the uplift history of source terranes using garnet and tourmaline chemistry and detrital geochronology.

## ACKNOWLEDGEMENTS

I must thank my major advisor, Dr. Ashraf Uddin, whose guidance and support benefited me throughout my graduate studies at Auburn University. I will never forget his contribution to my development as a geologist, and his kind efforts are highly appreciated. He always motivated me to “think three-dimensionally”. I also thank my committee members, Dr. Charles E. Savrda and Dr. David T. King, Jr. who supported me throughout my academic career and contributed invaluable scientific and editorial assistance to this research.

I would like to thank Dr. J.N Sarma, Professor of the Department of Applied Geology, Dibrugarh University, Assam, India for his kind help and valuable discussions. I also like to thank Mr. Chris Fleisher at University Georgia for his kind cooperation during microprobe analysis. Special thanks go to my fellow students Raju Sitaula, Shahadat Hossain, Thomas Key, Greg Dyer, and Deblina Bose with whom I shared many geological and nongeological discussions. I must appreciate the department of Geology and Geography staff, Sheila Arington, Eva Lilly, and John Simms who helped me during my tenure at Auburn University.

I wish to thank my beloved teachers Dr. D. Mukhopadhyay and Dr. Tapas Bhattacharyya for their kind suggestions and encouragements. I thank my parents who always believed in me. Finally, I would like to thank my wife, Oindrila who encouraged and supported in more ways than I can list.

Style manual or journal used

Geological Society of America Bulletin

Computer software used

Adobe Photoshop CS2

ArcGIS Desktop 9. 2

Golden Software Grapher 5<sup>®</sup>

Macromedia Freehand Drawing

Microsoft Office Excel 2003

Microsoft Office PowerPoint 2003

Microsoft Office Word 2003

Thompson EndNote 7.0



## TABLE OF CONTENTS

LIST OF FIGURES .....	xiii
LIST OF TABLES .....	xix
CHAPTER 1: INTRODUCTION .....	1
1.1 INTRODUCTION .....	1
1.2 STUDY AREA .....	3
CHAPTER 2: REGIONAL TECTONIC SETTING .....	7
2.1 INTRODUCTION .....	7
2.2 EASTERN HIMALAYA .....	9
2.3 MISHMI HILLS .....	10
2.4 SHILLONG PLATEAU AND MIKIR HILLS.....	12
2.5 INDO-BURMA RANGES .....	16
2.5.1 Schuppen Belt .....	16
2.5.2 Kohima-Patakai Synclinorium.....	17
2.5.3 Ophiolite Melange Zone.....	17
2.6 ASSAM SHELF .....	18
2.7 BENGAL BASIN .....	19
CHAPTER 3: STRATIGRAPHY AND SEDIMENTATION .....	24
3.1 INTRODUCTION .....	24
3.2 PRE-TERTIARY STRATIGRAPHY.....	27

3.2.1 GONDWANA ROCKS .....	27
3.2.2 GONDWANA ROCKS .....	28
3.2.3 CRETACEOUS ALKALINE INTRUSIVE AND LAVE FLOWS.	28
3.2.4 CRETACEOUS SEDIMENTS .....	29
3.3 TERTIARY SEDIMENTS .....	30
3.4 BRIEF SUMMARY ON CONDITION OF DEPOSTION .....	35
CHAPTER 4: SANDSTONE PETROGRAPHY .....	38
4.1 INTRODUCTION .....	38
4.2 METHODS .....	39
4.3 PETROGRAPHY .....	40
4.3.1 JAINTIA GROUP .....	40
4.3.2 BARAIL GROUP .....	43
4.3.3 SURMA GROUP .....	44
4.4 PETROFACIES EVOLUTION AND COLLISIONAL HISTORY.....	54
CHAPTER 5: HEAVY MINERAL ANALYSIS .....	55
5.1 INTRODUCTION.....	55
5.2 METHODS .....	56
5.3 RESULTS .....	58
5.4 PROVENANCE HISTORY .....	65
CHAPTER 6: MICROPROBE ANALYSIS .....	66
6.1 INTRODUCTION .....	66
6.2 MINERAL CHEMISTRY .....	67
6.3 METHODS .....	69

6.3.1 Sample Preparation.....	69
6.3.2 The Electron Microprobe .....	70
6.4 RESULTS .....	72
6.4.1 Tourmaline .....	74
6.4.2 Chrome Spinel .....	78
6.4.3 Garnet .....	82
6.5 DISCUSSIONS .....	86
6.5.1 Tourmaline.....	86
6.5.2 Chrome Spinel .....	86
6.5.3 Garnet.....	89
CHAPTER 7: MUDROCK GEOCHEMISTRY.....	91
7.1 INTRODUCTION .....	91
7.2 METHODS .....	92
7.3 RESULTS .....	93
7.3.1 Major and Trace Elements.....	93
7.3.2 Source Rock Weathering and Diagenesis .....	103
7.4 TECTONIC SETTING AND SOURCE ROCKS .....	105
CHAPTER 8: DISCUSSION .....	108
8.1 SYNTHESIS .....	108
8.2 EOCENE PROVENANCE .....	108
8.3 OLIGOCENE PROVENANCE .....	110
8.4 MIOCENE PROVENANCE .....	111
8.5 MICROPROBE ANALYSIS .....	112

8.5.1 Tourmaline .....	112
8.5.2 Chrome Spinel .....	112
8.5.3 Garnet .....	113
8.6 MUDROCK GEOCHEMISTRY.....	113
8.7 PALEOTECTONIC SETTING .....	114
8.8 CONCLUSIONS.....	118
REFERENCES .....	119
APPENDICES .....	132

## LIST OF FIGURES

Figure 1. Figure 1. Map showing various sedimentary basins of India. Assam is a category 1 basin with proven oil and gas production (after Bastia, 2006) .....	5
Figure 2. Digital elevation map surrounding the study area, which falls in the Assam-Bengal system. Shillong Plateau stands adjacent to the west and the Indo-Burman Ranges lie to the east (ONGC unpublished report) BAI: Bongaigaon, BPN: Barapani, CHP: Cherrapunji, GAU: Guwahati, SHL: Shillong, TEZ: Tezpur.....	5
Figure 3. Figure 3. Sample location sites plotted on Landsat imagery. Sample location sites are along National Highway 44 (NH 44) .....	6
Figure 4. Index map of Himalaya and Indo-Burma Ranges Abbreviation: DL - Delhi, ITS - Indus Tsangpo Suture Zone, IBR - Indo-Burma Ranges, KH - Kashmir Hazira Syntaxis, R - Rajmahal Hills, MBT – Main Boundary Thrust, MCT – Main Central Thrust, Sp – Shillong Plateau (modified after Acharyya, 2007a).....	11
Figure 5. Simplified map of eastern Himalaya and northeastern India. 1 - Neogene Siwalik molasse, 2 - Early Paleogene rocks, 3 - Low grade Proterozoic rocks, 4 - High-grade rocks, 5 - Tethyan Himalayan sediments, 6 - Ophiolite, 7 - Trans-Himalayan granitoids, 8 - Precambrian rocks of Peninsular India, 9 - Early Cretaceous volcanic rocks. ITO – Indus Tsangpo Ophiolite, SP – Shillong Plateau, M - Mikir Hills (modified after Acharyya, 2007a) .....	11
Figure 6. Map showing assemblages of Precambrian Cratonic blocks and adjacent mobile belts in eastern and northeastern India. Abbreviations: BF-Brahmaputra Fault, K-Kolkata, CGGC-Chhotanagpur Granite Gneiss Complex, DBF-Dhubri Fault, DF-Dauki Fault, EGMB-Eastern Ghat Mobile Belt, GB-Ganga Basin, KL-Kopili Lineament, M-Mikir Hills, NSL-Narmada Son Lineament, R-Rajmahal traps, SC-Singhbhum Craton, SMB-Satpura Mobile Belt, SP-Shillong Plateau (Rajasekhar and Mishra, 2008) .....	14
Figure 7. Complete Bouguer anomaly map of east India and Bangladesh. H1–H7 and L1–L2 represents gravity highs and lows. Epicenter of 1897 Shillong earthquake is shown by Red triangle. HZ-Hinge zone, SP-Shillong Plateau, K -Kolkata, G-Guwahati. BF - Brahmaputra Fault, OF-Oldham Fault, DF =Dauki Fault, K = Kolkata (Calcutta), KL = Kopili Lineament, P = Purulia, RF = Rajmahal Fault, SBF = Sainthia Bahmani Fault (modified after Rajasekhar and Mishra, 2008). .....	15
Figure 8. Map showing structural units of Indo-Burma Ranges and Central Burma Basin (modified after Acharyya, 2007b). .....	21

Figure 9. Schematic cross section of Indo-Burma Ranges and Central Burma Basin (modified after Acharyya, 2007b). .....	21
Figure 10. Tectonic map of Bengal Basin and its contiguous regions. Running between Calcutta-Mymensingh, the hinge zone separates stable shelf from central deep basin. Abbreviation: CTFB - Chittagong-Tripura Fold Belt (after Uddin and Lundberg, 1998b) .....	22
Figure 11. North-south cross section through Bengal Basin (after Uddin and Lundberg, 2004) .....	23
Figure 12. East-west cross section of Bengal Basin (after Uddin and Lundberg, 2004) ..	23
Figure 13. Geological map of northeast India (modified after Dasgupta and Biswas, 2000). Study area is indicated by the black box .....	26
Figure 14. Detailed geological map of Shillong Plateau 1 - Basement complex, 2 - Shillong Group, 3 - Khasi Greenstone, 4 - Porphyritic granite, 5 - Carbonatite, 6 - Sylhet trap, 7 - Cretaceous Sediments, 8 - Jaintia Group, 9 - Barail Group, 10 - Surma and Dupi Tila Group, 11 - Fault, 12 - Shear Zone (after Nandy, 2001) .....	30
Fig. 15. Outcrop photographs of different stratigraphic units of the study area. (A) Therria/Tura Sandstone of Jaintia Group. (B) Lakadong Limestone Member of lower Sylhet Formation. (C) Lakadong Sandstone Member of lower Sylhet Formation. (D) Lower Kopili Formation with alternating sandstones and shales. (E) Fine-grained sandstone with Laisong Formation of the lower Barail Group. (F) Fine-grained sandstone of Boka Bil Formation .....	37
Figure 16. QtFL triangular plot of sandstone samples from southeast of Shillong Plateau. Provenance fields are drawn after Dickinson (1985).....	45
Figure 17. QmFLt plot showing mean and standard deviation polygons of Lower Cenozoic stratigraphic units. Provenance fields are drawn after Dickinson (1985) .....	46
Figure 18. QmPK plot of sandstone samples from the study area, showing mean and standard deviation polygons for each stratigraphic units. ....	47
Figure 19. Ternary diagram showing lithic fragment composition (LsLm <sub>1</sub> Lm <sub>2</sub> ) of sandstones from study area. Mean and standard deviation polygons of each stratigraphic unit .....	48
Figure 20. Plot of plagioclase to total feldspar ratios in sandstones, showing mean and standard deviation of each studied stratigraphic units .....	48

Figure 21. Vertical variation of modal mineralogical composition of sandstone samples of the Tertiary clastic sequence from southeast of Shillong Plateau .....	49
Figure 22. (A) Representative photomicrograph of highly compacted and silica-cemented Tura Sandstone of the Eocene Jaintia Group showing dominance of monocrystalline quartz (Qm). (B) Representative photomicrograph of Tura Sand of the Eocene Jaintia Group, showing higher proportion of polycrystalline quartz (Qp) .....	50
Figure 23. (A) Representative photomicrograph of Kopili Sandstone of Eocene Jaintia Group, showing very low- to low-grade metamorphic lithic fragments (Lm <sub>1</sub> ). A few altered subhedral plagioclase is also seen. (B) Representative photomicrograph of Oligocene lower Barail Sandstone, showing sedimentary (Ls) and lower grade metamorphic lithic fragments (Lm <sub>1</sub> ). (Plag: Plagioclase feldspars) .....	51
Figure 24. (A) Representative photomicrograph of Oligocene upper Barail Sandstone, showing various framework grains (quartz, sedimentary lithic, and metamorphic lithic) (B) Representative photomicrograph of Miocene Surma Sandstone, showing k-spar feldspar (K-spar), and metamorphic fragments (quartzite, Lm <sub>1</sub> , Lm <sub>2</sub> ; quartzite = Lm <sub>1</sub> ) ...	52
Figure 25. Heavy mineral occurrence (weight percent) in different stratigraphic units from the study area .....	61
Figure 26. Heavy mineral distribution of Eocene, Oligocene, and Miocene sandstones from the study area.....	61
Figure 27. (A) Representative photomicrograph of heavy minerals from Jaintia Group sandstone. (B) Well-rounded tourmaline grain from upper Jaintia Group sandstone (Kopili Formation), indicating recycling of sediments (Op=opaque; Tr-tourmaline; Rt-Rutile; Zr-zircon). .....	62
Figure 28. Representative photomicrograph of heavy minerals in sandstones from the (A) Barail Group and (B) Surma Group (Op= Opaque; Tr= tourmaline; Ser= serpentine; Gt= garnet; Rt= rutile; Zr= Zircon; and Cr-sp= chrome-spinel).....	63
Figure 29 (A) Abundance of chrome-spinel and chlorite grains in Surma sandstone. (Chl-chlorite; Zr= Zircon; and Cr-sp= chrome-spinel). (B) Backscattered scanning electron images of chrome spinel from same sample .....	64
Figure 30. Classification of detrital tourmalines from southeast of Shillong Plateau .....	75
Figure 31. Detrital tourmalines plotted on X-site occupancy diagram.....	75
Figure 32. Al-Fe(tot)-Mg plot (in molecular proportion) of tourmalines from southeast of Shillong plateau. Fe(tot) represents the total iron in the tourmaline. Several end members are plotted for reference. Numbered fields correspond to the following rock types: (1) Li-rich granitoid, pegmatites, and aplites, (2) Li-poor granitoids and associated pegmatites	

and aplites, (3) Fe<sup>3+</sup>-rich quartz-tourmaline rocks (hydrothermally altered granites), (4) Metapelites coexisting with an Al-saturating phase, (5) Metapelites without an Al-saturating phase, (6) Fe<sup>3+</sup>-rich quartz-tourmaline rocks, calc-silicate rocks, and metapelites, (7) Low-Ca meta-ultramafics and Cr and V-rich metasediments, and (8) Metacarbonates and meta-pyroxenites.....76

Figure 33. Ca-Fe(tot)-Mg plot (in molecular proportion) for tourmalines from the southeast of Shillong Plateau. Several end members are plotted for reference. The numbered fields correspond to the following rock types: (1) Li-rich granitoid pegmatites and aplites, (2) Li-poor granitoids and associated pegmatites and aplites, (3) Ca-rich metapelites and calc-silicate rocks, (4) Ca-poor metapelites and quartz-tourmaline rocks, (5) Metacarbonates, and (6) Meta-ultramafics.....77

Figure 34. Ternary plot of major trivalent cations in chrome spinel. Three major provenance fields have been drawn to show the data distribution. The colored area denotes the field for chrome spinel of mantle melting origin, including ultramafic xenoliths, abyssal dunites, spinel and plagioclase peridotites, and Alpine-type peridotites (Dick and Bullen, 1984) .....80

Figure 35. Plot of Mg/(Mg+Fe<sup>2+</sup>) against the ratio of trivalent cations Fe<sup>3+</sup>/(Fe<sup>3+</sup>+Al+Cr) for detrital spinel showing that Alpine and stratiform types overlap one another (Irvine, 1977) .....81

Figure 36. Mg/(Mg+Fe<sup>2+</sup>) versus Cr/(Cr+Al) plot for detrital chrome spinel showing the distribution of samples relative to different provenance fields. Note that although some data points fall in the overlap between the stratiform complex field (layers rich in chromite in a layered igneous complex) and Alpine-type peridotite (ophiolites), data generally reflect an Alpine-type peridotite provenance (after Dick and Bullen, 1984) ...82

Figure 37. Chemical composition of garnets from southeast of Shillong Plateau plotted on a (Sp+Gro)-Py-Alm diagram. Sp - Spessartine; Gro - Grossular; Alm – Almandine; Py – Pyrope (after Nanayama, 1997) .....84

Figure 38. Chemical composition of garnets from southeast of Shillong Plateau plotted on a (Py+Alm)-Sp-Gro diagram. Sp-Spessartine; Gro-Grossular, Alm-Aalmandine, Py-Pyrope (after Nanayama, 1997) .....84

Figure 39. Chemical composition of garnet grains from southeast of Shillong Plateau, plotted on Sp-Alm-Py ternary diagram. Sp - Spessartine; Gro - Grossular; Alm – Almandine; Py – Pyrope, after (Nanayama, 1997) .....85

Figure 40. Chemical composition of garnet grains from southeast of Shillong Plateau, plotted on (Alm+Sp)-Gr-Py ternary diagram. Sp - Spessartine; Gro - Grossular; Alm – Almandine; Py – Pyrope (after Nanayama, 1997). Fields I, II and III are various garnet groups that are discussed in the text .....85



Figure 41. Mg/(Mg+Fe <sup>2+</sup> ) versus Cr/(Cr+Al) plot is compared with mid-oceanic ridge basalt (MORB) (gray shaded area) derived peridotites (abyssal peridotite, basalts; Dick and Bullen, 1984). Chrome spinels from this area has wide range of Cr# (Cr/(Cr+Al)) than abyssal spinels (including both MORB and abyssal peridotites).....	88
Figure 42. Plot of TiO <sub>2</sub> vs. Cr # of detrital chrome spinel from southeast of Shillong Plateau. All chrome spinels have very low TiO <sub>2</sub> . MORB = Mid-oceanic ridge basalt (after Arai, 1992) .....	88
Figure 43. Pressure-temperature diagram for garnet data from southeast of Shillong Plateau, Meghalaya. Dashed lines are garnet Fe/(Fe+Mg) isopleths, constructed for the two garnet compositions observed in this study and assuming that garnet formed in equilibrium with biotite (Spear, 1993). Garnet shows a wide spectrum of metamorphic P-T conditions.....	90
Figure 44. (A) Stratigraphic variation of major element oxide concentrations. Data are recalculated as volatile free. (B) Stratigraphic variation of post-Archean Australian average shale (PAAS; Taylor and McLennan, 1985)-normalized major element composition.....	99
Figure 45. Harker variation diagrams of major elements for mudrocks from the study area .....	100
Figure 46. Stratigraphic variation of K <sub>2</sub> O /Al <sub>2</sub> O <sub>3</sub> ratios of mudrock samples from study area. Stratigraphically older sediments are to the right. All samples are within the clay mineral field .....	101
Figure 47. (a) Stratigraphic variation of trace element concentrations. (b) Spider plot of trace element composition of mudrocks from the study area normalized against PAAS .....	102
Figure 48. Al <sub>2</sub> O <sub>3</sub> -CaO*+Na <sub>2</sub> O-K <sub>2</sub> O (Nesbitt and Young, 1984) diagram for mudrock samples from the study area. Solid black lines show weathering trend of these samples. Average CIA (chemical index of alteration) values for these are moderate to high (i.e., 80%) .....	104
Figure 49. Plot of discrimination functions F1 and F2 for mudrocks from the study area. Provenance fields are after Roser and Korsch (1988). P1 -mafic and intermediate igneous provenances; P2 -intermediate igneous provenances; P3 -felsic igneous provenances; and P4 -recycled-mature polycyclic quartzose detritus .....	106
Figure 50. (A) Tectonic discrimination diagram for mudrocks from southeast of Shillong Plateau. Boundaries are after Roser and Korsch (1986). PM – passive margin, ACM – active continental margin, ARC – oceanic island arc margin. (B) TiO <sub>2</sub> -Zr discrimination diagram from southeast of Shillong Plateau (Hayashi et al., 1997a) .....	107

Figure 51. QtFL diagrams showing lower Cenozoic sandstone compositions from Assam Basin, Bengal Basin, and present study area (Uddin et al., 2007) .....110

Figure 52. Paleogeographic reconstruction of the present study area (in gray box) with reference to Assam and Bengal basin. Red body is the deposition lobe prograding basinward with of time and progressive uplift of the hinterland blocks .....117

## LIST OF TABLES

Table 1. Cenozoic stratigraphy of the study area (after Rangarao, 1983; Singh and Singh, 2000) .....	33
Table 2. Recalculated modal parameters of sand and sandstone ( Uddin and Lundberg, 1998a) .....	41
Table 3. Normalized modal compositions of sandstones from southeast of Shillong Plateau, Meghalaya .....	42
Table. 4 Normalized abundances of heavy minerals from southeast of Shillong Plateau, India (ZTR-Zircon-tourmaline-rutile) .....	60
Table 5. Electron microprobe standards used in this study .....	73
Table 6. Results of whole-rock chemical analysis of mudrock samples from southeast of Shillong Plateau .....	96

## **CHAPTER 1: INTRODUCTION**

### **1.1 INTRODUCTION**

Provenance analysis is commonly used to reconstruct parent rock assemblages of sediments and the physio-climatic conditions under which sediments originally formed. The term provenance is derived from the Latin verb “provenire,” meaning to come forth or originate. Determining the provenance of clastic sedimentary rocks is often an important component of geological investigations of any sedimentary sequence or basin. Mineralogy of siliciclastic rocks reflects the character of sedimentary provenance and the nature of sedimentary processes within a depositional basin. Provenance and depositional basins are governed by tectonic regimes, which in turn control the distribution of siliciclastic rocks. In broad perspective, provenance studies include all queries that will help in reconstructing lithospheric history of the Earth (Basu, 2003). The ultimate goal of provenance analysis is to deduce the characteristics of the source area from compositional and textural parameters of clastic sediments, supported by the other lines of evidence (Pettijohn et al., 1987). Sandstone petrography is widely used as one of the tools for determining the origin and tectonic reconstruction of ancient terrigenous deposits (Dickinson, 1970). Many studies have correlated the composition of sandstones, their provenances, and tectonic settings (e.g., Dickinson and Suczek, 1979). Petrofacies analysis, using various ternary plots (QtFL, QmFLt, etc), infers various tectonic settings and helps to understand and interpret plate interactions in the geologic past (Graham et al., 1976; Ingersoll, 1978; Dickinson and Suczek, 1979; Dickinson et al., 1982).

Composition of siliciclastic rocks is controlled by a number of factors involved in clastic sediment systems (i.e., climate, relief, transport, and diagenesis) which provide valuable information for paleogeographic reconstruction (Suttner, 1974; Ingersoll et al., 1984; Johnson, 1993).

Basin evolution and unroofing history of mountain belts can be best inferred through provenance studies that focus on key attributes of detrital mineralogy (Cerveny, 1986; Dorsey, 1988; Uddin and Lundberg, 1998a). Provenance reconstruction through detailed mineralogical analyses is based on the assumption that modes of transportation, depositional environments, climates, and diagenesis have not significantly altered detrital grain compositions (Basu, 1976).

In recent years, single grain heavy mineral chemistry using microprobe has added a new dimension to provenance studies. Among the minerals used for such studies by different authors are garnet, tourmaline, chrome-spinel, zircon, rutile, amphibole, pyroxene, epidote, and illmenite (Cookenboo et al., 1997; Sabeena et al., 2002; Kumar, 2004; Morton et al., 2004; Zahid, 2005; Rahman, 2008). Garnet and tourmalines have proven to be most useful for provenance studies due to their mineralogical and chemical diversity, abundance in sediments and rocks of different origins, physico-chemical resistance, and stability under various extreme geological conditions (Morton, 1985). Chrome spinel chemistry is useful in discriminating various mafic and ultramafic sources (Dick and Bullen, 1984; Cookenboo et al., 1997).

Major and trace element geochemistry of mudrock and sandstones are being successfully used to study sediment provenance (Bhatia and Crook, 1986; McLennan et al., 1993; Fedo et al., 1996).

The Assam Basin is located in the northeastern part of India, between the upper Assam Basin at the foothills of the eastern syntaxis of the eastern Himalaya to the northeast and the Bengal Basin of Bangladesh to the southwest (Figs. 1 & 2). Ongoing and recent research on these two basins provide interesting provenance information (Uddin and Lundberg, 1998a, 1998b, Kumar, 2004, Zahid, 2005, Uddin et al., 2007a,b; Rahman, 2008). Major objectives of the current study are to determine the provenance of lower Cenozoic sequences from southeast Shillong Plateau of northeast India and to reconstruct regional paleogeography of the area during the lower Cenozoic (Fig. 2). Methodologies used for this study are conventional sandstone petrography, heavy mineral analysis, selected mineral chemistry, and mudrock chemistry. This study provides information on provenance and sedimentation history for the middle part of one of the world's largest depositional lobes (Assam-Bengal system) that evolved from the eastern syntaxis of the Himalayas and the Indo-Burma Ranges.

## **1.2 STUDY AREA**

The Cenozoic Himalayan mountain chain, located along the northern edge of the Indian shield, was formed by the collision of India with Eurasia (Uddin and Lundberg, 1998a; Uddin et al., 2007b). The other Cenozoic mountain belt, the Indo-Burma Ranges, formed due the collision between the Indian plate with the Burmese platelet (Curry et al., 1979). The history of the collision is recorded in part within thick clastic wedges derived from these two orogenic belts and deposited in subsiding foreland troughs of the Assam and Bengal basins to the south and southeast of the Shillong Plateau. Previous study on provenance analysis of Paleogene rocks from upper Assam Basin revealed

sediment sources from the eastern Himalayas and the Indo-Burma Ranges (Kumar, 2004). Paleogene sediments from the northeastern part of the Bengal Basin indicate provenance from both the stable Indian craton west of the Bengal Basin and the Indo-Burma Ranges to the east (Zahid, 2005). The present study area is located in the southeastern part of the Meghalaya State and in the lower (southern) part of Assam State of northeastern India (Fig. 2). The study area is bounded to the north and west by the Shillong Plateau, to the south by the Dauki fault, and to the east by the Naga thrust (Fig. 2). This area is located between upper Assam Basin and the Bengal Basin section in the Sylhet trough. A continuous Eocene to Miocene sequence is exposed along the Jowai-Badarpur Road, National Highway (NH) 44 in the field area (Fig. 3). To investigate the source of the sediments southeast of Shillong Plateau, sandstone and mudstone samples ranging in age from Eocene to lower Miocene were collected (in collaboration with Dr. J.N Sarma from Dibrugarh University, Assam, India) along NH 44 from south of Jowai to Lubha River section (Fig. 3).

The study area is situated in a place that is expected to have received detritus from the Himalayas and the Indo-Burma Ranges during their uplift in various phases in the Cenozoic. Detrital history from this area has provided important data pertaining to uplift and erosional history of these two orogenic belts.

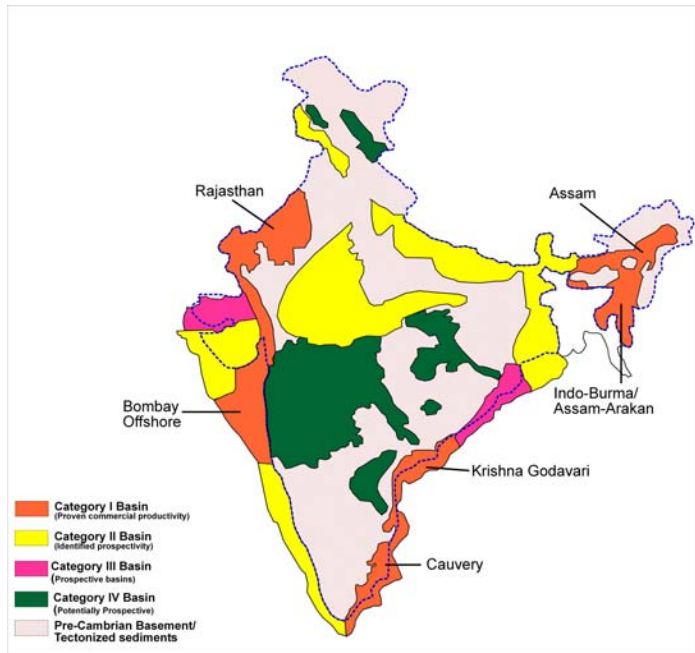


Figure 1. Map showing various sedimentary basins of India. Assam is a category 1 basin with proven oil and gas production (after Bastia, 2006).

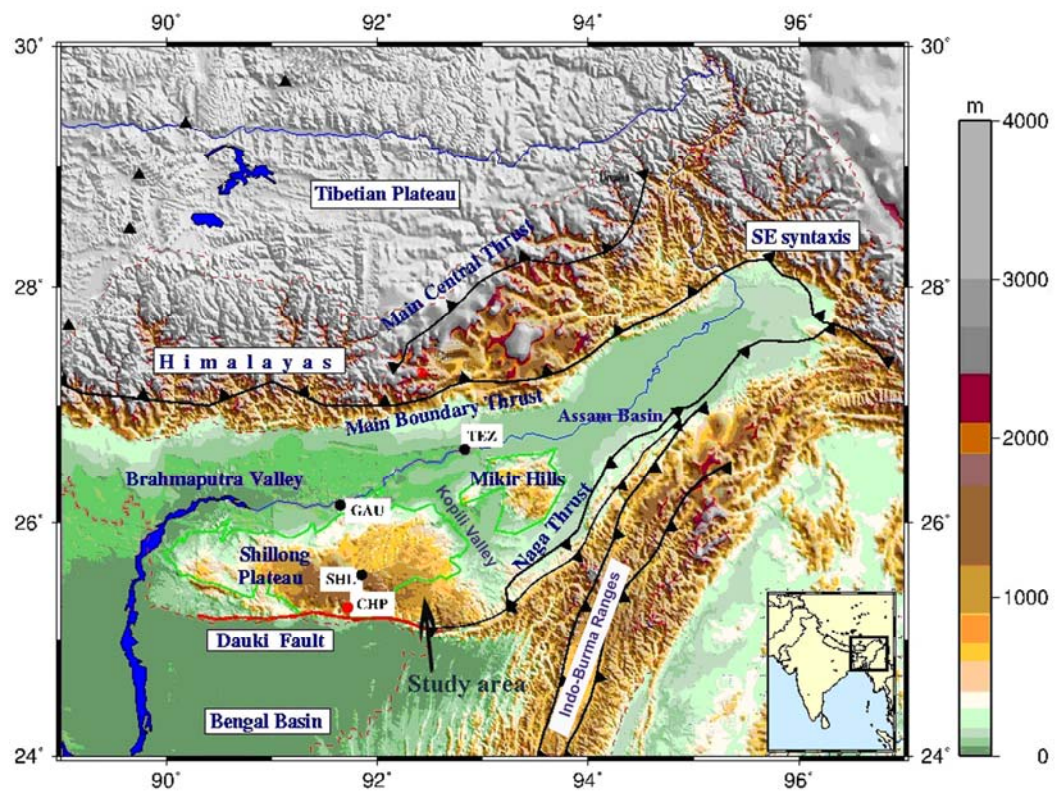


Figure 2. Digital elevation map surrounding the study area, which falls in the Assam-Bengal system. Shillong Plateau stands adjacent to the west and the Indo-Burman Ranges lie to the east (ONGC unpublished report) BAI: Bongaigaon, BPN: Barapani, CHP: Cherrapunji, GAU: Guwahati, SHL: Shillong, TEZ: Tezpur.



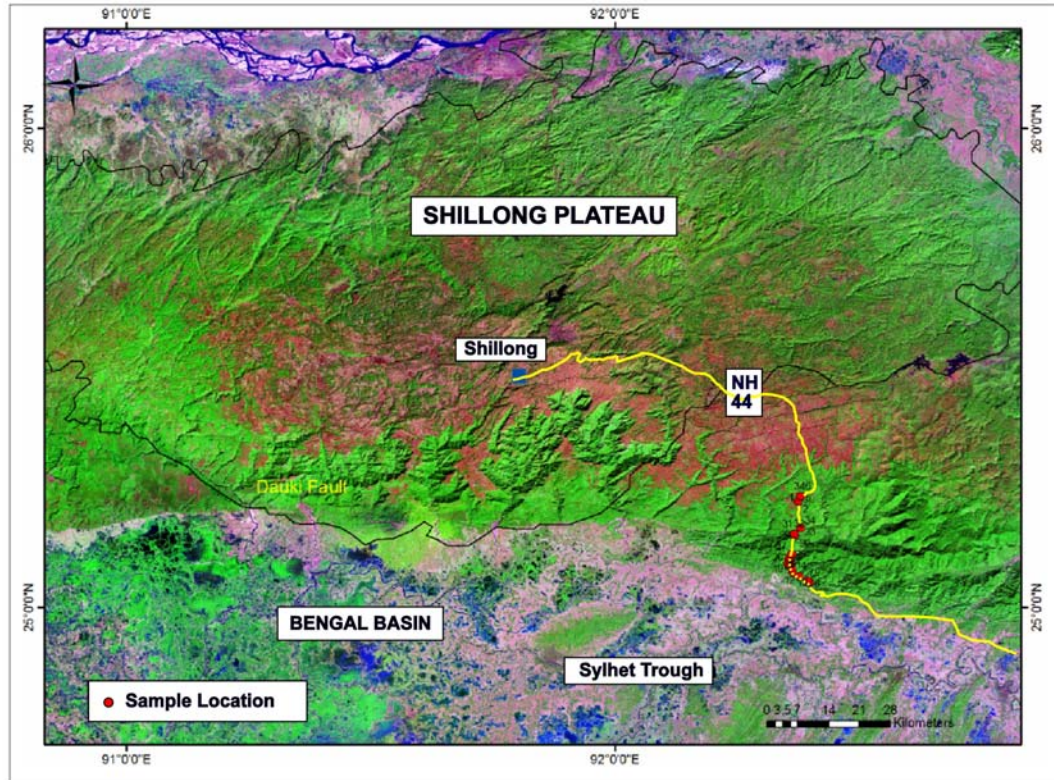


Figure 3. Sample location sites plotted on Landsat imagery. Sample location sites are along National Highway 44 (NH 44).

## **CHAPTER 2: REGIONAL TECTONIC SETTING**

### **2.1 INTRODUCTION**

The northeastern part of India is bounded by two young orogenic belts; the east-west trending Himalayas and north-south trending Indo-Burma Range (Fig. 4). These belts formed due to collision of the Indian plate with the Tibetan (Eurasian) plate to the north and with the Burmese plate to the east. Two foreland basins, the Assam and Bengal basins (Fig. 5), formed as a result of this collision during the early Cenozoic. Basin architecture and sedimentation styles within these two foreland basins have varied with the temporal changes in the intensity and pattern of plate-to-plate interaction (Alam et al., 2003).

Several attempts have been made to reconstruct plate interaction in the southeast Asia region (Falvey, 1974). Northeastern India is considered to have passed through five important geologic phases (Dasgupta and Biswas, 2000). The first of these relates to when India was part of the Gondwanan supercontinent (Lee and Lawver, 1995; Acharyya, 1998; Dasgupta and Biswas, 2000). The second phase came in the Permian-Carboniferous, when adjoining areas were rifted and the coal-bearing Gondwana sediments were deposited. This phase, during which the area was still part of the Gondwanaland, seems have been accompanied locally by some volcanic activity. The third phase was in the late Triassic/early Jurassic when, with the drifting away of Southern Tibet, the northern fringe of India (including the part that is now Assam) became a site of marine sedimentation. The Sung valley carbonatite, located northwestern

part of present study area near Jowai, was intruded during this period (Kumar et al., 1996). The fourth phase started when the eastern boundary of India also broke apart in late Jurassic-early Cretaceous and the southern and eastern shore became open to marine sedimentation. This phase also saw the beginning of igneous activity with the outpouring of the Garo Hills, Sylhet, and Mikir Hills basaltic traps, and the intrusion of mafic-ultramafic bodies. The fifth phase started with collision of India with the Burmese plate to the east and Tibet to the north during the early Eocene and continued with all stages of collisional tectonics thereafter (Sengupta et al., 1990; Hodges, 2000). During this phase, the entire zone was caught between the two collision zones of Himalaya and the Indo-Burman Ranges.

The geology and the tectonic setting of northeastern India were discussed by Acharyya (1980, 2007b), Evans (1964), and Saikia (1999). The distinctive tectono-geological subdivisions of northeast India (Fig. 2) are as follows (Nandy, 2001):

- Eastern Himalayan orogenic belt
- Precambrian Mishmi Hills
- Indo-Burma Ranges
- Precambrian Shillong plateau and the Mikir Hills
- The foredeep between the eastern Himalayan and Naga thrusts, which extends from the Shillong plateau to upper Assam (the Assam Shelf); and
- The Bengal Basin, covering part of the West Bengal of India and Bangladesh

## 2.2 EASTERN HIMALAYA

The eastern Himalayan orogenic belt is made up of a succession of northerly dipping thrust sheets. From south to north, the Himalaya is divided into the Siwalik Hills or Sub-Himalaya, Lesser Himalaya, and the Higher Himalaya. The Siwalik Hills or Sub-Himalaya contains mostly Neogene foreland basin sediments deposited in the foredeep (Burbank et al., 1996). The Lesser Himalaya is made up of lower Cenozoic sediments of both continental and marine origin, overlain by an older sequence of carbonates, orthoquartzites, and low-grade schists (Vance and Harris, 1999; Hodges, 2000). The Lesser Himalaya is separated from the Siwalik Hills by the Main Boundary Thrust (MBT). North of the Lesser Himalaya, the Higher Himalaya is made up of high-grade schists (Fig. 4), gneisses with Oligocene-Miocene and younger mineral ages resulting from Himalayan metamorphism (Vance and Harris, 1999; Hodges, 2000), and patches of intrusive granite that form the “Central Crystalline” belt. The Lesser Himalaya is separated from the Higher Himalaya by the Main Central Thrust (MCT), a ductile shear zone forming the tectonic base of the “Central Crystalline” belt. The structural trend of the folds and thrusts in the Eastern Himalaya is east-west. North of the “Central Crystalline” belt, the area consists of ophiolites and Paleozoic to lower Cenozoic Tethyan Himalayan sediments, followed up further north by Trans-Himalayan rocks (Fig. 5).

According to Acharyya and Ray (1982), Paleogene foreland basin sediments are tectonically concealed in the eastern Himalaya, but DeCelles et al. (2004) suggested that Paleogene sediments are discontinuous in their development and are largely absent in the eastern Himalayas. The evolution of the Himalayan foreland basin and its lateral continuity to the eastern Himalaya where it is concealed below the older rocks is a

subject matter of continuous debate. The exposed width of pre-Cenozoic Lesser Himalaya and the Neogene Siwalik rocks is very narrow in the eastern Himalaya due to the southward advancement of crystalline nappes that brought MBT and MCT into close proximity to each other (Acharyya, 2007b). Some thrust slivers of Eocene fossiliferous marine sediments are exposed discontinuously for a strike length of 300 km in Arunachal foothills of easternmost Himalaya, close to and beneath the MBT (Acharyya, 2007b).

### **2.3 MISHMI HILLS**

The Mishmi Hills trend northwest-southeast across the northeastern corner of India (Fig. 5). The Mishmi Hills are made up of a frontal high-grade schist, migmatites, and an inner low-grade mafic-ultramafic schist with crystalline serpentinite lenses to the southwest and diorite-granodiorite to the northeast (Nandy, 2001). An important tectonic structure of this block is the Mishmi thrust, which dips towards northeast. The grade of metamorphism in the frontal metamorphic belt increases up structural section from chlorite to staurolite–kyanite zones, reflecting inverted metamorphic gradient. The relationship between deformation and metamorphism shows that the metamorphic peak was syn- to post-tectonic in relation to the main ductile shearing event of the Mishmi thrust. Movement along these shear zones has resulted in inversion of metamorphic zones (Nandy, 2001; Gururajan and Choudhuri, 2003). The frontal metamorphic belt can be closely associated with the Mogok schist belt of Myanmar to the southeast.

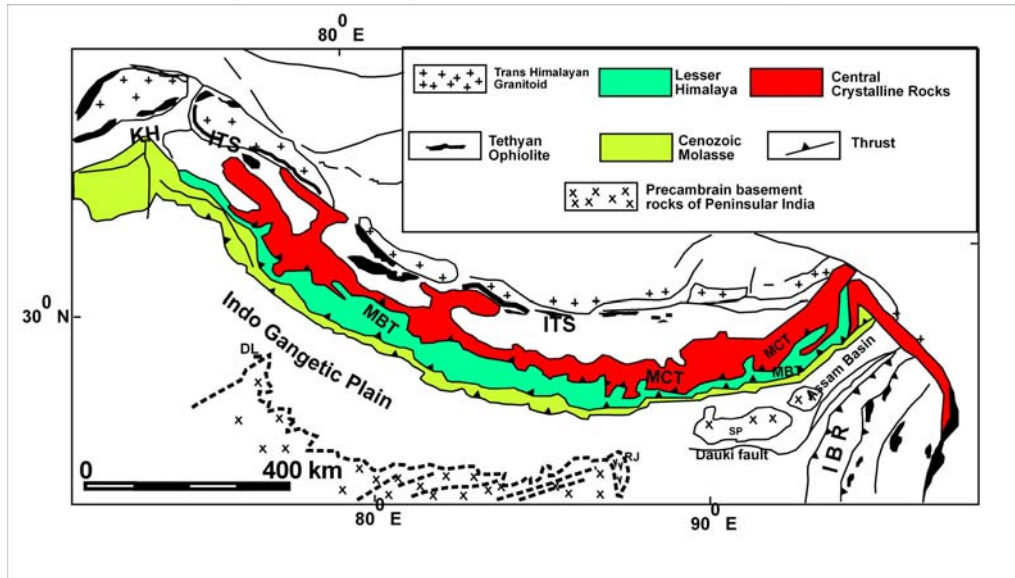


Figure 4. Index map of Himalaya and Indo-Burma Ranges Abbreviation: DL - Delhi, ITS - Indus Tsnagpo Suture Zone, IBR - Indo-Burma Ranges, KH - Kashmir Hazira Syntaxis, R - Rajmahal Hills, MBT – Main Boundary Thrust, MCT – Main Central Thrust, Sp – Shillong Plateau (modified after Acharyya, 2007a).

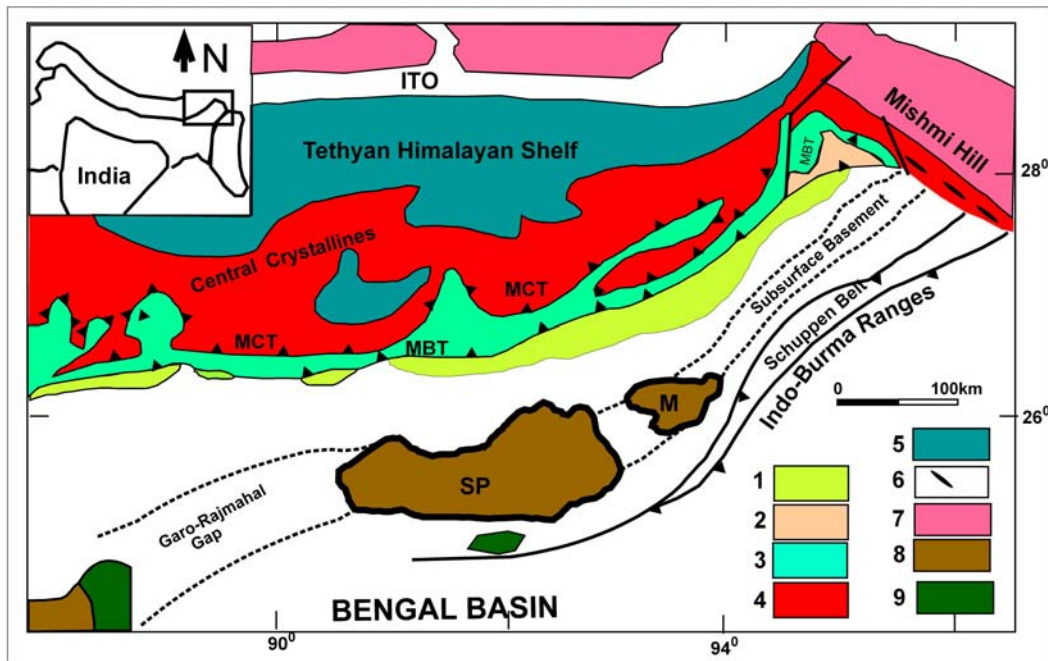


Figure 5. Simplified map of eastern Himalaya and northeastern India. 1 - Neogene Siwalik molasse, 2 - Early Paleogene rocks, 3 - Low grade Proterozoic rocks, 4 - High-grade rocks, 5 - Tethyan Himalayan sediments, 6 - Ophiolite, 7 - Trans-Himalayan granitoids, 8 - Precambrian rocks of Peninsular India, 9 - Early Cretaceous volcanic rocks. ITO – Indus Tsangpo Ophiolite, SP – Shillong Plateau, M - Mikir Hills (modified after Acharyya, 2007a).

## 2.4 SHILLONG PLATEAU AND MIKIR HILLS

The Shillong Plateau (Figs. 5 & 6) is a flat high land of nearly 1.0-1.5 km average regional elevation covering an area of about 3000 km<sup>2</sup>. It is flanked by the Himalayan foredeep to the north and the Bengal Basin to the south. The Shillong Plateau is separated from the Mikir Hills by the northwest-southeast-trending Kopili lineament (Fig. 6), which extend up to the MBT to the northwest and the Naga Thrust to the southeast (Rajasekhar and Mishra, 2008). Gneisses and migmatites with enclaves of amphibolite and high-grade supracrustal rocks form the basement rock of the Shillong Plateau (Nandy, 2001; Ghosh et al., 2005a). The basement rocks are overlain by Proterozoic metasediments of the Shillong Group (1530-1550 Ma) and are intruded by several younger granitic plutons of 885-480 Ma (Mitra and Mitra, 2001). Coeval ( $\approx$ 1600 Ma) rocks of similar types and metamorphic grades are reported from peninsular India to the west of Shillong Plateau, (i.e., the Chhotnagpur Granite Gneiss Complex, or CGGC; Fig. 6; Mitra and Mitra, 2001) and are reflected by a high Bouguer anomaly (Fig. 7). The CGGC, part of the Satpura Mobile Belt, represents a Mesoproterozoic collision zone with the Precambrian Singbhum Craton to the south. Chatterjee et al. (2007) considered the Shillong Plateau as Shillong-Meghalaya Gneissic Complex (SMGC) with Mesoproterozoic ages ( $1596\pm 15$  Ma) and considered the SMGC as a part of the Pan-African and Antarctic amalgamation along the east coast of India. Similar ties in crustal structure and geomorphological alignment between the CGGC and Satpura Mobile Belt suggest that the Shillong Plateau is an eastward extension of the Satpura Mobile Belt (Rajasekhar and Mishra, 2008). A large continued crustal bulge under the Shillong Plateau caused by lithospheric flexure

under the Himalaya is considered to be responsible for uplift of the Shillong plateau (Rajasekhar and Mishra, 2008).

The Bouguer anomaly map of eastern India (Fig. 7) shows three major gradients of decreasing gravity field to the north, east, and northeast of the Shillong Plateau. These are related to crustal loading in these directions during Himalayan orogenesis.

The Shillong Plateau is cut by several east-west, north-south, northeast-southwest, and northwest-southwest trending faults and lineaments. Among them, Dauki fault to the south is the prominent one (Bhattacharyya and Kayal, 2002). The Dauki fault separates the Shillong Plateau from the adjacent Sylhet trough of the Bengal Basin to the south. The nature and the displacement of the Dauki fault (Figs. 6 & 7) is a matter of debate. Evans (1964) suggested that the Dauki fault is a strike slip fault along which the Shillong Plateau was displaced about 200-250 km eastward from the eastern part of Peninsular India. The Shillong Plateau is bounded by the Dhubri fault, Bramhaputra fault, and Kopili lineament to the west, north and the east, respectively (Figs. 6 & 7). The eastern and southern part of this plateau is covered by Cretaceous to Eocene shelf deposits. Johnson and Nur Alam (1991) suggested that the Shillong Plateau was uplifted during Pliocene time. However, recent data suggest that the uplift initiated in the mid- to late Miocene (Clark and Bilham, 2008).



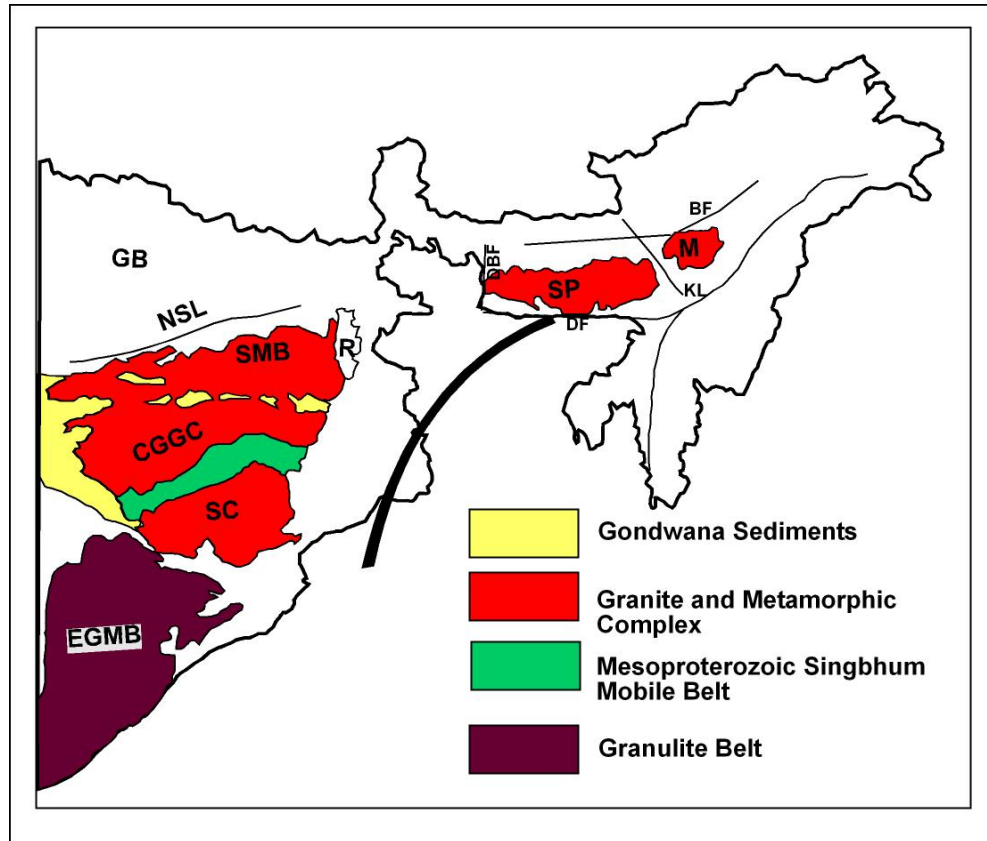


Figure 6. Map showing assemblages of Precambrian Cratonic blocks and adjacent mobile belts in eastern and northeastern India. Abbreviation: BF-Brahmaputra Fault, K-Kolkata, CGGC-Chhotanagpur Granite Gneiss Complex, DBF-Dhubri Fault, DF-Dauki Fault, EGMB-Eastern Ghat Mobile Belt, GB-Ganga Basin, KL-Kopili Lineament, M-Mikir Hills, NSL-Narmada Son Lineament, R-Rajmahal traps, SC-Singbhum Craton, SMB-Satpura Mobile Belt, SP-Shillong Plateau (Rajasekhar and Mishra, 2008).

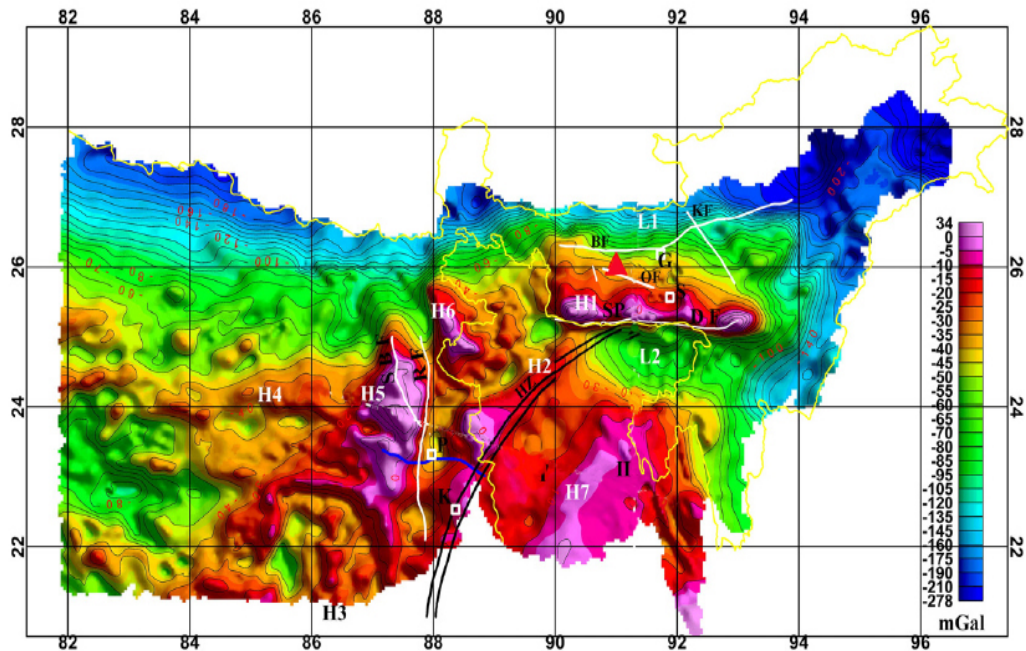


Figure 7. Complete Bouguer anomaly map of east India and Bangladesh. H1–H7 and L1–L2 represents gravity highs and lows. Epicenter of 1897 Shillong earthquake is shown by Red triangle. HZ-Hinge zone, SP-Shillong Plateau, K -Kolkata, G-Guwahati. BF - Brahmaputra Fault, OF-Oldham Fault, DF =Dauki Fault, K = Kolkata (Calcutta), KL = Kopili Lineament, P = Purulia, RF = Rajmahal Fault, SBF = Sainthia Bahmani Fault (modified after Rajasekhar and Mishra, 2008).

## **2.5 INDO-BURMA RANGES**

The Indo-Burma Ranges, also known as the Assam-Arakan Mountain Belt, is an arcuate active orogenic belt that trends NW-SE at its southern extreme and ENE-WSW at the northern end. It is bounded to the west by Kaladan fault and to the east by the Central Burma Basin (Figs. 8 & 9). The Eastern Boundary Thrust (EBT) separates the Indo-Burma mobile belt from Central Burma Basin (Nandy, 2001). This mobile belt formed due to subduction of the Indian plate beneath the Burmese platelet, and is regarded as an arc-trench deposit on oceanic Indian crust. The Indo-Burma Ranges contain Cretaceous to Eocene pelagic sediments overlain by Eocene to Oligocene flysch, upper Miocene to Pleistocene mollasse, and ophiolitic suites that were scraped off an oceanic part of the Indian plate (Curry et al., 1979; Sengupta et al., 1990; Kumar, 2004).

The Indo-Burma Mobile Belt is divided into the following tectonic sub-units: (1) Schuppen Belt; (2) Central Kohima-Patakai Synclinorium; and (3) Eastern Ophiolite Mélange Zone (Figs. 5 & 6).

### **2.5.1 Schuppen Belt**

The Schuppen Belt (Fig. 8) is bounded by the Naga Thrust to the northwest and Disang Thrust to the northeast, a zone of imbricated thrusts on thin-skinned crust (Kent et al., 2002). This belt developed due to differential movement between the Indian and Burma plates. Before the collision, this area was the eastward facing margin of the Indian plate (Kent et al., 2002). This belt is 20 to 25 km wide, runs for a strike length of 200 km (Kumar, 2004), and is made up dominantly of shelf sediments. The Naga and Disang thrusts join south of this belt where it is known as the Halflong Thrust, which continues

as the Dauki fault further west (Johnson and Alam, 1991). This belt consists of six to eight major thrust sheets and related folds. Activity on the frontal fault is considered to have started during middle Miocene (Kent et al., 2002). Structurally, the Naga thrust delimits the shelf from the deeper basin.

### **2.5.2 Kohima-Patakai Synclinorium**

The Kohima-Patakai Synclinorium occupies the central part of the Indo-Burma Ranges. The Bouguer anomaly map (Fig. 7) shows a linear negative anomaly in this area, which can be interpreted as thick sedimentary succession. This belt is separated from the Sylhet trough to the west by a north-south trending fault, considered to be the Paleogene accretionary prism (Nandy, 2001). Paleogene sediments are deformed into open upright folds with vertical to subvertical axial planes. The anticlines are characterized by narrow hinges, whereas synclines are very broad and rounded. The general nature of these folds are doubly plunging (Nandy, 2001). This belt shows structural complexity to the east. Axial planes trend north-south in the southern part and become northeast-southwest in the northern part of the belt.

### **2.5.3 Ophiolite Mélange Zone**

This zone demarks the eastern boundary of the Indo-Burma Ranges (Figs. 8 & 9), which is made up of unfossiliferous pre-Mesozoic low- to medium-grade metasediments and ophiolite suites (Acharyya, 2007a). The metasediments are mostly quartzite, phyllite, carbonaceous phyllite, crystalline limestone/marble, and sheared granite, while serpentinite is subordinant (Brunnschweiler, 1966). The ophiolite suites in Nagaland

consist of the following units: (1) ultramafic complexes consisting of tectonized peridotite and ultramafic cumulates; (2) a gabbro complex of layered and massive gabbro; (3) a diabase complex; (4) a mafic volcanic complex; (5) plagiogranite; and (6) a capping package of pelagic sediments (Brunnschweiler, 1966; Bhattacharyya, 1991; Nandy, 2001). The sharp tectonic contact of these rocks with epi-metamorphosed slates and phyllites in Naga Hills (Ganju et al., 1986), combined with the absence of intrusive contacts suggest that they are rootless subhorizontal bodies (Fig. 9) (Acharyya, 2007a) representing obducted masses of the oceanic crust. Acharyya (2007a) suggested that two juxtaposed sets of ophiolites were accreted during Early Cretaceous and mid-Eocene and both are considered to have alpine-type affinities (Daurah et al., 1983).

## **2.6 ASSAM SHELF**

The Assam Shelf (Fig. 5), considered as a vast intermontane basin, is bounded by the Himalaya in the north, Indo–Burma Ranges to the east, the Mishmi block to the northeast and the Shillong Plateau and Mikir Hills to southwest (Rangarao, 1983). This basin, through which the Brahmaputra River flows, is covered by thick alluvium and is structurally less complex and tectonically less deformed than the thrust zone (Schuppen Belt) to the east (Mathur et al., 2001). The subsurface geology of the upper Assam basin is known best from oil exploration data. Uplift of the Shillong Plateau has been a major influence on sedimentation and the structural configuration of young strata of the Assam Shelf. Thickness of Lower Cenozoic sediments in the shelf zone ranges from 3.6 km to more than 7 km. Sediments includes shallow marine Paleogene to continental Neogene sediments overlying a granitic basement. Rocks with lithological affinities with the

Shillong-Meghalaya Gneissic Complex (SMGC) are believed to form the basement of the Assam Shelf (Clark and Bilham, 2008). During the major part of Cretaceous to early Paleogene, the Assam Shelf is considered to have been a passive continental margin upon which sediments were deposited in near shore to shallow marine depositional environments. The shelf hosted deltaic to deep water depositional environments during the later part of Eocene and Oligocene, followed by a fluvial environment in Miocene and younger times (Dasgupta and Biswas, 2000).

## **2.7 BENGAL BASIN**

The Bengal Basin (Fig. 10), situated at the eastern part of Indian subcontinent, is bounded by the Indian Shield, Shillong Plateau, and Indo-Burma Ranges to the west, north, and east, respectively. Two major river systems, the Ganges and Brahmaputra, pass through this basin. The Bengal Basin covers an area of nearly 200,000 km<sup>2</sup> and contains a thick (up to 16 km) package of orogenic sediments derived from the Himalayas to the north and the Indo-Burma Ranges to the east (Uddin and Lundberg, 1999).

The Bengal Basin has been subdivided into the following geotectonic elements (Figs. 10, 11 & 12): (1) Stable Shelf; (2) Central Deep Basin, which extends from the Sylhet Trough in the northeast to the Hatia Trough in the south; and (3) Chittagong-Tripura Fold Belt. The Stable Shelf to the west is separated from the deeper part of the basin by a hinge zone that runs from Kolkata (Calcutta) in the southwest to Mymensingh in the northeast (Fig. 10). The gravity map (Fig. 7) shows that there is a significant Bouguer gravity anomaly ( $L_2$ ) in the Sylhet Trough, reflecting the thick accumulation of

basinal sediments. Rajasekhar and Mishra, (2008) suggested that sediments thicken from 5 km to 13 km east of the hinge zone, and that the depth of Moho increases from 29 to 34 km across the hinge zone. A northeast-southwest trending linear gravity anomaly is evident in the central part of the basin. This is interpreted as a transition from thin continental crust to oceanic crust (Clark and Bilham, 2008; Rajasekhar and Mishra, 2008). The Chittagong-Tripura fold belt is a Neogene accretionary prism complex, and the western boundary of this fold belt is interpreted as a Miocene subduction zone. The right-lateral Kaladan Fault separates the Chittagong Fold Belt from the Indo-Burma Ranges (Fig. 10). Sedimentation in the Bengal Basin started during the Gondwana period as a half-graben, like the other Gondwana basins in India (Alam et al., 2003). The basin became a stable shelf after India broke apart from its counterparts during the Cretaceous and since then sedimentation has been continuous in the most parts of the basin.

According to Alam et al. (2003), sedimentation within the Bengal Basin took place in five distinct phases: (1) Permo-Carboniferous to early Cretaceous; (2) Cretaceous–Mid-Eocene; (3) Mid-Eocene–Early Miocene; (4) Early Miocene–Mid-Pliocene; and (5) Mid-Pliocene–Quaternary. Each of these phases of sedimentation was controlled by the tectonic cycles, which involved the interaction and collision pattern of the major plates. Sedimentation in the basin has been divided into several stages: (1) syn-rift stage; (2) drifting stage; (3) early collision stage; and (4) early and late collision stage (Johnson and Alam, 1991; Alam et al., 2003). East-west and north-south cross sections through the Bengal Basin are shown in figures 11 & 12.

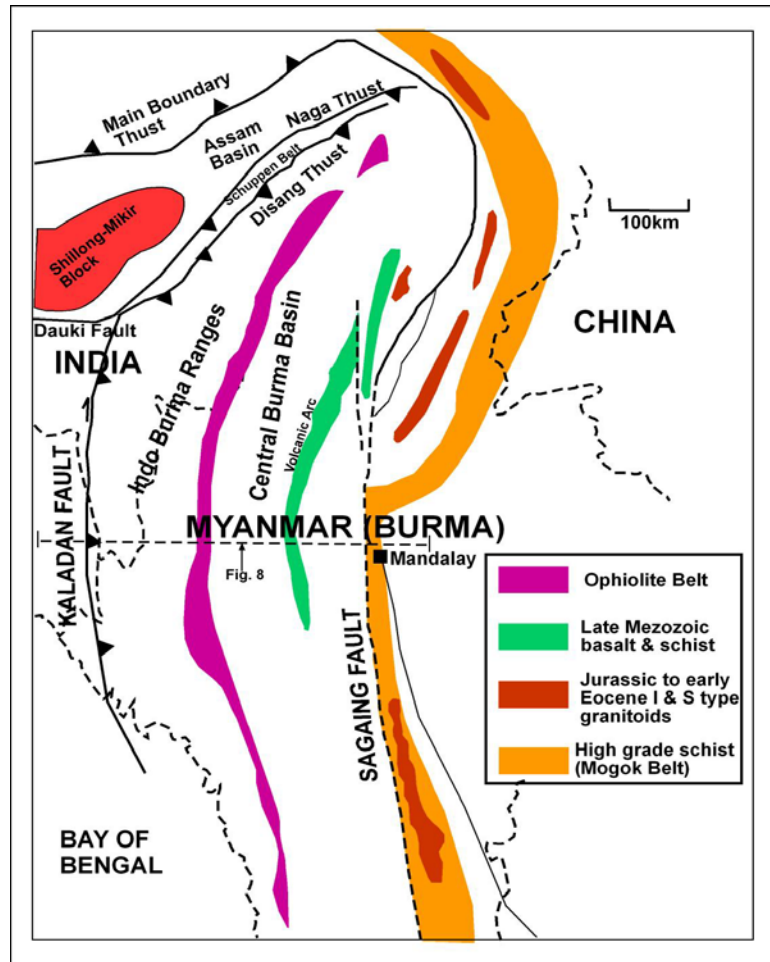


Figure 8. Map showing structural units of Indo-Burma Ranges and Central Burma Basin (modified after Acharyya, 2007b).

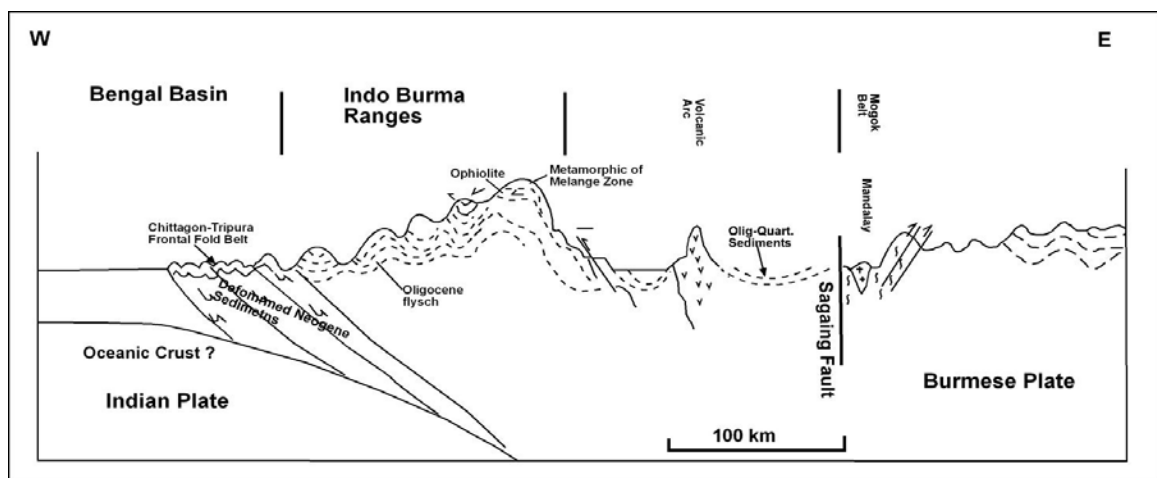


Figure 9. Schematic cross section of Indo-Burma Ranges and Central Burma Basin (modified after Acharyya, 2007b).



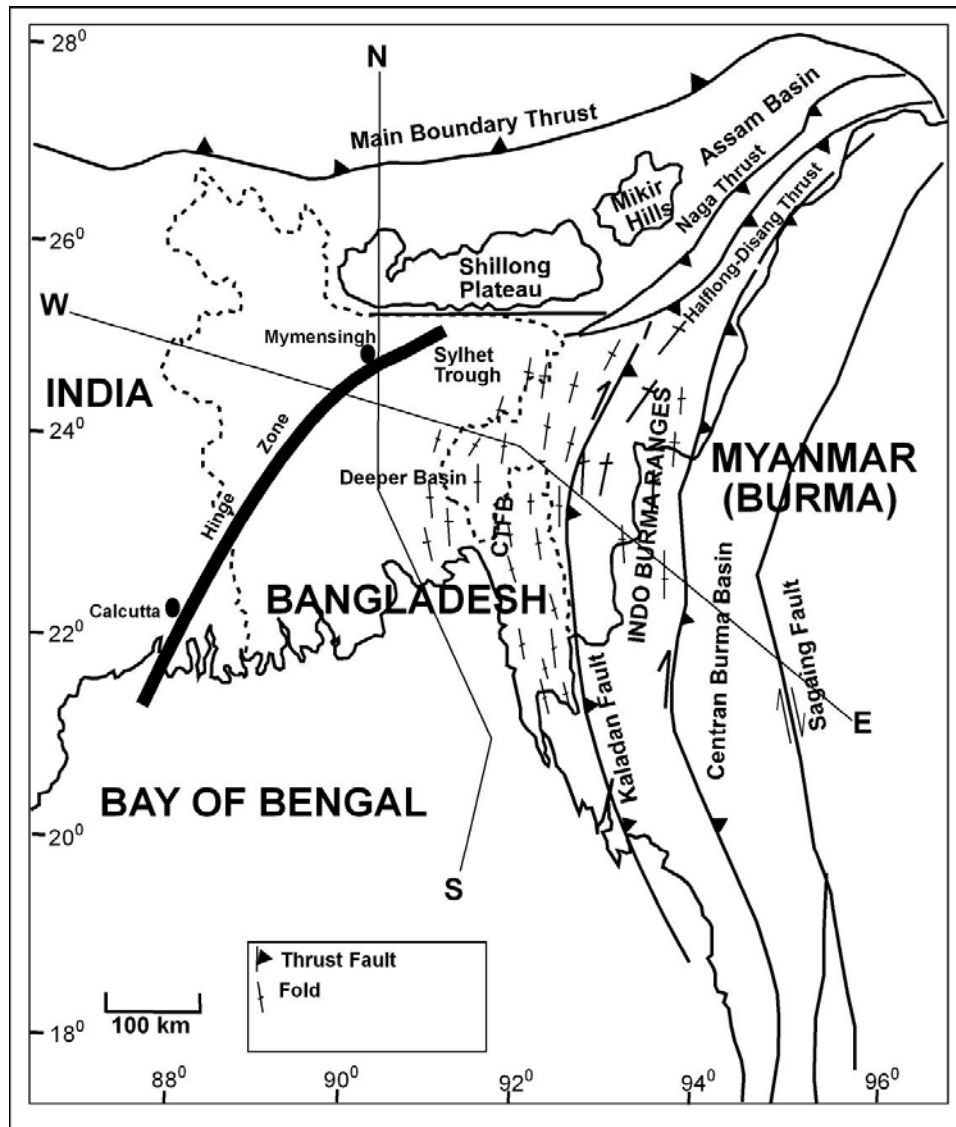


Figure 10. Tectonic map of Bengal Basin and its contiguous regions. Running between Calcutta-Mymensingh, the hinge zone separates stable shelf from central deep basin. Abbreviation: CTFB - Chittagong-Tripura Fold Belt (after Uddin and Lundberg, 1998b).

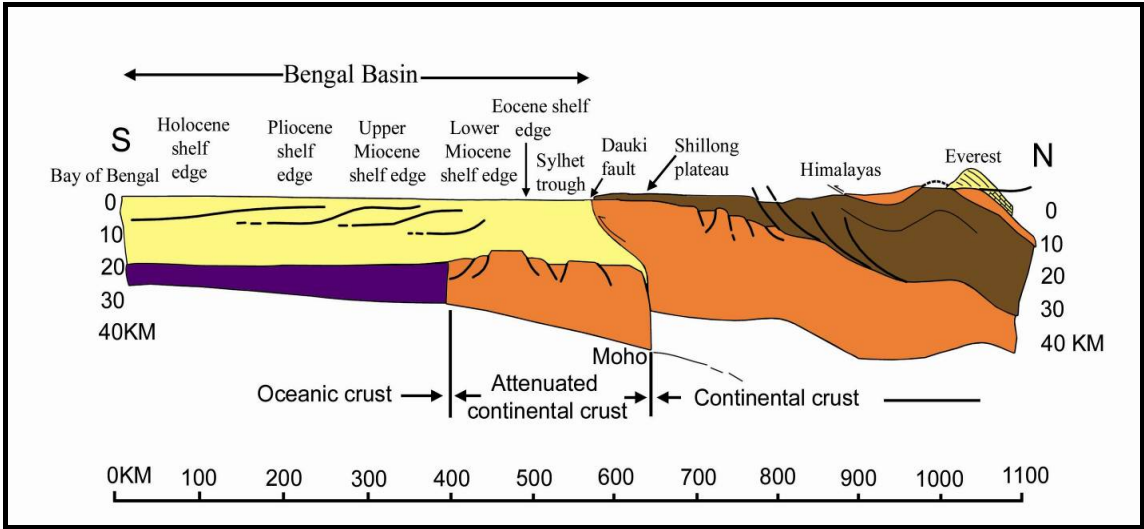


Figure 11. North-south cross section through Bengal Basin (after Uddin and Lundberg, 2004).

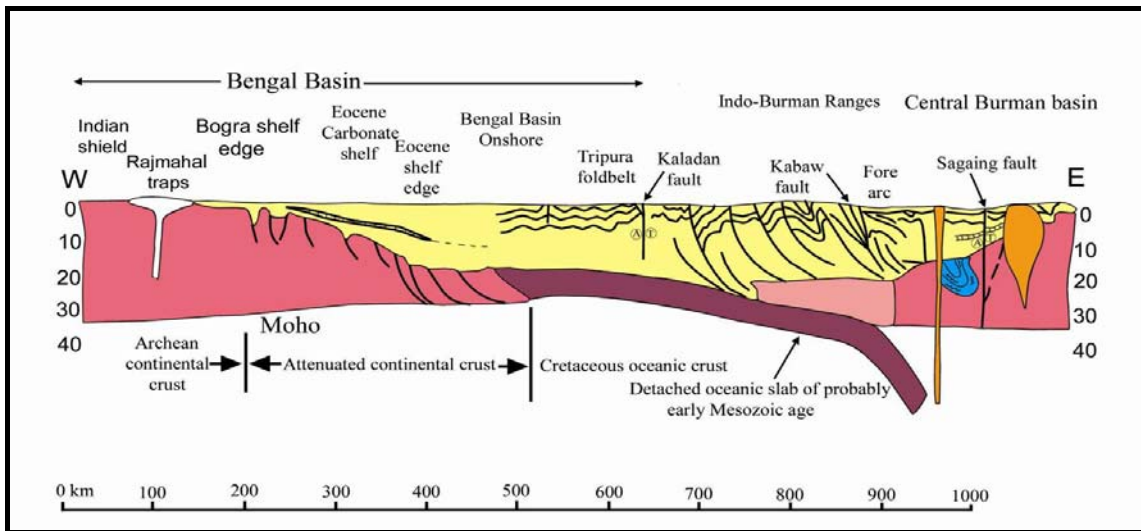


Figure 12. East-west cross section of Bengal Basin (after Uddin and Lundberg , 2004).

## **CHAPTER 3: STRATIGRAPHY AND SEDIMENTATION**

### **3.1 INTRODUCTION**

To the south and southeast, the Precambrian Shillong Plateau is unconformably overlain by younger sedimentary cover, both of orogenic and non-orogenic origin. The present study area falls to the southeast of the Shillong Plateau (Fig. 13) where sediments are nearly 11 km thick. The present study area is located at the junction between Assam and Bengal foreland basins of Himalaya and Indo-Burma orogenic belts. This area is considered as the lower extent of the Assam Basin, commonly known as lower Assam Basin, which covers the southeastern part of Meghalaya state and southern part of Assam state in India. Earlier workers divided the Assam Basin into a geosynclinal part or deeper basin and a shelf part (Dasgupta and Biswas, 2000). Based on this division, the present study area falls in the shelf part. However, the present study area anomalously contains a large sedimentary thickness. This area has been studied well for large Eocene coal reserves (Singh, 1989; Singh and Singh, 2000), but other lower Cenozoic strata have not been carefully studied. The stratigraphic framework of Assam Basin is based primarily on paleontological criteria (Sinha and Sastri, 1973; Bhandari et al., 1973; Rangarao, 1983). The present study area contains sedimentary sequences spanning from Cretaceous to lower Cenozoic (notably Cretaceous rocks are exposed only at the south side of the Shillong Plateau).

The Phanerozoic history of Assam Basin can be placed in four phases. During phase 1, the Assam Basin was a part of the Gondwana supercontinent. In phase 2, rifting

took place and coal-bearing fluvial deposits were deposited during Permo-Carboniferous time. Phase 3 began with the initial rifting of the Gondwanaland in the late Triassic/early Jurassic continued to the early Eocene. During phase 3, the area became open to marine sedimentation as a passive margin developed. During phase 4, beginning the early Eocene, India collided with the Burmese block. Since then, the entire landmass has been caught up between two collision zones; Burma to the east and Tibet to the north. The Mishmi Hills added a third compressional force from northeast (Saha et al., 2006).

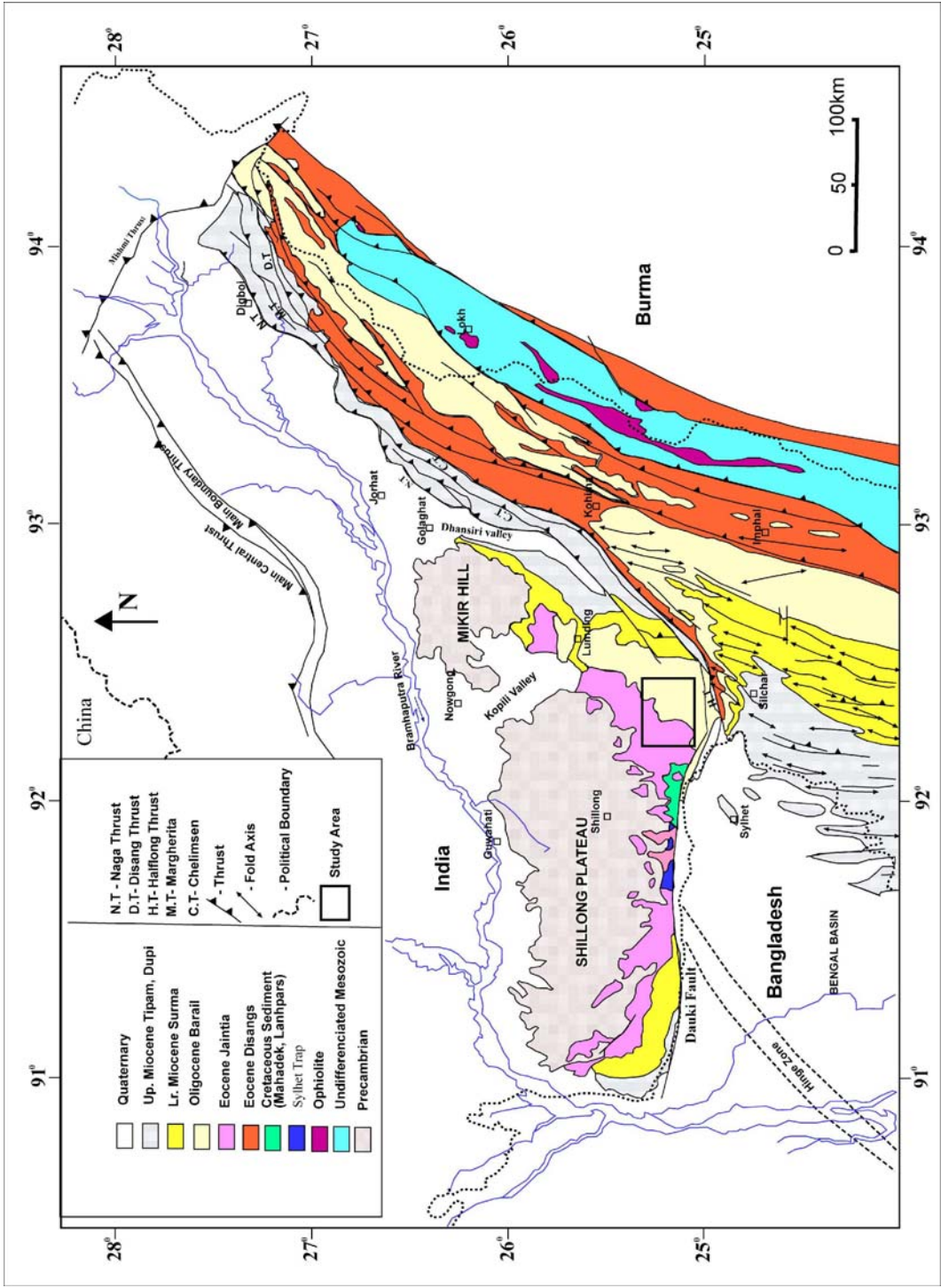


Figure 13. Geological map of northeast India (modified after Dasgupta and Biswas, 2000). Study area is indicated by the black box.

## **3.2 PRE-CENOZOIC STRATIGRAPHY**

### **3.2.1 PRECAMBRIAN BASEMENT COMPLEX**

Precambrian basement rocks that crop out in Shillong Plateau and Mikir Hills area (Fig. 14) are composed of a Precambrian Gneissic Complex with felsic and mafic intrusives, the Proterozoic Shillong Group of supracrustal material, and younger porphyritic granitoid rocks. The Gneissic Complex consists of two different units, viz. Gneissic Complex proper and migmatites. The gneissic complex proper contains abundant granitic gneisses of amphibolite facies. Other associated rocks consist of basic bands containing diopsidic-clinopyroxene and sillimanite-garnet-potassium feldspar-quartz gneiss without muscovite. These form a common assemblage and represent the highest grade amphibolite facies (Nandy, 2001). Towards the southern part of the Shillong Plateau, this Gneissic Complex contains assemblages of quartz, muscovite, biotite, garnet, staurolite, porphyroblastic andalusite, and dispersed grains of tourmaline (Mazumdar, 1976; cited in Nandy, 2001). The younger granitoid intrusions (450 - 700 Ma) are dioritic, granodioritic and granitic in composition (Ghosh et al., 1994; Srivastava and Sinha, 2005). The dioritic rocks are made up of biotite, sphene, apatite, zircon, epidote-zoisite, and minor plagioclase and quartz (Mazumdar, 1976).

These basement rocks are overlain by the intra-cratonic Shillong Group of supracrustal rocks. The Shillong Group mostly contains clastic sequences with oligomictic conglomerate, quartz arenite, and siltstone with interlayered metavolcanics (i.e. amphibolites) (Ghosh et al., 2005b).

### **3.2.2 GONDWANA ROCKS**

A few patches of lower Gondwana sediments with poorly preserved leaf impressions are exposed to the west of Shillong Plateau (Naik et al., 2004). These Gondwana sediments may be correlated with the Gondwana sequences drilled at the Hinge zone of northwestern Bengal Basin. These Gondwana sediments consist of pebble conglomerates, sandstones, and carbonaceous shale with lenticular coal seams. A nearly 340m thick Gondwana sequences was recently discovered in an oil well drilled to the north of Mikir Hills in Dhansiri Valley (Dasgupta, 1977; Nandy 2001).

### **3.2.3 CRETACOUS ALKALINE INTRUSIVES AND LAVA FLOWS**

Several alkaline ultramafic intrusive rocks occur along a northeast-trending zone. These intrude the Shillong Group (Fig. 14). They comprise pyroxenite, gabbro, mafic dikes and nepheline syenite (Srivastava, 2005). Mamallan et al. (1994) also reported the presence of trachyte, alkali pegmatite, ijolite, carbonatite, and fenite from the intrusives. Among the several alkaline bodies, the Sung Carbonatite is well-studied. Five distinct stages of evolution are recognized in the Sung Valley carbonatite, viz. 1) earliest ultramafic phase, 2) melilite-pyroxinite rocks, 3) ijolite, 4) syenite, and 5) carbonatite. Such complex magmas are considered to be generated by small-scale melting and segregation at depths of 100-200 km. Chattopahyay et al. (1983) suggested that this complex formed around  $84 \pm 13$  to  $90 \pm 10$  Ma, in response to up-arching of the basement along a NE-SW axis and a deep-seated fault parallel to this axis.

The Sylhet trap, part of the Rajmahal-Sylhet continental flood basalt province, is well exposed in the southern part of the Shillong Plateau. This flood basalt system is

associated with the rifting of the Indian plate from its Gondwanaland counterparts. The maximum thickness of the Sylhet trap is 550-600 m. The Sylhet trap comprises basalts with minor volumes of rhyolite and acid tuff. The basalts are mainly micro-porphyritic with phenocrysts of labradorite and augite (Baksi et al., 1987). Petrochemically, the Sylhet basalt belongs to the calc-alkaline volcanic suite with minor alkaline and acid differentiates. The main basalts are tholeiites as they are saturated with SiO<sub>2</sub>, with 0.5% norm quartz. The alkali basalt contains 15% diopside phenocrysts by volume (Talukdar et al., 1971; cited in Nandy, 2001).

### **3.2.4 CRETACEOUS SEDIMENTS**

Dasgupta (1977) and Samanta and Raychoudhury (1983) described the lithostratigraphic development of Upper Cretaceous to lower Cenozoic deposits south and southeast of the Shillong Plateau (Figs. 13 & 14). Sedimentation in the area began with the accumulation of a thick, shallow marine Upper Cretaceous clastic sequence on top of the Sylhet trap. This sequence includes massive, coarse, ferruginous and glauconitic sandstones that become progressively more calcareous and argillaceous towards the top (i.e. the Mahadeo/Mahadek Formation). The upper part of this sequence is considered to be of early Paleocene (Danian) age (Pandey, 1990; Jauhri and Agarwal, 2001). Sandstones are overlain by calcareous shales, mudstone, and carbonaceous sandstone of the Langpar Formation. The Langpar Formation is thought to have been deposited in deeper neritic through shallow marine setting. Planktonic microfossils suggest that it is early Paleocene in age (Nagappa, 1959; Pandey, 1978, cited in in Misra, 1992; Jauhri and Agarwal, 2001).



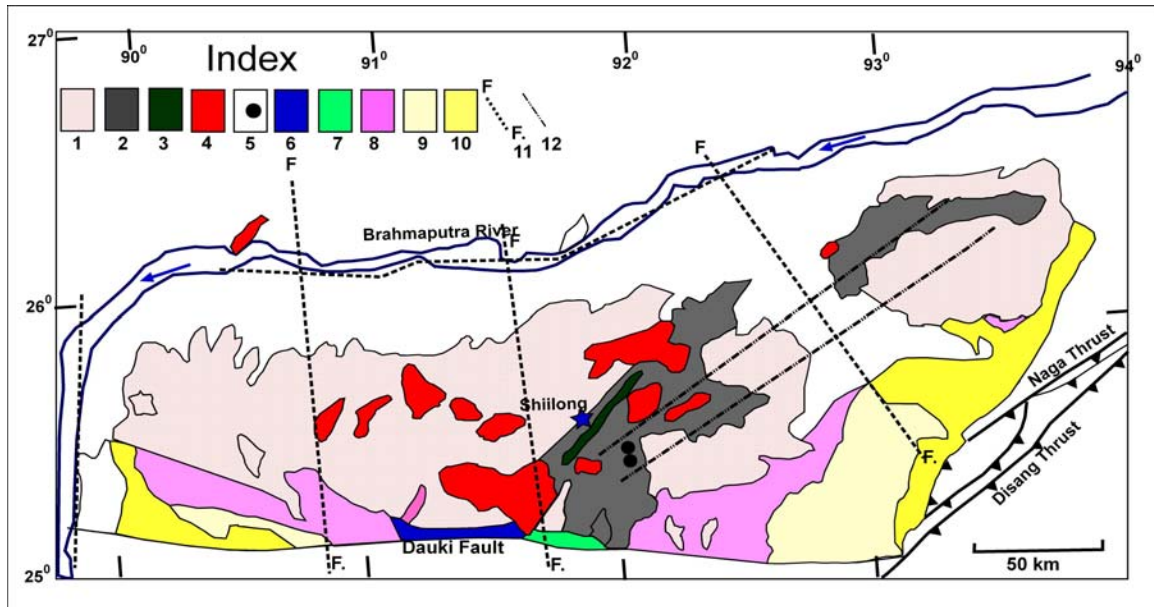


Figure 14. Detailed geological map of Shillong Plateau 1 - Basement complex, 2 - Shillong Group, 3 - Khasi Greenstone, 4 - Porphyritic granite, 5 - Carbonatite, 6 - Sylhet trap, 7 - Cretaceous Sediments, 8 - Jaintia Group, 9 - Barail Group, 10 - Surma and Dupi Tila Group, 11 - Fault, 12 - Shear Zone (after Nandy, 2001).

### 3.3 LOWER CENOZOIC SEDIMENTS

A thick sequence (10+ km) of lower Cenozoic sediments was deposited to south and southeast of the Shillong Plateau. The stratigraphy of Cenozoic sequences from the study area is presented in Table 1. The lowermost unit of this sequence is the Therria/Tura Formation of the Jaintia Group (Figs. 13 & 14), which conformably overlies the Langpar Formation. The Therria/Tura Formation is 100 m thick and is composed of sandstone, calcareous sandstone, and limestone. Tura sandstone (Fig. 15A) is coarse grained, and is generally exposed only in relatively lower level ground. The Jaintia Group is believed to have formed in Eocene shelf settings that formed when the southwestern, southern and southeastern parts of the Shillong Plateau were submerged (Misra, 1992; Dasgupta and Biswas, 2000). The Therria Formation is conformably overlain by the Sylhet Limestone and the Kopili Formation. The Sylhet Limestone contains bluish,

massive to thinly-bedded limestone and coarse- to medium-grained sandstone with bands of sandy limestone.

The Sylhet Limestone has been divided into five members: (1) Prang Limestone, up to 270 m of fossiliferous limestone; (2) Nurpuh Sandstone, 20 m of sandstone with calcareous bands; (3) Umlatdoh Limestone, up to 60 m of limestone with sandstone bands; (4) Lakadong Limestone (Fig. 15B), up to 150 m of fossiliferous limestone; and (5) Lakadong Sandstone (Fig. 15C), 24 m of sandstone with thin coal layers.

The Sylhet Limestone has been traced northeastwards to the Mikir Hills and has been found in deep wells in upper Assam, where a thickness of 400 m have been recorded (Dasgupta and Biswas, 2000). The Umlatodoh Limestone is lower Eocene in age, whereas the Prang Limestone is middle to upper Eocene. The alternation of sandstone and limestone within the Sylhet Limestone reflects changes in depositional environment and differential clastic influx over time. Predominantly brownish, medium-grained arkosic sandstone with carbonaceous shale and coal seams reflects shallow-water deltaic environments (Singh and Singh, 2000). The Sylhet Limestone is absent in the upper Assam Basin but is well developed in the Bengal Basin toward the southwest (Uddin et al., 2007).

The Kopili Formation (Fig. 15D) conformably overlies the Sylhet Limestone. It hosts an alternating sequence of sandstone, siltstone, and black shale, commonly called the Kopili alternation, and grades upward into the overlying Barail Sandstones. The Kopili Formation is well exposed in the southern and eastern parts of the Shillong Plateau and in the Mikir Hills. In the southeastern part of Shillong Plateau, the Kopili Formation

is nearly 500 m thick. The Kopili Formation is late Eocene age (Chandra et al., 1983; Singh and Singh, 2000).

The Eocene Disang Formation is made up of a monotonous sequence of deep-water dark-gray shales with thin bands of sandstone toward the top. The Disang Formation is not exposed in the study area but is well exposed towards the east across the Haflong thrust (Fig. 13). In part of the Indo-Burma Ranges, Disang shales are splintery in nature, with thin quartz veins and a few serpentinized intrusions (Dasgupta, 1977). The thickness of the Disang Formation has not been confirmed in the Indo Burma Ranges. The beds are invariably crumpled and dip steeply toward the Indo Burma Ranges (Dasgupta, 1977; Dasgupta and Biswas, 2000).

The Kopili Formation is conformably overlain in the Shelf Zone by deep-water facies of the Laisong, Renji, and Jenum formations of the Oligocene Barail Group. The lowest part of the Barail Group certainly passes by lateral variation into the upper part of the Disang Group. The Barail Group is arenaceous and crops out in relatively higher grounds. Thickness of the Barail Group varies in different parts of the basin. In the present study area, the Laisong Formation (Fig. 15E) is mainly composed of medium-to fine-grained sandstone with subordinate shale and conglomerate, whereas the Renji Formation is an argillaceous unit. The Jenum Formation is composed of well-indurated, medium- to fine-grained, massive sandstone.

Table 1. Cenozoic stratigraphy of the study area (after Rangarao, 1983; Singh and Singh, 2000).

Age	Group	Formation	Thickness (m)	Lithology
Pliocene to Pleistocene	Dupi Tila	Dupi Tila	1200	Massive to cross bedded sandstone at the lower part with increasing mud units toward the top
Unconformity (?)				
Upper Miocene to Pliocene	Tipam	Girujan Clay	1900	Not exposed in this area
		Tipam Sandstone		Massive, thick-bedded sandstone
Lower Miocene	Surma	Boka Bil	2500	Fine-grained, laminated sandstone and shale.
		Bhuban		Fine-grained, indurated sandstone alternating with shale.
Unconformity (?)				
Oligocene	Barail	Renji	4650	Argillaceous sandstone
		Jenum		Medium- to fine-grained, hard massive sandstone.
		Laisong		Medium to fine sandstone with subordinate shale and conglomerate.
Eocene	Jaintia	Kopili	500	Alternating sandstone & black shale
		Sylhet	500	Bluish, massive to thinly bedded limestone. Coarse- to medium-grained sandstone with bands of sandy limestone. Gray to pinkish gray limestone, sandy limestone, and calcareous sandstone. One member, known as Lakadong Sandstone, is made up of medium-grained arkosic sandstone with carbonaceous shale and coal seams.
		Therria/Tura	100	Medium to coarse sandstone with thin bands of pyrite-rich siltstone

In the present study area, the Barail Group is unconformably overlain by thick, sequences of the Bhuban and Boka Bil formations of the Surma Group and the upper Miocene Tipam Sandstone. The Bhuban Formation is composed of indurated fine-grained sandstone alternating with shale. The Boka Bil Formation (Fig. 15F) is chiefly composed of fine-grained, laminated sandstone and shale. The Tipam unit is characterized by massive, thick-bedded sandstone. There is a basin-wide unconformity at the Barail-Surma boundary that can be traced into the Bengal Basin and in upper Assam Basin (Dasgupta and Biswas, 2000; Kent and Dasgupta, 2004).

The Surma Group, also subdivided into lower Bhuban and upper Boka Bil formations, is thickest in the Sylhet trough. Surma Group sediments thin rapidly northward, largely by the lower beds being truncated by the overlying Tipam Sandstone. At Badarpur, southeast of the present study area, fairly thick and coarse massive sandstones in the lower part of the Surma Group provided reservoirs for oil (Dasgupta, 1977). In Bangladesh, large quantities of natural gas deposits have been found in the Surma Group. The thickness of the Surma Group is commonly more than 2,500 m in Assam-Arakan Basin and the Indo-Burma Region. In the upper Assam, the Surma Group is not subdivided as the beds are very thin.

The Tipam Sandstone, although defined best in upper Assam, is readily recognizable in the Sylhet trough of Bangladesh and Tripura-Mizoram states of India. In the Surma Valley of Tripura, south-southeast of present study area, the full thickness of the Tipam Sandstone is about 1,200-1,400 m. However, in many areas the upper part is missing represented by an unconformity below the Dupi Tila Formation. In the North Cachar Hills, just east of present study area, the formation is about 1,300 m thick but

increases northwards (2,300 m) in the Naga Hills (Rangarao, 1983). In the Surma Valley, the Tipam Sandstone is composed of thick, fairly coarse, massive ferruginous sandstone with subordinate beds of shale.

### **3.4 BRIEF SUMMARY ON DEPOSITIONAL CONDITIONS**

Although much information has been obtained about the lower Cenozoic rocks of Assam, the conditions of deposition are poorly known. In the Eocene, there was a clear distinction between calcareous shelf facies and an argillaceous deep water facies. The shelf facies was deposited over a spur of the Indian Shield that extended toward the northeast (Fig. 5). In upper Assam, the location of the hinge zone is near to the Naga thrust (Fig. 13). In the present study area, Eocene marine shelf limestone alternates with coal-bearing sandstone.

The contrast between the two facies was minimal during the Oligocene with the principal difference being in thickness. However, in the north Cachar Hills and especially in the Mikir Hills (Fig. 13), the thinner shelf facies is on the whole more arenaceous, with an abundance of thick massive sandstones. The Barail deposits are mainly of shallow water origin, although the presence intraformational conglomerates and coal seams in the Schuppen Belt region of upper Assam indicate interruptions in subsidence.

The Sylhet Limestone was deposited in response to extensive and prolonged marine transgression in the study area. Deposition occurred in carbonate platform environments, which tended to become reefal throughout the course of deposition of the Sylhet Limestone. Carbonate deposition, however, was occasionally interrupted due to

increased supply of clastics. The lower part of the Kopili Formation has yielded age-diagnostic foraminifera that suggest a late Eocene age.

After the Oligocene-Miocene break, deposition began in the south long before resumption in the north. In the southern part of Assam, the earlier northeast to southwest trend was no longer obvious, and the separation of shelf and deep basinal parts is not clearly distinguished. The Miocene deposits of the south contain few marine fossils, but in the north the units were deposited in brackish water environments (Dasgupta, 1977). Continental environments spread southwards, as shown by the occurrence of mottled clays and sandstones in the Girujan Clay in the Sylhet trough.



Fig. 15. Outcrop photographs of different stratigraphic units of the study area. (A) Therria/Tura Sandstone of Jaintia Group. (B) Lakadong Limestone Member of lower Sylhet Formation. (C) Lakadong Sandstone Member of lower Sylhet Formation. (D) Lower Kopili Formation with alternating sandstones and shales. (E) Fine-grained sandstone with Laisong Formation of the lower Barail Group. (F) Fine-grained sandstone of Boka Bil Formation.



## **CHAPTER 4: SANDSTONE PETROGRAPHY**

### **4.1 INTRODUCTION**

Sandstone petrography is widely used to infer the paleotectonic setting and provenance of ancient clastic sequences. Sandstones from similar tectonic settings tends to have similar compositions. Petrofacies analyses, wherein the proportions of the detrital framework grains are plotted on different ternary diagrams, have demonstrated intimate relationship between detrital sand composition and tectonic setting (Ingersoll, 1978; Dickenson and Suczek, 1979; Dickinson et al., 1983; Decelles and Hertel, 1989). Mack (1984) suggested that factors other than the source-rock composition also are important in determining the ultimate composition of sandstones. Sandstone composition is sensitive to several factors, such as climate, relief, transport, and diagenesis, which provide valuable information for paleogeographic reconstructions (Suttner, 1977; Ingersoll et al., 1984; Johnson, 1993). Basin evolution and unroofing history of mountain belts can be best inferred through provenance studies that focus on key attributes of detrital mineralogy (Dorsey, 1988; Cervený et al., 1989; Uddin and Lundberg, 1998a, b). Provenance reconstruction through detailed mineralogical analyses is based on the assumption that modes of transportation, depositional environments, climates, and diagenesis have not significantly altered detrital grain composition (Basu, 1976). This chapter deals with sandstone petrology and modal analysis of Lower Cenozoic clastic sequences deposited southeast of the Shillong Plateau. Systematic compositional study of sandstones from this area helps in understanding the detrital history,

paleotectonic evolution, and unroofing history of the adjacent mountain belts (Uddin and Lundberg, 1998a).

## 4.2 METHODS

A total of twenty-six samples of sand and sandstone, ranging in age from Eocene to Miocene, were collected along the Jowai-Badarpur Road of southeast Meghalaya state of India (Fig. 3). Fresh outcrop samples were collected from all representative sequences guided by regional geological experts. Mineralogical composition of sandstone was determined by modal analysis of thin sections following the Gazzi-Dickinson method (Ingersoll et al., 1984); i.e. sand-sized minerals included in lithic fragments were counted as mineral phases rather than the host lithic fragments in order to normalize for grain-size variations (Table 2; Dickinson, 1970; Ingersoll et al., 1984). Thin sections were stained for plagioclase and potassium feldspars. A minimum of 300 grains were counted per each thin section, with 350 points counted for samples with larger compositional variability. Modal analysis data were recalculated on a matrix free basis.

Modal sandstone compositions were plotted on standard ternary diagrams (QtFL, QmFLt, QmPK, LsLvLm, LsLm<sub>1</sub>Lm<sub>2</sub>, etc.) and used to assess temporal changes in provenance (Dickinson, 1970; Dorsey, 1988). The following compositional parameters were evaluated: Qt = total quartz; Qm = monocrystalline quartzose grains; Qp = polycrystalline quartz grains, including chert grains; F = total feldspar grains; P = plagioclase feldspar grains; K = potassium feldspar grains; L = lithic fragments; Lt = total lithic fragments; Ls = sedimentary lithic fragments; Lv = volcanic lithic fragments; Lm = metamorphic lithic fragments; Lsm = sedimentary and metasedimentary lithic fragments; Lvm = volcanic, hypabyssal, metavolcanic lithic fragments; Lm<sub>1</sub> = very low-

to low-grade metamorphic lithic fragments; and  $Lm_2$  = low- to intermediate-grade metamorphic lithic fragments (Table 2). In the QmFlt diagram, polycrystalline quartz and chert grains were placed at the Lt (lithic fragments) pole. In QtFL diagrams, all quartzose grains were plotted together to emphasize grain stability, weathering, and relief in the source areas, and transport mechanism.

### **4.3 PETROGRAPHY**

Composition of lower Cenozoic sandstones from southeast of Shillong Plateau vary from quartzose to quartzofeldspathic (see Table 3). Feldspar content is very low in all samples. In general, the older Eocene Tura sandstones are medium-to coarse-grained, whereas the younger sandstones are mostly medium- to fine-grained. Lithic fragments are more common in late Eocene and younger sequences. Data from modal analyses of the major stratigraphic units are presented in Table 2 and plotted in figures 16 to 19. Variation in plagioclase/total feldspar and modal mineralogical composition in all sandstones are shown in figures 20 & 21. Representative photomicrographs of sandstones are provided in figures 22 through 24.

#### **4.3.1 JAINTIA GROUP**

A total of fourteen sand and sandstone samples from the Eocene Jaintia Group were studied. Ten samples are from Tura and Sylhet formations and the remaining four are from the Kopili Formation. The Tura and Sylhet formations of Jaintia Group are similar in framework grain composition. However, the Kopili Formation is distinct in having higher percentages of lithic fragments. The average composition of the Sylhet and

Tura formations of Eocene Jaintia Group is  $Qt_{98}F_2L_0$ , whereas the average composition of the overlying Kopili Formation is  $Qt_{73}F_4L_{23}$ .

In general, the older Eocene units (e.g., Tura and Sylhet formations) are very rich in quartz. Qm is the dominant framework grain in Sylhet and Tura formations (Fig. 22A), although a few samples show Qp dominant over Qm (samples T1 & T4). Quartz grains present are both monocrystalline and polycrystalline, and sub-angular to sub-rounded (Fig. 22B).

Table 2. Recalculated modal parameters of sand and sandstone (Uddin and Lundberg, 1998a).

1. Primary parameters (after Graham et al., 1976; Dickinson and Suczek, 1979; Dorsey, 1988)

$Qt = Qm + Qp$ , where

Qt = total quartzose grains

Qm = monocrystalline quartz (> 0.625 mm)

Qp = polycrystalline quartz (or chalcedony)

Feldspar Grains ( $F = P + K$ ), where

F = total feldspar grains

P = plagioclase feldspar grains

K = potassium feldspar grains

Unstable Lithic Fragments ( $Lt = Ls + Lv + Lm$ ), where

Lt = total unstable lithic fragments

Lv = volcanic/metavolcanic lithic fragments

Ls = sedimentary/metasedimentary lithic fragments

2. Secondary parameters (after Dickinson, 1970a; Uddin and Lundberg, 1998a)

P/F = plagioclase/total feldspar

$Lm_1$  = very low- to low-grade metamorphic lithic fragments

$Lm_2$  = low- to intermediate-grade metamorphic lithic fragments

Table 3. Normalized modal compositions of sandstones from southeast of Shillong Plateau, Meghalaya (Gr. 1= Tura and Sylhet formations, Gr.2=Kopili Formation, Gr.3= Barail Group, and Gr.4= Surma Group).

	Gr.1			Gr.2			Gr.3			Gr.4										
	Sample no.	Qt	F	L	Qm	F	Lt	Qm	P	K	Ls	Lv	Lm	Ls	Lm <sub>1</sub>	Lm <sub>2</sub>				
	SM 3	100	0	0	92	0	8	100	0	0										
	SM 4	100	0	0	82	0	18	100	0	0										
	SM 5	98	2	0	92	2	6	97	0	3										
	SM 6	98	2	0	69	2	29	98	2	0										
	SM 33	99	1	0	63	1	36	98	2	0										
	T 1	96	4	0	18	4	78	91	1	8										
	T 3	98	2	0	83	2	15	97	0	3										
	T 4	98	2	0	32	2	66	94	0	6										
	T 6	99	1	0	79	1	20	97	0	3										
	T 7	99	1	0	83	1	16	97	0	3										
	MEAN:	98	2	0	MEAN:	69	2	29	MEAN:	97	1	3								
	STDEV	1	1	0	STDEV	25	1	24	STDEV	3	1	3								
	SM 25	66	2	32	36	2	62	95	0	5	3	0	97	3	13	84				
	SM 28	47	1	52	22	1	77	98	2	0	26	0	74	26	21	53				
	SM 29	63	6	31	12	6	82	90	10	0	34	0	66	34	26	40				
	SM 30	73	4	23	52	4	44	91	7	2	38	0	62	38	16	46				
	MEAN:	63	3	35	MEAN:	31	3	66	MEAN:	94	5	2	MEAN:	25	0	75	MEAN:	25	19	56
	STDEV	11	2	12	STDEV	17	2	17	STDEV	4	5	2	STDEV	16	0	16	STDEV	16	6	20
	SM 18	53	1	46	35	1	64	95	2	3	30	0	70	30	41	29				
	SM 17	64	2	34	39	2	59	94	1	5	22	0	78	22	40	38				
	SM 16	62	4	34	49	4	47	93	2	5	17	0	83	17	27	56				
	SM 20	64	5	31	20	5	75	80	14	6	22	0	78	22	30	48				
	SM 21	73	3	24	39	3	58	93	0	7	33	0	67	33	9	58				
	SM 22	73	6	21	52	6	42	88	6	7	46	0	54	46	11	43				
	SM 23	65	4	31	17	4	79	82	5	13	15	0	85	15	12	73				
	SM 24	67	5	28	38	5	57	86	8	6	32	0	68	28	16	56				
	MEAN:	65	4	31	MEAN:	36	4	60	MEAN:	89	5	6	MEAN:	27	0	73	MEAN:	27	23	50
	STDEV	6	2	7	STDEV	12	2	13	STDEV	6	5	3	STDEV	10	0	10	STDEV	10	13	14
	SM 07	52	16	32	22	16	62	57	9	34	5	0	95	4	15	81				
	SM 08	61	7	32	38	7	55	84	3	13	7	0	93	7	16	77				
	SM 09	50	5	45	39	5	56	89	1	10	13	0	87	13	16	71				
	SM 14	59	3	38	54	3	43	94	2	4	14	0	86	14	30	56				
	MEAN:	56	8	37	MEAN:	38	8	54	MEAN:	81	4	15	MEAN:	10	0	90	MEAN:	10	19	71
	STDEV	5	6	6	STDEV	13	6	8	STDEV	17	4	13	STDEV	5	0	4	STDEV	5	7	11

The average P/F (plagioclase/total feldspar) ratio for Tura and Sylhet samples is 0.12. Silica cement in the form of quartz overgrowth occurs in the highly indurated Tura Sandstone. A few samples of the Tura Sandstone contain sillimanite and other heavy mineral inclusions.

The late Eocene Kopili Formation is quartzolithic in composition ( $Qt_{73}F_4L_{23}$ ), containing higher amount of metamorphic rock fragments. Rock fragments were altered diagenetically, which created secondary matrix (pseudomatrix) in the sandstones (Fig. 23A). Some samples of the Kopili Formation contain sub-rounded glauconite and zircon grains that suggest recycling of sediments in the basin. Framework-grain contacts are concavo-convex to sutured indicating moderate to strong post-depositional compaction. The P/F ratio in Kopili Formation samples is less than that of the Sylhet and Tura formations (P/F=0.20).

#### **4.3.2 BARAIL GROUP**

Eight Oligocene Barail sandstone samples were analyzed. The Oligocene Barail Group contains 85% to 92% framework grains and is quartzolithic ( $Qt_{65}F_4L_{31}$ ). Quartz constitutes about 53-73% of the samples. Lithic grains consist of sedimentary and metamorphic fragments; volcanic fragments are rare. Some of the labile framework grains were altered to form secondary matrix (Figs. 23B, 24A). The lower part of Barail Group is relatively rich in lithic fragments compared to the upper part. Grain contacts are concavo-convex. Potassium feldspars are more common than plagioclase, except in one sample (SM 20). P/F ratio for Barail sandstone (0.33) is higher than those for the underlying Kopili Formation.

### **4.3.3 SURMA GROUP**

The early Miocene Surma Group is similar in composition ( $Qt_{56}F_8L_{36}$ ) to the underlying Barail Group. Surma Group samples are characterized by more common matrix (upto 20%) (Fig. 24B) which is mainly secondary in origin. This unit contains less Qp and slightly more feldspars compared to the underlying Barail Group. Generally, sands from this unit are very poorly sorted and subrounded to subangular. Quartz and lithic fragments are the dominant framework grains; feldspars are much less common. Muscovite is very common in the sandstones from the Surma Group. Grain contacts are mainly line to concavo-convex. This unit contains higher percentages of upper grade metamorphic rock fragments than the underlying Barail Group. P/K ratios for this unit (0.20) are similar to those for the Kopili Formation but less those of the Barail Group.

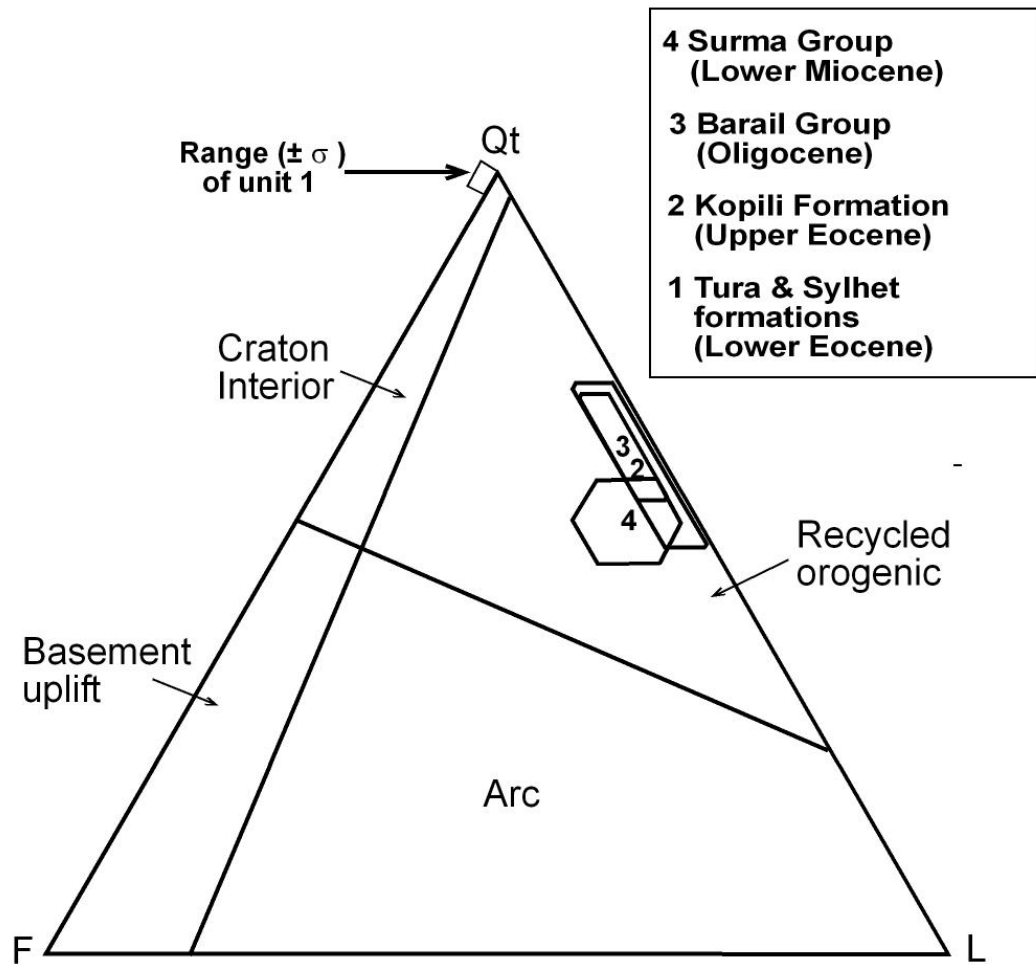


Figure 16. QtFL triangular plot of sandstone samples from southeast of Shillong Plateau. Provenance fields are drawn after Dickinson (1985).



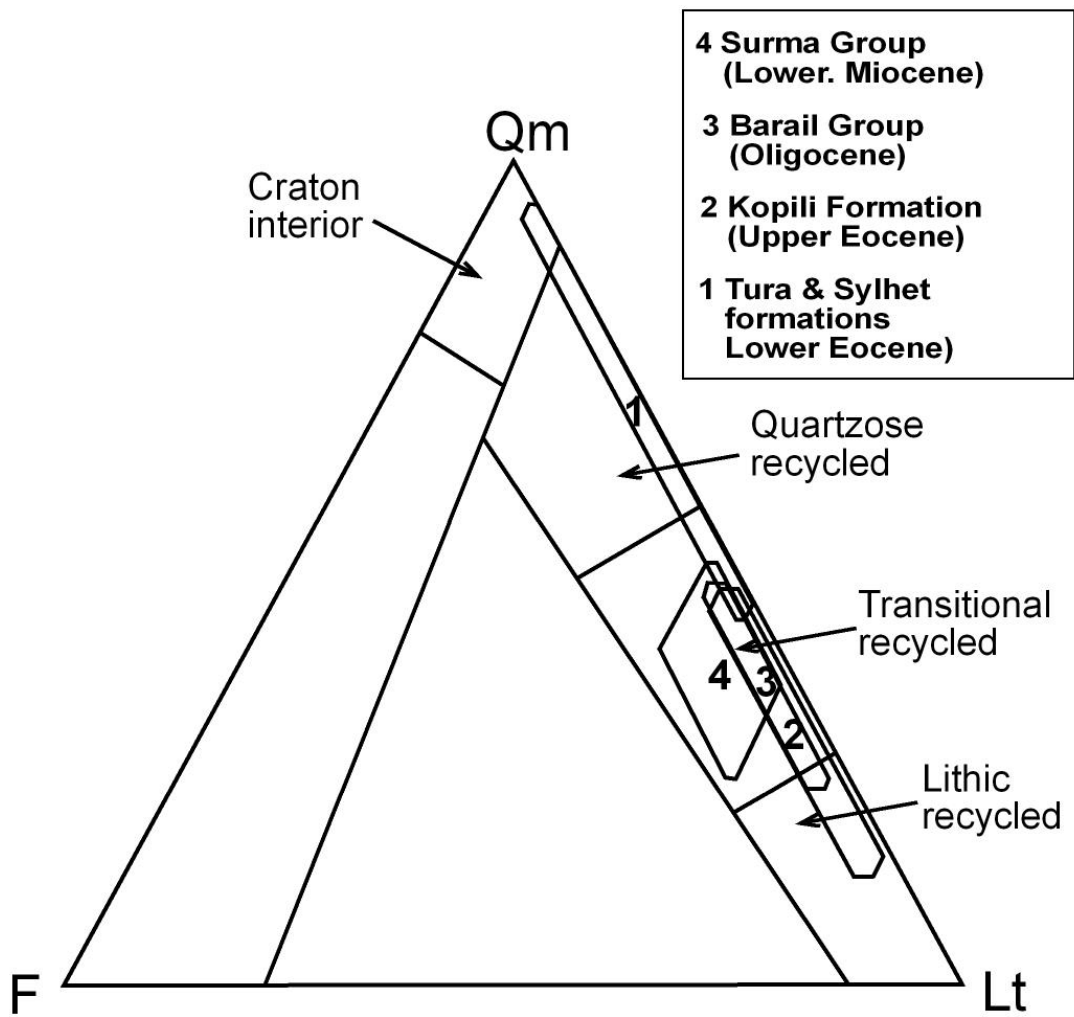


Figure 17. QmFLt plot showing mean and standard deviation polygons of Lower Cenozoic stratigraphic units. Provenance fields are drawn after Dickinson (1985).

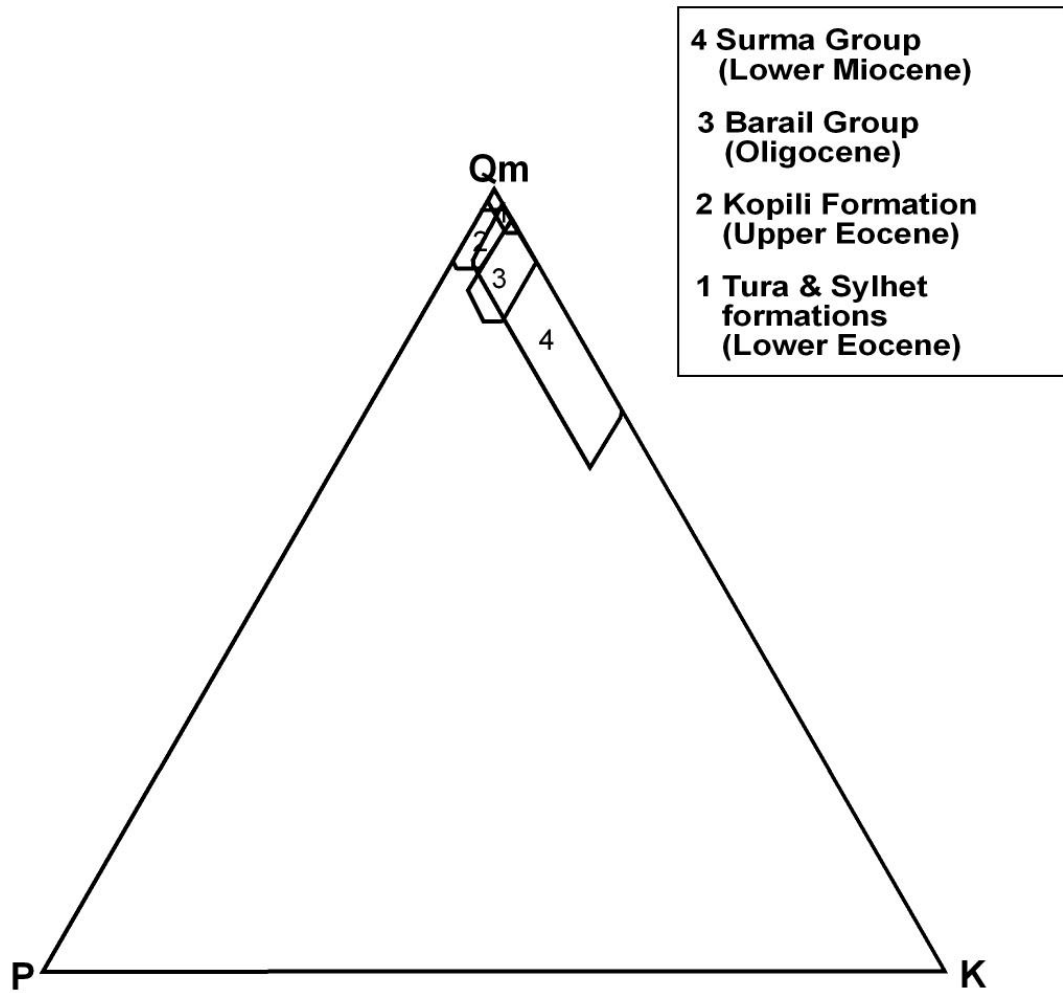


Figure 18. QmPK plot of sandstone samples from the study area, showing mean and standard deviation polygons for each stratigraphic units.

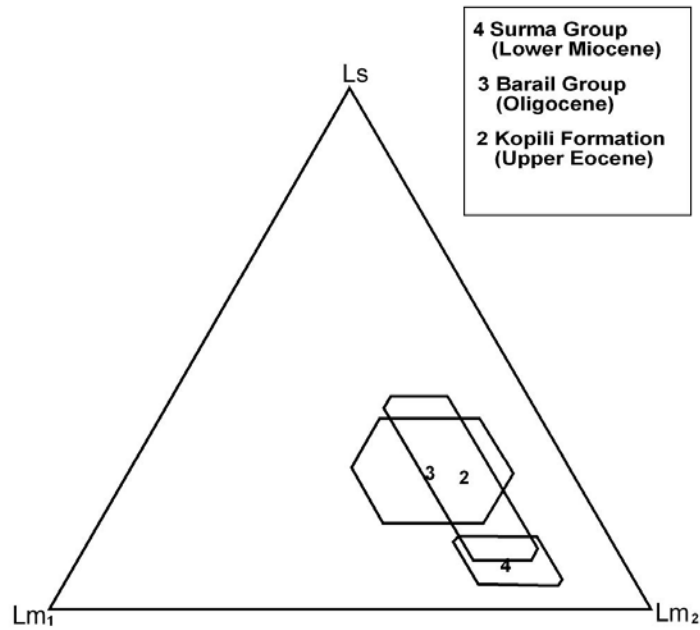


Figure 19. Ternary diagram showing lithic fragment compositions (LsLm<sub>1</sub>Lm<sub>2</sub>) of sandstones from the study area. Mean and standard deviation polygons of each stratigraphic units.

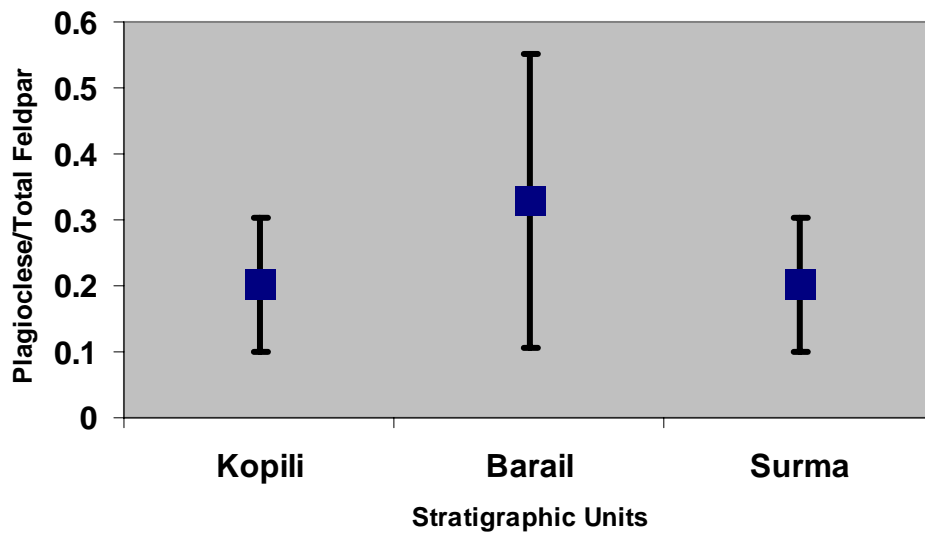


Figure 20. Plot of plagioclase to total feldspar ratios in sandstones, showing mean and standard deviation of each studied stratigraphic units. Feldspar counts in Eocene Tura and Sylhet formations are absent to negligible and not plotted here.

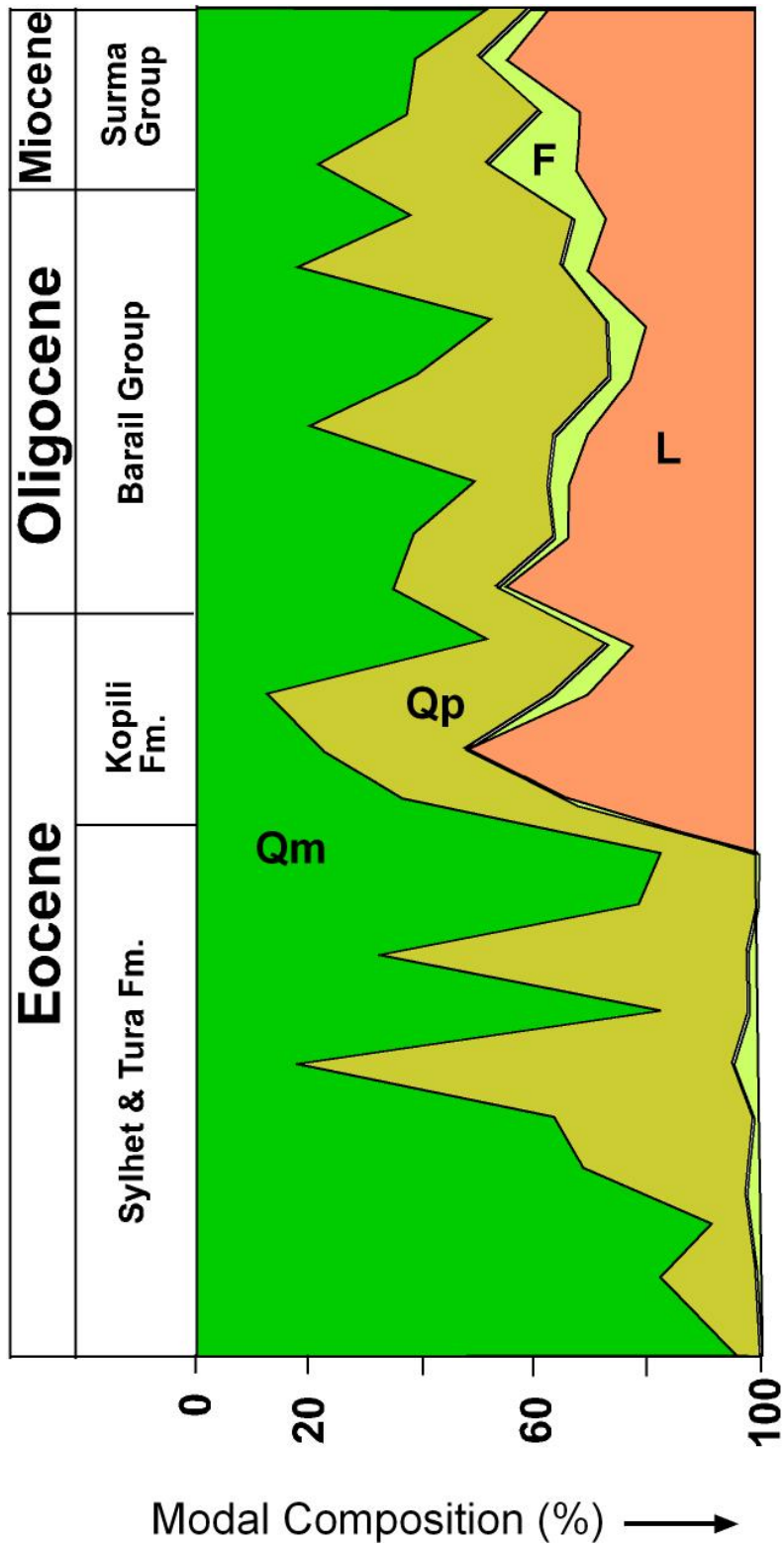
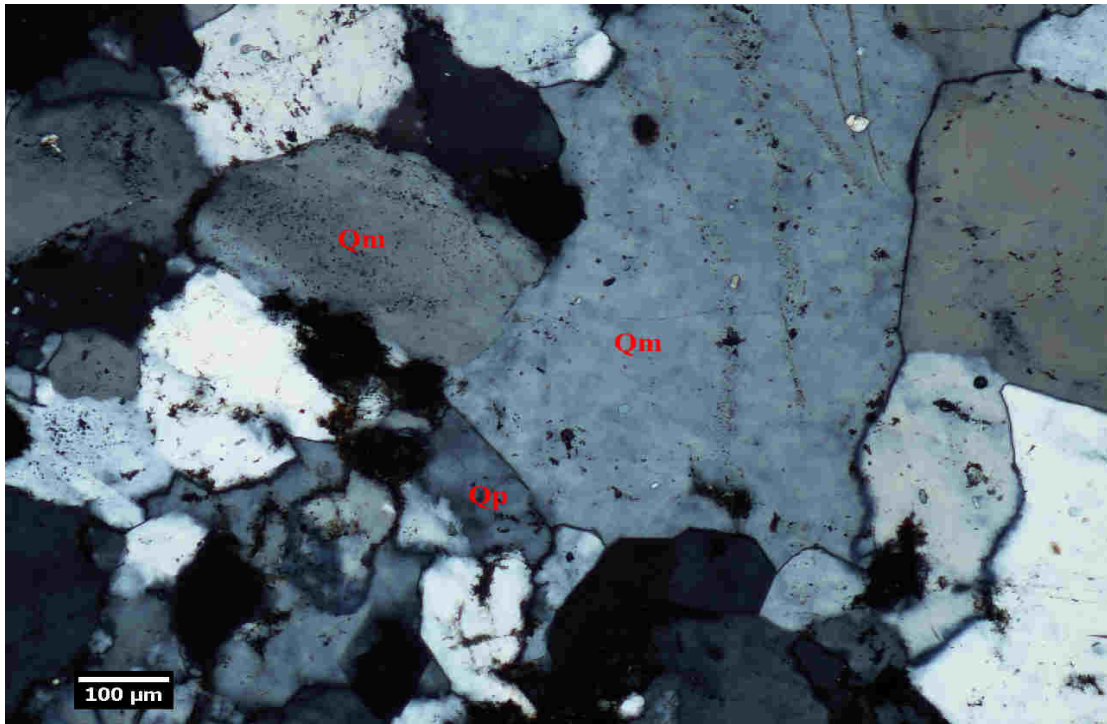
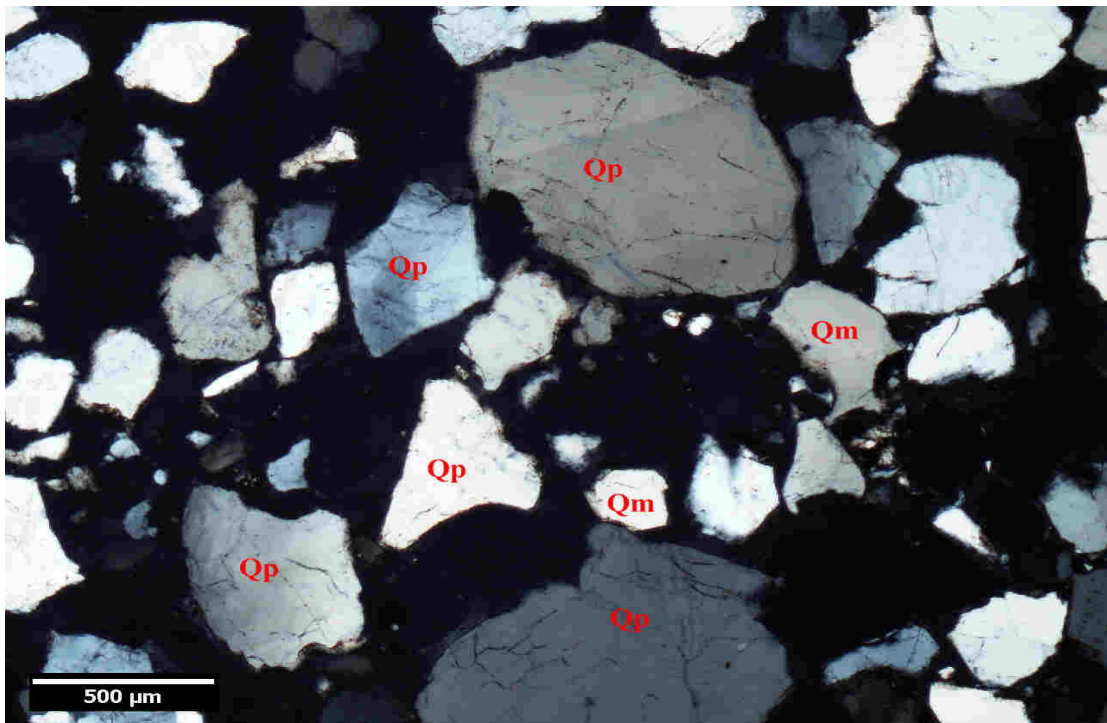


Figure 21. Vertical variation of modal mineralogical compositions of sandstone samples of the Lower Cenozoic clastic sequence from southeast of Shillong Plateau.



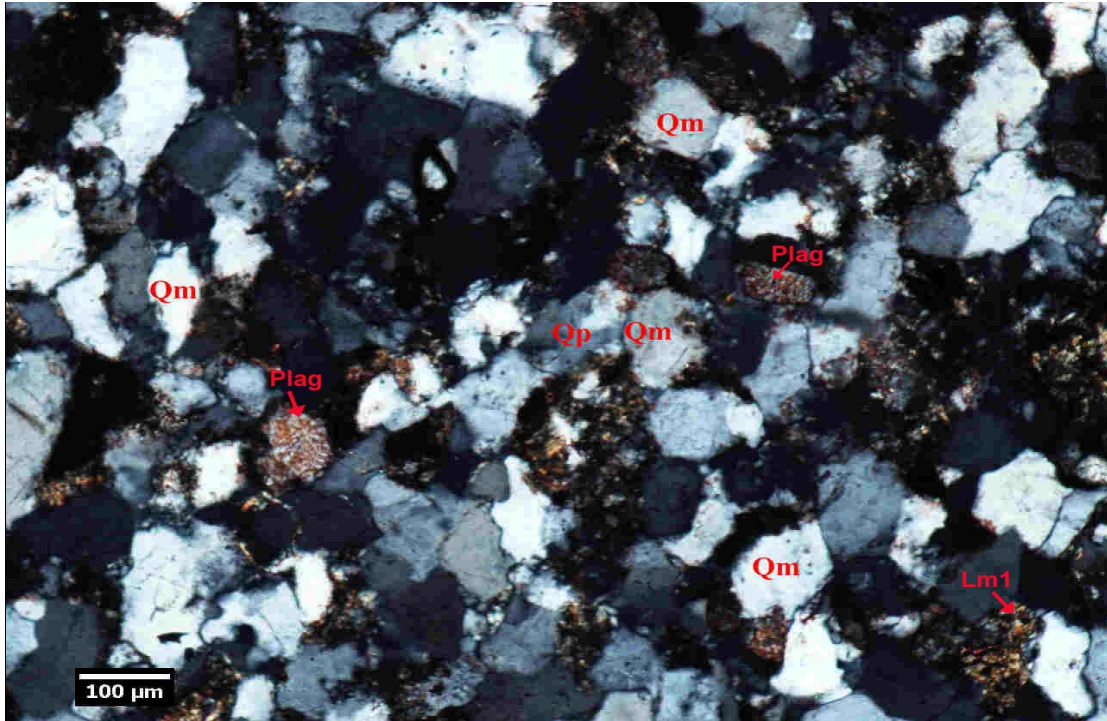
(A)



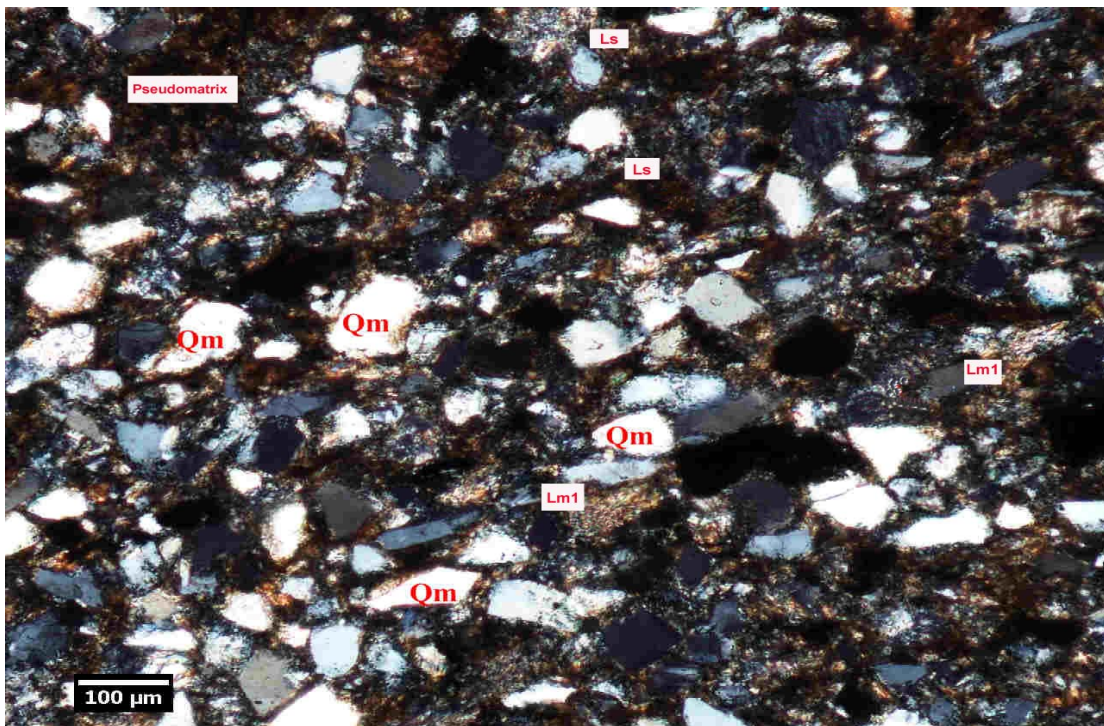
(B)

Figure 22. (A) Representative photomicrograph of highly compacted and silica-cemented Tura Sandstone of the Eocene Jaintia Group showing dominance of monocrystalline quartz (Qm). (B) Representative photomicrograph of Tura Sand of the Eocene Jaintia Group, showing higher proportion of polycrystalline quartz (Qp).





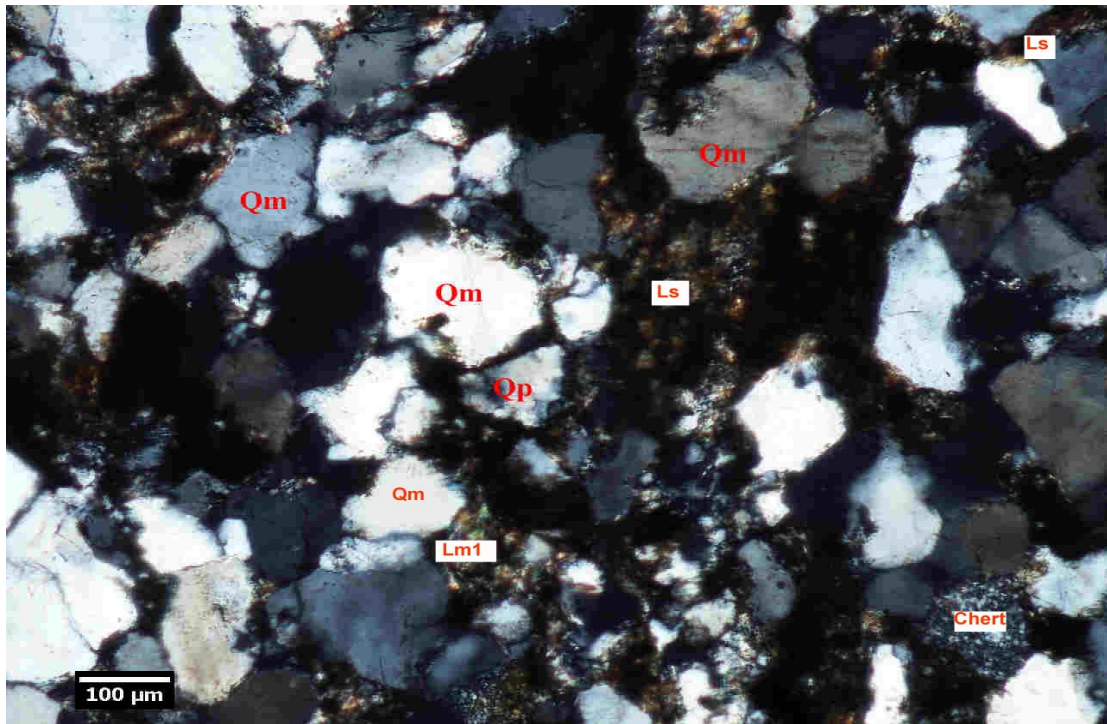
(A)



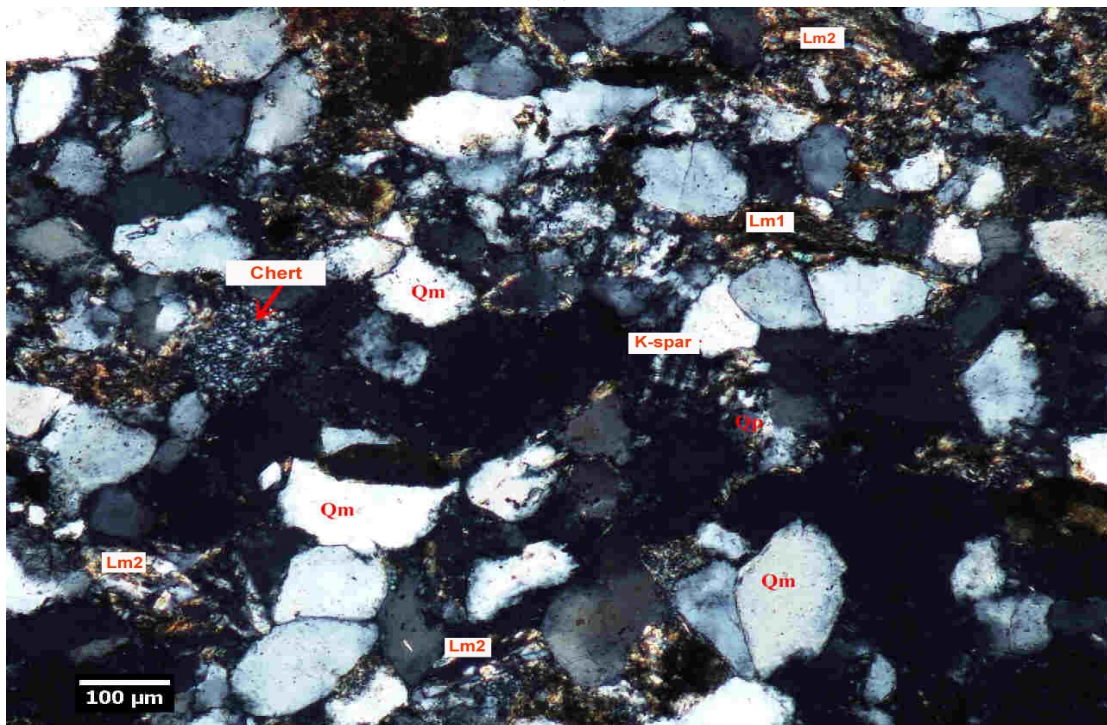
(B)

Figure 23. (A) Representative photomicrograph of Kopili Sandstone of Eocene Jaintia Group, showing very low- to low-grade metamorphic lithic fragments (Lm<sub>1</sub>). A few altered subhedral plagioclase is also seen. (B) Representative photomicrograph of Oligocene lower Barail Sandstone, showing sedimentary (Ls) and lower grade metamorphic lithic fragments (Lm<sub>1</sub>). (Plag: Plagioclase feldspars).





(A)



(B)

Figure 24. (A) Representative photomicrograph of Oligocene upper Barail Sandstone, showing various framework grains (quartz, sedimentary lithic, and metamorphic lithic) (B) Representative photomicrograph of Miocene Surma Sandstone, showing k-spar feldspar (K-spar), and metamorphic fragments (quartzite, Lm<sub>1</sub>, Lm<sub>2</sub>; quartzite = Lm<sub>1</sub>).

#### 4.4 PETROFACIES EVOLUTION AND COLLISIONAL HISTORY

Early Eocene sandstones of Sylhet and Tura formations from southeast of Shillong Plateau are quartzose, which suggests possible derivation from cratonic or mature terranes as shown by “craton interior” provenance field in QtFL diagram (Fig. 16). The Tura and Sylhet formations are considered to have been deposited in shallow marine to deltaic environments on a passive margin. Higher amount of quartz suggest mineralogical maturity. The sandstones are generally devoid of matrix; intergranular spaces are filled by quartz and iron cement. QmFLt diagrams (Fig. 17) show a shift to “recycled orogen” provenance field of Dickinson (1985) due to incorporation of Qp into the Lt pole in QmFLt diagram. These highly mature sandstones are interpreted to have been derived from the Indian craton.

Late Eocene Kopili sands are quartzolithic, suggesting an orogenic source as shown in both QtFL and QmFLt diagrams (Figs. 16 & 17). The Kopili sandstones (Figs. 16 & 17) are rich in lithic fragments and feldspars compared to the underlying formations. LsLm<sub>1</sub>Lm<sub>2</sub> plot shows that the Kopili sandstones are rich in high-grade metamorphic lithic fragments. The probable source of these sediments is considered to be the nearby Shillong Plateau. The LsLm<sub>1</sub>Lm<sub>2</sub> plot (Fig. 19) shows that the Kopili Formation has high proportions of Lm<sub>2</sub> (upper grade metamorphic lithic fragments), which can be attributed to derivation from the adjacent Shillong Plateau.

The Oligocene Barail Group is quartzolithic in composition, similar to underlying Kopili Formation. The provenance of the Barail sandstone is interpreted as “recycled orogenic” as shown in QtFL and QmFLt plots (Figs. 16 & 17). The lower part of Barail sandstone has higher quartz contents, whereas lithic fragments are dominant in upper part



of the Barail sandstone. The higher proportion of lithic fragments, similar to the underlying Kopili Formation, reflects continuous derivation from a proximal orogenic source. The QmPK plot (Fig. 18) of Barail Sandstone samples reflects a higher proportion of potassium feldspars compared to the underlying Kopili sandstones, which may indicate a granitic or gneissic source. The LsLm<sub>1</sub>Lm<sub>2</sub> plot (Fig. 19) shows that the Barail sandstone is slightly rich in Ls and Lm<sub>1</sub>, compared to the underlying Kopili sands. This could be due to a greater influx of recycled orogenic sediments from the adjacent Indo-Burma Ranges or Himalaya.

The early Miocene Surma Sandstone is also quartzolithic (Qt<sub>56</sub>F<sub>8</sub>L<sub>36</sub>). Compared to the underlying formations, Surma sandstone contains less quartz (including polycrystalline quartz), and feldspar and lithic fragments. Surma Group of sandstones falls within the “recycled orogenic” fields on QtFL and QmFLt plots (Figs. 16 & 17). Higher chert contents within this formation suggest possible derivation from pelagic units of the eastern ophiolite belt of the Indo-Burma Ranges. The QmPK plot (Fig. 18) shows that the Surma sandstones contain more potassium feldspars than the other underlying formations. This can be interpreted to reflect the unroofing of the adjacent Shillong granite-gneiss complex and Himalayan and Indo-Burma orogenic belts during the early Miocene. Higher contents of Lm<sub>2</sub> in this unit support this interpretation.

Overall, the sandstone modal analyses of lower Cenozoic strata in the area reflect the following: (1) a gradual increase in lithic fragments in stratigraphic up-section; (2) a gradual increase of potassium feldspar since the Eocene; and (3) a temporal decrease in P/F ratios.

## **CHAPTER 5: HEAVY MINERAL ANALYSIS**

### **5.1 INTRODUCTION**

Heavy minerals have specific gravity of 2.9 or more and occur in sandstones generally in less than 1 wt% (Tucker, 1988). Heavy mineral analysis is quite useful in provenance analysis of clastic sedimentary rocks (Morton, 1985; Uddin and Lundberg, 1998b). Several provenance studies have been carried out successfully in Himalayan foreland basins using heavy mineral (Sinha and Sastri, 1973; Amano and Taira, 1992; Kumar, 2004; Zahid, 2005; Najman et al., 2008). Heavy mineral assemblages closely reflect source rock composition if the sediments were deposited proximal to the source without long transportation and extensive weathering (Uddin et al., 2007a). This is one of the most widely used techniques in provenance studies, because certain suites of heavy minerals are restricted to distinct source rocks. The limitation of using heavy minerals in provenance analysis is that the composition of heavy mineral assemblages in sandstone is generally affected by processes like sediment-transport, depositional environments, and diagenesis. Certain features of heavy mineral suites, however, are inherited directly from the source area without significant modification (Morton, 1985). Heavy mineral analysis has aided in determining the nature of the source rocks, in reconstructing the routing of a paleo-fluvial systems, and in establishing relationships of source rocks (Kumar, 2004; Zahid, 2005; Rahman, 2008).

Examining suites of less common to rare minerals such as rutile, zircon, apatite, magnetite, garnet, tourmaline and others provide greater constraints on possible source

rocks because of their narrow paragenesis (Lihou and Mange-Rajetzky, 1996). Heavy mineral analysis benefits from the general chemical and mechanical stability of the minerals although variations in properties exist. To be most effective, suites of minerals with similar hydrodynamic behavior (size, shape and density) should be used (Morton, 1991).

This chapter describes an alternative approach that concentrates on relative abundances of minerals that are stable during diagenesis and have similar hydraulic behavior. In the present study, semi-quantitative analysis of heavy mineral assemblages was performed on sandstones in each of the lower Cenozoic formations southeast of the Shillong Plateau. The major objective of this study is to better constrain the source rock composition, orogenic events, and erosional history in the source area. This study also attempts to recognize dominant varieties of mineral groups in Eocene-Lower Miocene sequences, and identifies index minerals for those stratigraphic horizons.

## **5.2 METHODS**

Heavy minerals were separated from 20 sand and sandstone samples. Fourteen of these samples were selected for study. Five samples are from the Eocene Jaintia Group, five are from the Oligocene Barail Group, and four are from Miocene Surma Group.

Several steps were followed to separate the heavy minerals (Mange and Maurer, 1992). First, sand grains in sandstone and loose sand were disintegrated. The very fine- to fine-grained sand fraction (63-250  $\mu\text{m}$ ) was selected because they generally contain the highest concentrations of heavy minerals. For routine point-count studies, the 2-3 phi fractions (fine sand) were used because the grains were easier to identify under a

petrographic microscope. Fine and very fine sands were treated with HCL and H<sub>2</sub>O<sub>2</sub> to eliminate carbonate grains and organic matter.

Heavy minerals were separated using a high-density liquid, tetrabromoethane (Br<sub>2</sub>CHCHBr<sub>2</sub>, density 2.89 gm/cc) through a gravity settling process. Nearly 15 hours were allowed to settle the entire heavy minerals to the bottom of the funnel above the pinch clip. Afterwards, the stopcock was opened slowly, and heavy fractions were allowed to pour into filter paper in the lower funnel. The stop cock was then closed immediately to leave a layer of clear liquid below the lighter fraction. The light fraction was then drained into a new funnel. Both fractions were washed thoroughly with acetone and put into the oven for drying.

Identification of heavy minerals was made convenient by grouping them into different magnetic fractions. The 2-3 phi fractions were separated into low, medium, and high (0.4, 0.8, and 1.2 ampere) magnetic fractions based on mass magnetic susceptibility using a Frantz magnetometer at the Department of Geology and Geography, Auburn University. The 0.4-ampere magnetic group at slide slope of 20° separates illmenite, garnet, olivine, chromite, and chloritoid. The 0.8-ampere group at 20° slide slope isolates hornblende, hypersthene, augite, actinolite, staurolite, epidote, biotite, chlorite, and tourmaline (dark). The 1.2-ampere group at slide slope of 20° separates diopside, tremolite, enstatite, spinel, staurolite (light), muscovite, zoisite, clinozoisite, and tourmaline (light). At a slide slope of 5°, the magnetic fraction at 1.2-ampere includes sphene, leucosene, apatite, andalusite, monazite, and xenotime.

Slide mounts were prepared with the magnetically defined heavy-mineral separates by sprinkling mineral grains (usually more than 300) onto a slide in a drop of

oil with a refractive index of 1.550. All mineral identifications were carried out with a petrographic microscope using a modification of the Fleet method (Fleet, 1926), in which nearly all grains on each microscope slide were counted. Identified grains from each magnetically separated fraction were then added together to calculate frequency percentage of heavy minerals present in the 2-3 phi size fractions for all slides.

### **5.3 RESULTS**

Semi-quantitative point-counting results of heavy minerals in sandstones from the study area are presented in Table 4. Total heavy mineral contents vary from 0.07% to 0.95%. In Eocene Jaintia Group, weight percent of heavy mineral ranges from 0.07 % to 0.4%. The Oligocene Barail Group is comparatively rich in heavy minerals, with contents ranging from 0.15% to 0.95%. In the uppermost Surma sandstones, heavy mineral contents range from 0.08% to 0.3% (Fig. 25).

Heavy mineral assemblages in Eocene Jaintia Sandstone are dominated by opaque minerals (Fig. 26). In terms of non-opaque minerals, Eocene Jaintia Group is very rich in ultrastable heavy minerals, excluding garnet (Figs. 27A & B). In some samples, subangular to subrounded rutile grains are bound together by silica cement. The ZTR (zircon, rutile and tourmaline) index for the Eocene Jaintia sandstones is very higher than that of the other units (28.35%; Fig. 26) and indicates high compositional maturity. Higher maturity index suggests long transportation of detritus from the source area. Absence of garnet can be explained either as loss of garnet during transportation and diagenesis, or low influx of garnet to the basin from the source area. Zircon grains are colorless, prismatic to well-rounded and sometime show zoning. Tourmaline grains are strongly pleochroic and exhibit variable morphologies (e.g., irregular, prismatic, rounded;

Fig. 27B). Morphologic variations of tourmaline grains suggest a range of source rocks and/or transport paths.

The average opaque content in the Oligocene sandstones is 49.6%, less than those of the underlying Jaintia Group. The ZTR index of 23.83% in Barail sandstones is quite less than the Jaintia sandstones (Fig. 26). The Barail sandstones also contain a more diverse assemblages of heavy minerals (Fig. 28A) compared to the Jaintia sandstones. Amphibole, chrome-spinel, garnet, biotite-muscovite, chlorite-chloritoid and serpentine are more abundant than in the underlying unit. The low ZTR index and presence of unstable heavy minerals suggest rapid and deep erosion in the source area, limited transport, and rapid deposition of the sediments.

In the uppermost unit (Surma sandstones), the average opaque mineral content is 30.50% and the ZTR index is 18.34% (Fig. 26). Some unstable heavy minerals (e.g., amphibole, chrome-spinel, chlorite-chloritoid, and serpentine) are much higher in Surma Group sandstones (Fig. 28B). Figures 29A & B show the occurrence of subangular to prismatic chrome-spinel grains in Surma sandstones. In some samples, biotite altering into chlorite is also seen. This may indicate retrograde metamorphism in the source area. Overall, Surma sediments have lowest ZTR index indicating compositional immaturity. The low maturity index and presence of higher percentages of unstable heavy minerals suggest that the transportation route was very short and that the orogenic front was in close proximity during Surma deposition.

Table. 4 Normalized abundances of heavy minerals from southeast of Shillong Plateau, India (ZTR= (Zircon-tourmaline-rutile/Total Heavy)×100).

	Eocene Jaintia Group		Oligocene Barail Group		Micocene Surma Group	
	N= 5	%	N= 5	%	N= 4	%
Opaque	149	66.60	103	49.60	67	30.50
Non opaque						
Zircon	17	26.52	10	9.12	8	5.19
Rutile	12	17.13	20	20.46	13	8.46
Tourmaline	34	43.63	20	17.80	19	12.68
Amphibole	0	0.00	6	5.36	12	7.79
Chrome-spinel	1	0.89	6	5.77	18	12.23
Garnet	0	0.00	11	9.96	3	1.68
Biotite & muscovite	0	0.00	7	7.44	14	8.95
Staurolite	3	2.67	0	0.00	1	0.45
Apatite	0	0.00	4	3.78	8	5.43
Chlorite & Chloritoid	0	0.00	6	6.27	37	24.10
Serpentine	0	0.00	8	7.44	15	9.79
Others	7	9.17	7	6.61	5	3.26
Total Non-opaque	74	100.00	105	100.00	152	100
ZTR %		28.35		23.83		18.34

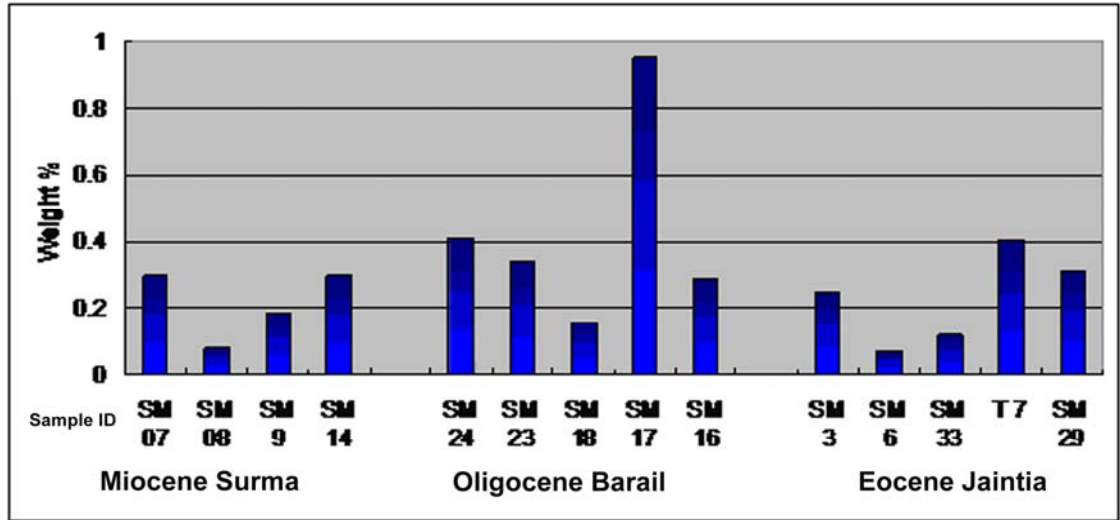


Figure 25. Heavy mineral occurrence (weight percent) in different stratigraphic units from the study area.

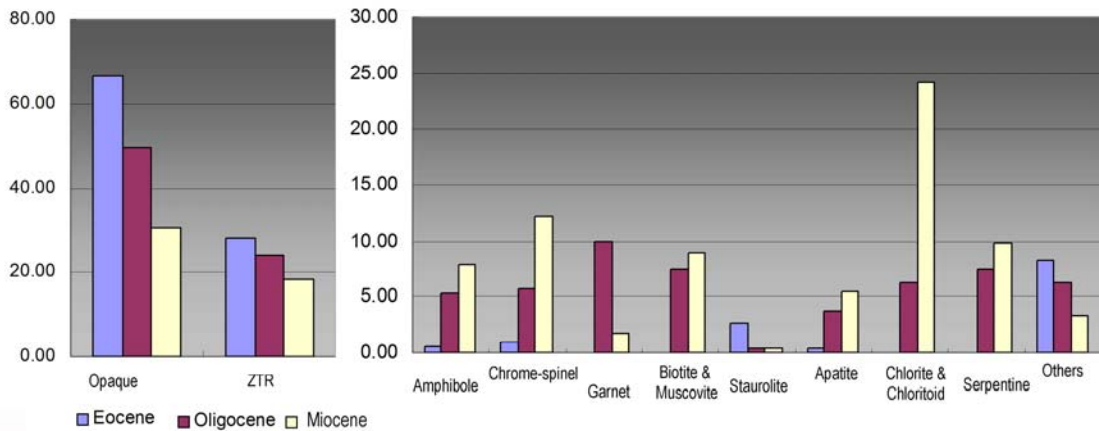
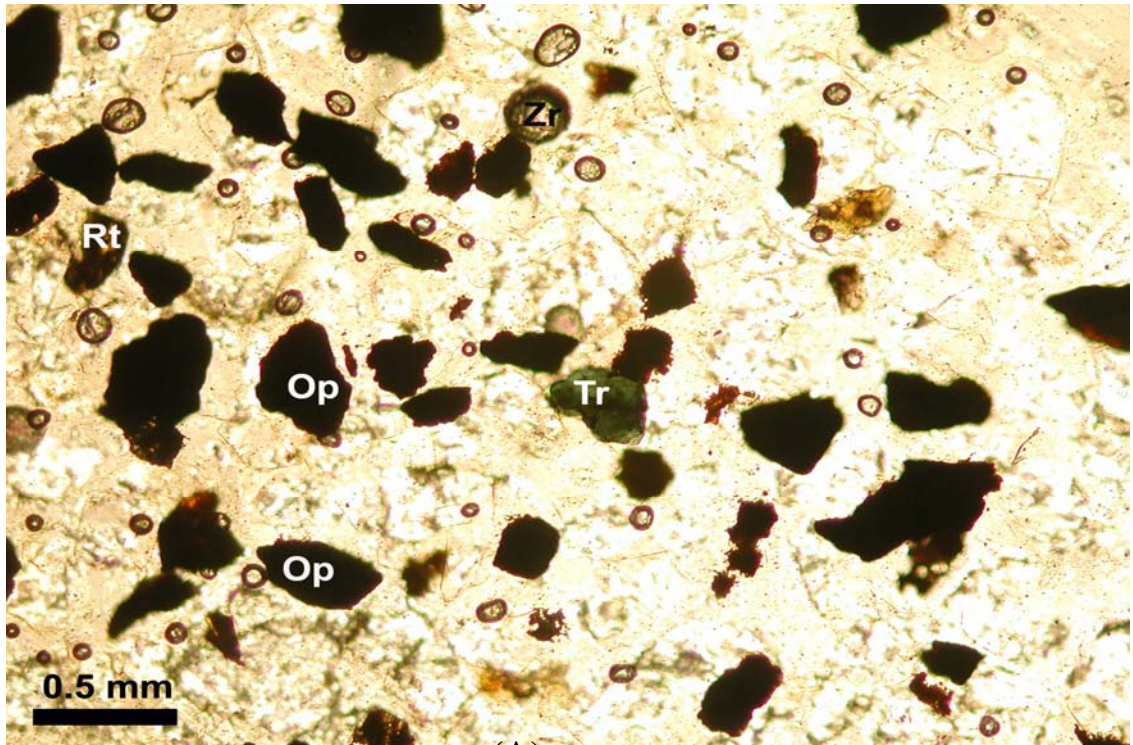


Figure 26. Heavy mineral distribution of Eocene, Oligocene, and Miocene sandstones from the study area.





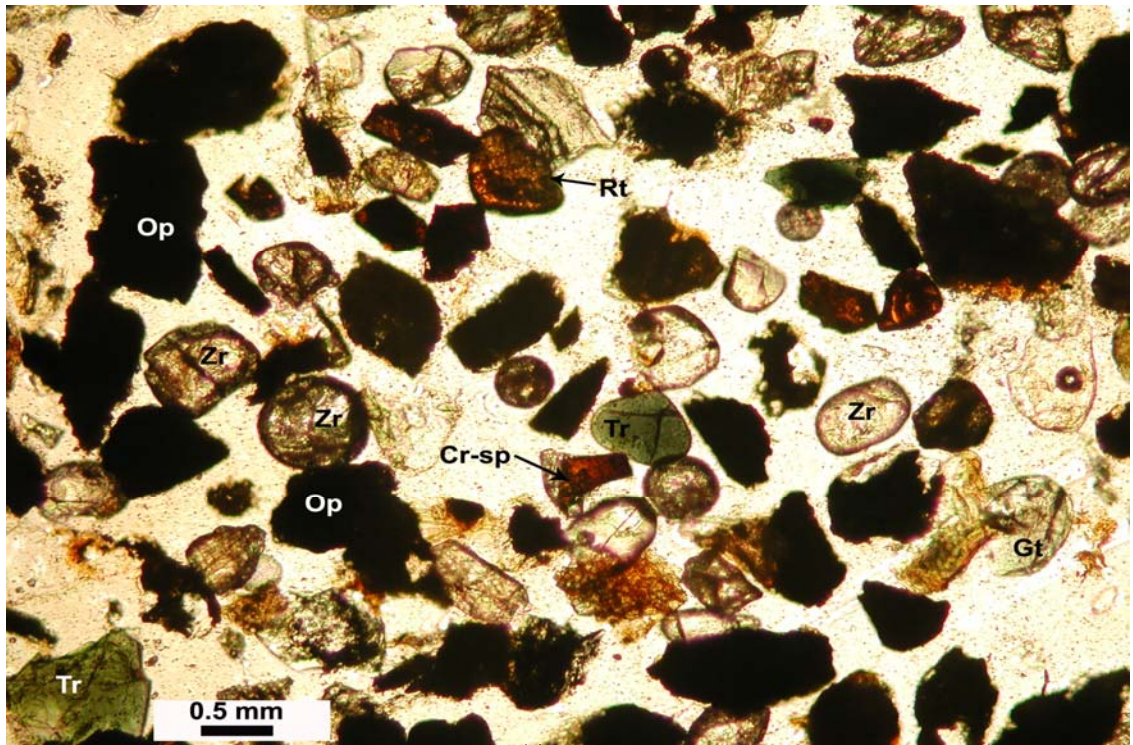
(A)



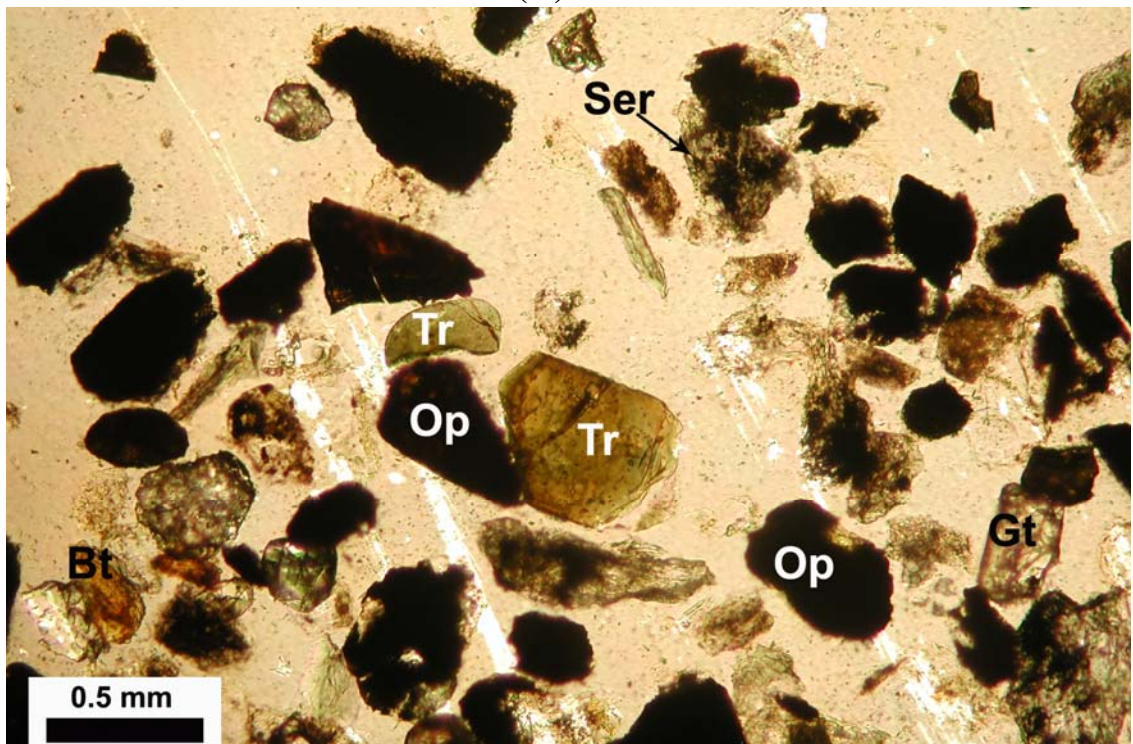
(B)

Figure 27 (A). Representative photomicrograph of heavy minerals from Jaintia Group sandstone. (B). Well rounded tourmaline grain from upper Jaintia Group sandstone (Kopili Formation) indicating recycling of sediments (Op=opaque; Tr-tourmaline; Rt-Rutile; Zr-zircon).





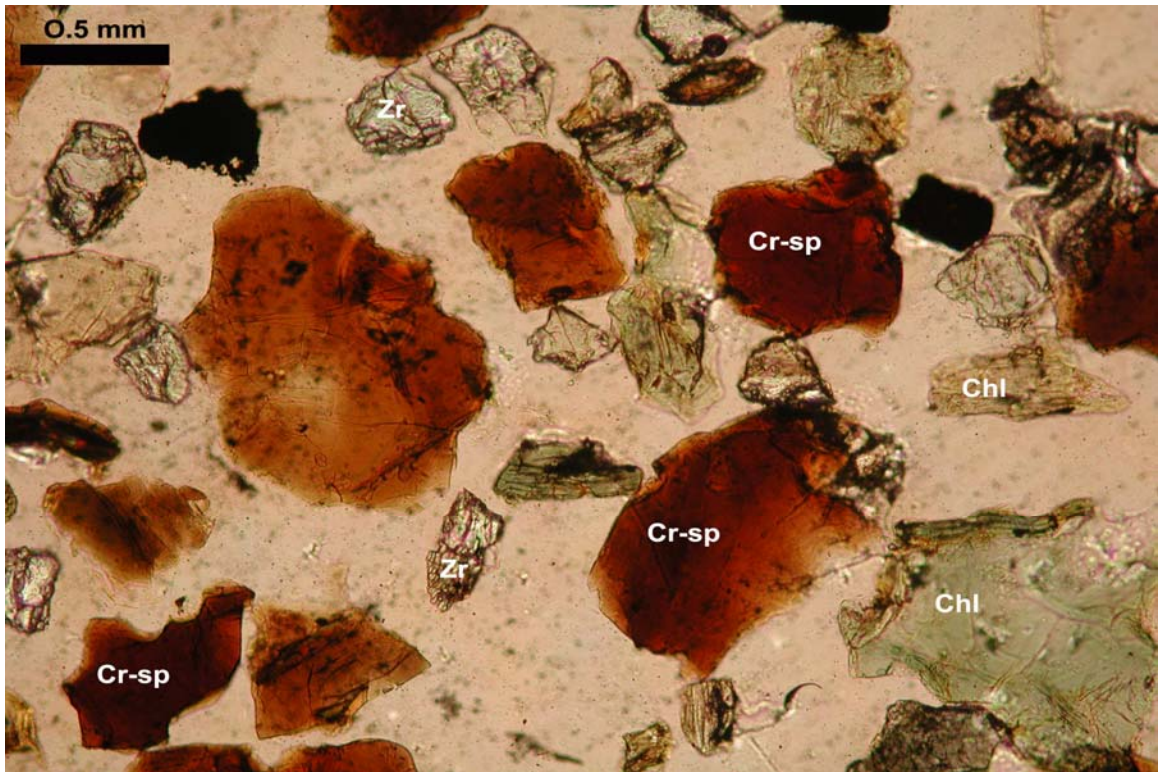
(A)



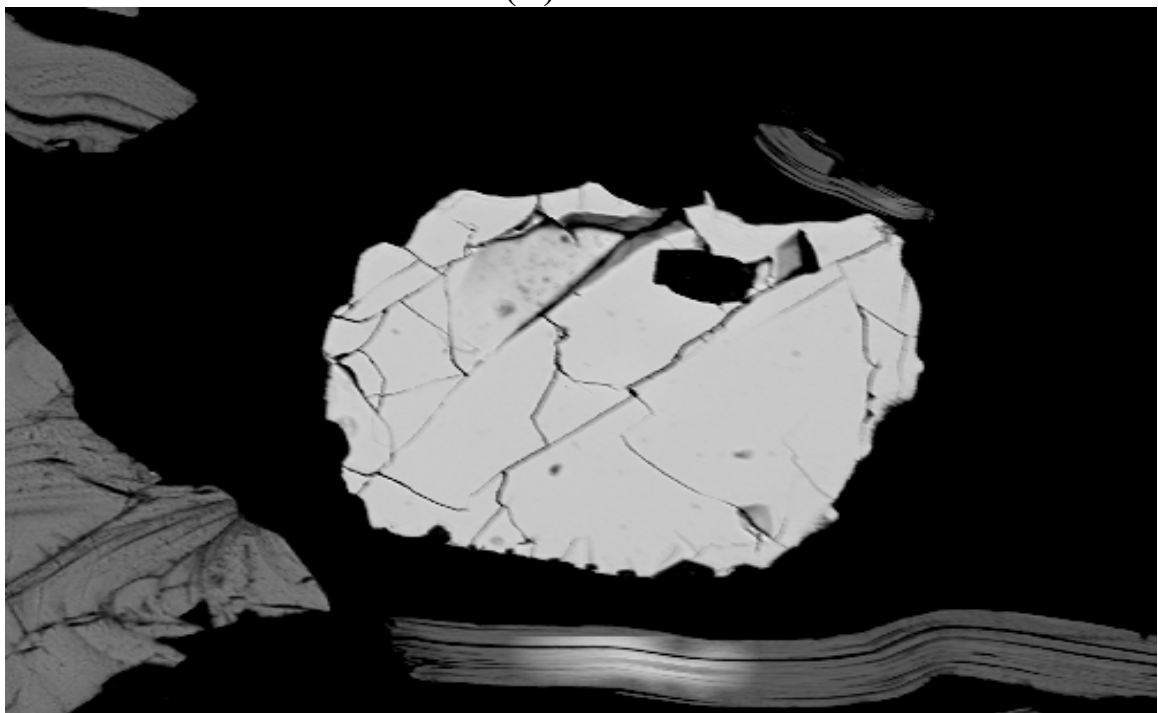
(B)

Figure 28. Representative photomicrograph of heavy minerals in sandstones from the (A) Barail Group and (B) Surma Group (Op= Opaque; Tr= tourmaline; Ser= serpentine; Gt= garnet; Rt= rutile; Zr= Zircon; and Cr-sp= chrome-spinel).





(A)



BEI SM-8 Cr-Spinel

(B)

Figure 29. (A) Abundance of chrome-spinel and chlorite grains in Surma sandstone (Chl=chlorite; Zr= Zircon; and Cr-sp= chrome-spinel). (B) Backscattered scanning electron images of chrome spinel from same sample.

## 5.4 PROVENANCE HISTORY

Semi-quantitative analysis of heavy mineral assemblages indicates the nature of source rocks from which they have derived. In the study area, the abundance of the opaque and the ZTR index progressively decrease and the abundance of unstable heavy minerals increase up section (Fig. 26). The gradual increase of ZTR index and decrease of abundance of heavy minerals suggest a change in sedimentation patterns. The high ZTR contents of Eocene Jaintia Group suggest long transport histories where as the very low ZTR index in Surma sandstone suggests deposition close to the orogenic front. The presence of well rounded tourmaline and zircon grains in Barail and Surma sandstones reflect the origination of sediments from a recycled orogenic source. Presence of chrome-spinel and serpentine suggest input from ultramafic sources. These two mafic minerals are commonly found in Miocene sandstones indicating an uplifted and eroded ultramafic source during the Miocene. Presence of chlorite and biotite indicate low-grade metamorphic source terranes for the Miocene units.

## **CHAPTER 6: MICROPROBE ANALYSIS**

### **6.1 INTRODUCTION**

Heavy minerals have been used to study the provenance of clastic sequences using systematic point-count analysis. An obvious weakness of determining the provenance from conventional point-count methods is the lack of geochemical data linking sediments to possible source rocks. The chemical composition of a number of heavy minerals can be used as indicators of provenance. Although the chemistry of such heavy minerals varies enough to be of petrogenetic significance, density and stability remain relatively homogenous within each mineral species. Thus, varieties of key mineral that are present in a sedimentary sequence are independent of influences such as hydrodynamic sorting and diagenesis (Hallsworth and Chisholm, 2000; Kumar, 2004). Tracing the provenance using mineral chemistry is most effective for minerals in which compositional variability reflects relatively narrow environments formation.

The recent advent of readily available microanalysis equipment, such as the electron microprobe, has enabled varietal studies to be carried out on the basis of single-grain geochemical analysis. This has considerable advantages over optical methods of varietal studies, because it provides objective numerical data that can be treated with considerably more confidence and because it provides a basis for direct comparison with source-rock mineralogy. The method can be applied to a wide variety of detrital heavy minerals, both translucent (Morton, 1991) and opaque (Basu

and Molinaroli, 1991), because many species show some degree of compositional variation (Morton and Hallsworth, 1994).

The purpose of this chapter is to trace the provenance of the Lower Cenozoic clastic sequences deposited at southeast of Shillong Plateau using mineral chemistry data from selected heavy minerals (e.g., tourmaline, chrome-spinel, and garnet). Specifically, mineral chemistry was employed in attempts to evaluate the relative contributions of detrital sediments from the Himalaya and Indo-Burma Ranges.

## **6.2 MINERAL CHEMISTRY**

Three mineral species – tourmaline, chrome-spinel, and garnet were chosen for this study. Both tourmaline and chrome-spinel are abundant in the study area. Tourmaline is a complex borosilicate with a considerable range of composition. Its general formula is  $XY_3(T_6O_{18})(BO_3)_3V_3W$  (Hawthorne et al., 1993). The X site may be occupied by Na, Ca or possibly by K, but can be largely vacant. The Y site is occupied by  $Li^{1+}$ ,  $Mg^{2+}$ ,  $Fe^{2+}$ ,  $Mn^{2+}$ ,  $Al^{3+}$ ,  $Cr^{3+}$ ,  $V^{3+}$ ,  $Fe^{3+}$  or  $Ti^{4+}$ . The T site is usually occupied by Si, occasionally by Al, and possibly by B. The V site contains  $OH^{1-}$ , and  $O^{2-}$ . The wide range of tourmaline compositions makes tourmaline an ideal mineral to use for geochemical discrimination of provenance. Henry and Guidotti (1985) and Henry and Dutrow (1992) demonstrated that tourmaline geochemistry reflects the local environment in which the mineral was developed. Ternary plots, Al- $Fe_{total}$ -Mg, Ca- $Fe_{total}$ -Mg, can discriminate tourmalines from a wide range of rock types. Moreover, as tourmaline is stable in both weathering and diagenetic environments (Morton, 1991; Morton and Hallsworth, 2007), tourmaline analysis can be used on

any sandstone irrespective of the extent to which its grains have been modified during the sedimentary cycle. Several studies using tourmaline grains have been carried out successfully for provenance analysis in various parts of the world. For example, tourmaline proved useful to constrain the provenance of Jurassic sandstone in Slovakia (Aubrecht and Kristin, 1995), Jurassic to Cretaceous sandstone of Papua New Guinea (Morton et al., 2000), lower Cenozoic sandstones of the Bengal Basin (Zahid, 2005), and modern sand of Black Hills, South Dakota (Viator, 2003).

Chrome-spinel  $[(\text{Mg}, \text{Fe}^{2+})(\text{Cr}, \text{Al}, \text{Fe}^{2+})_2\text{O}_4]$  is a ubiquitous accessory mineral in ultramafic and mafic rocks. It is considered as a petrogenetic indicator because its chemistry is extremely sensitive to bulk rock composition and petrogenesis of the host rock. The principal constituents of chrome-spinel, Cr and Mg, are compatible elements with respect to the solid phase, whereas Al is incompatible and is strongly partitioned into melt. Partitioning of Mg and  $\text{Fe}^{2+}$  between spinel, silicate melts, and minerals is strongly temperature dependent (Irvine, 1977; Hisada et al., 1999). The ratio of these cations change according to the physicochemical conditions and equilibrium temperature, and can reveal the petrogenetic signature of the geodynamic setting in which the chrome-spinel was formed. For graphical evaluation, cation ratios are calculated as  $\text{Cr}\# = \text{Cr}/(\text{Cr} + \text{Al})$  and  $\text{Mg}\# = \text{Mg}/(\text{Mg} + \text{Fe}^{2+})$  and plotted as bivariate plots (Dick and Bullen, 1984; Barnes and Roeder, 2001). Ternary plots of trivalent cations,  $\text{Cr}^{3+}$ ,  $\text{Al}^{3+}$  and  $\text{Fe}^{3+}$  delineate different types of ophiolitic and ultramafic sources (Barnes and Roeder, 2001). Detrital chrome-spinels fingerprint Cenozoic sediment provenances and previously used to understand tectonic settings in the study region (Kumar, 2004; Zahid, 2005; Rahman, 2008).

Garnet geochemistry also is a widely used tool for determination and discrimination of sediment provenance for several reasons. First, it is a common component in many heavy mineral assemblages. Second, it is relatively stable under burial diagenesis and weathering (Morton, 1991; Morton and Hallsworth, 2007). Third, garnet has a wide range of composition that reflect source rocks. Garnet is especially interesting in that it varies not only by bulk composition (protolith), but also reflects P and T conditions during the formation of both igneous and metamorphic rocks. The general formula for common garnet is  $(\text{Mg}, \text{Fe}^{2+}, \text{Mn}, \text{Ca})_3(\text{Al}, \text{Cr}, \text{Ti}, \text{Fe}^{3+})_2\text{Si}_3\text{O}_{12}$ , but there are several possible substitutions (Deer et., 1997). Garnet falls into two isomorphous series: pyrospite  $[(\text{Mg}, \text{Fe}^{2+}, \text{Mn})_3\text{Al}_2\text{Si}_3\text{O}_{12}]$  and ugrandite  $[\text{Ca}_3(\text{Al}, \text{Cr}, \text{Ti}, \text{Fe}^{3+})_2\text{Si}_3\text{O}_{12}]$ . Significant occupation of the octahedral site by cations other than  $\text{Al}^{3+}$  (i.e.,  $\text{Cr}^{3+}$ ,  $\text{Fe}^{3+}$ ) is used in constraining the chemical conditions of crystallization. Garnet chemistry has been used to evaluate provenance in a number of studies (Yokoyama et al., 1990; Morton and Taylor, 1991; Zahid, 2005). Garnets however, are relatively rare in the stratigraphic units of the study area.

## **6.3 METHODS**

### **6.3.1 Sample Separation**

All samples were sieved into whole-phi fractions; the 2-3 and 3-4 phi fractions were used for this study. Highly magnetic fractions were removed from the heavy-mineral separates using hand held magnets and a Franz magnetic separator. The remaining "heavy" fraction was divided further into three to four groups using a Franz magnetic separator, with the aim of concentrating the mineral species that



would be analyzed with electron microprobe. Slides were prepared by drilling 1/8" holes in 1.5" X 0.75" Plexiglas sheets, pouring grains from each magnetic sub-fraction (low, medium to high magnetic susceptibility) into different holes, and then setting them with epoxy. The Plexiglas sheets were then mounted on glass slides, ground to standard optical thickness of 30 micrometers, and polished for microprobe analysis. Before the samples were put into the microprobe sample chamber, electrically non-conductive samples were carbon-coated to ensure conduction. Standards and samples were coated to the same thickness. Carbon coating was carried out by carbon evaporation under vacuum. A polished brass block was used to monitor the thickness of the carbon coat. As the thickness of coat increases on the brass, it changes color from orange (150 Å) to indigo red (200 Å), then to blue (250 Å), and then to bluish green (300 Å).

### **6.3.2 The Electron Microprobe**

The electron microprobe provides a complete micron-scale quantitative chemical analysis of inorganic solids. The method is nondestructive and utilizes 63 characteristic x-rays excited by an electron beam incident on a flat surface of the sample. In the electron microprobe, x-rays are emitted by the sample in response to a finely focused electron beam incident on the sample at a right angle. Some of the beam electrons are scattered backward. The backscattered electrons, as well as the characteristic x-rays of the elements, carry information about chemical composition. Backscattered electrons results from multiple elastic scattering and have energies between 0 and  $E_0$  (the beam energy). Secondary electrons, which are specimen electrons mobilized by the beam through inelastic scattering, have energies in the

range of 0-50 eV with a most probable energy of 3-5 eV. Because of energy differences between backscattered, characteristic X-rays, and secondary electrons, different detector setups are required for the detection of the three types of electron signal.

The electron microprobe serves two purposes: (1) it provides a complete quantitative chemical analysis of microscopic volumes of solid materials through x-ray emission spectral analysis; and (2) it provides high-resolution scanning electron and scanning x-ray (concentration) maps. There are two types of scanning electron images: backscattered electron (BSE) images, which show compositional contrast; and secondary electron (SE) images, which show enhanced surface and topographic features. Scanning-cathodoluminescence images form by light emission in response to the interaction between the scanning electron beam and the sample.

This study employed a JEOL JXA 8600 microprobe housed at the University of Georgia microprobe lab and under the supervision of Mr. Chris Fleisher. This microprobe is equipped with Geller Micro analytical laboratory dQANT automation. Analyses were done using a 64 accelerating voltage of 15 K.V. and a beam current of 15 nanno amps. Both natural and synthetic standards were used to calibrate the data. A PRZ metric correction was used.

**Standard intensity calibration:** Standard x-ray intensities of the elements to be measured were obtained on appropriately chosen standards. Different standards were used for different elements. Secondary standards were analyzed as unknowns to check if their known compositions are reproduced. The analytical conditions (e.g., accelerating voltage, beam current, etc.) were maintained throughout the session.

Table 5 lists the standards that have been used for this analysis. Most of them come from the C. M. Taylor Corp. The USNM standards come from the National Museum of Natural History, a branch of the Smithsonian Institution. This study used two synthetic standards obtained from the University of Oregon microprobe lab, and an almandine standard obtained from the Harvard Mineral Museum. Calibration for each analysis session was checked using the Kakanui Hornblende (USNM) and Pryope #39 (C. M. Taylor) standards.

## **6.4 RESULTS**

A total of 39 heavy mineral grains on 11 slides were analyzed (23 tourmalines, 11 chrome-spinel, and 5 garnets) Analyzed grains were scanned thoroughly by EDAX and those the three mineral species were analyzed for chemical composition. One spot analysis per grain was conducted. Results are provided in appendices A-D, and summarized below.

Table 5. Electron microprobe standards used in this study.

<b>Electron Microprobe Standards</b>			
<b>Element</b>	<b>Standard</b>	<b>Source</b>	<b>Comment</b>
Cr	Chromite #5	C M Taylor Corp	
Mn	Spessartine #4b	C M Taylor Corp	
TiO <sub>2</sub>	Rutile	C M Taylor Corp	
Ca	Sphene #1A	C M Taylor Corp	
Fe	Hematite #2	C M Taylor Corp	Used for oxide (spinel) analyses
Fe	Syn. Fayalite Ol-11	Univ. of Oregon	Used for silicate analyses
Ni	Ni metal	C M Taylor Corp	
Si	Diopside 5A	C M Taylor Corp	Si standard for all phases except garnet
Mg	Olivine #1	C M Taylor Corp	
Al	Syn. Spinel	C M Taylor Corp	
K	Orthoclase MAD-10	C M Taylor Corp	
Na	Ameila Albite	USNM	This is a ubiquitous Na standard
Si standard #112140	Almandine	Harvard Mineral Museum oxygen	Si standard for garnet analyses
F	Syn. Fluoro-Phlogopite	University of Oregon M-6)	
Cl	Scapolite	USNM R 6600-1	

### 6.4.1 Tourmaline

Fourteen tourmaline end-members have been officially recognized by the International Mineralogical Association (IMA). Many of the IMA recognized tourmaline species exhibit partial to complete solid solution among each other (Henry and Dutrow, 1992). Three of the most common alkali species exist in two solid solution series: schorl – dravite and schorl – elbaite. The schorl – dravite series is continuous between  ${}^Y\text{Mg}^{2+}_3$  and  ${}^Y\text{Fe}^{2+}_3$ . The schorl – elbaite series is continuous between  ${}^Y\text{Fe}^{2+}_3$  and  ${}^Y\text{Li}_{1.5}\text{Al}_{1.5}$ . However, there is a miscibility gap between dravite and elbaite (Deer et al., 1992). Other species are of more restricted paragenesis but have minor solid solution.

Most detrital tourmalines from the study area have compositions characteristic of the schorl-dravite series, although a few Oligocene sample falls outside this series (Fig. 30). Analyzed tourmalines fall in Alkali groups (Fig. 31), where the X site is primarily filled with Na, but significant levels of Ca and/or vacancy can be present. Plotted on Henry and Guidotti's (1985) Al-Fe(tot)-Mg environmental diagram (Fig. 32), the majority of the tourmalines cluster in field 4, which corresponds to metapelites coexisting with an Al-saturating phase. A few younger Miocene samples cluster in field 2, linked to Li-poor granitoids and associated pegmatites and aplites. The Ca-Fe(tot)-Mg ternary plots (Fig. 33) show that these tourmalines fall in field 4, which indicates the source for majority of the grains are Ca-poor metapelites, metapsammites, and quartz-tourmaline rocks. Very few grains plotted in the field associated with Li-poor granitoids and associated pegmatites and aplites. Tourmaline samples from the area are rich in Fe-Mg, compared to Ca. Therefore, these

tourmalines may have been derived from recycled metasedimentary rocks from adjacent orogenic belts that contain metasedimentary rocks. Alternatively, they could have been derived from any rocks of the Shillong Group. Rounding of some tourmaline grains, however, suggests derivation from a more distal source.

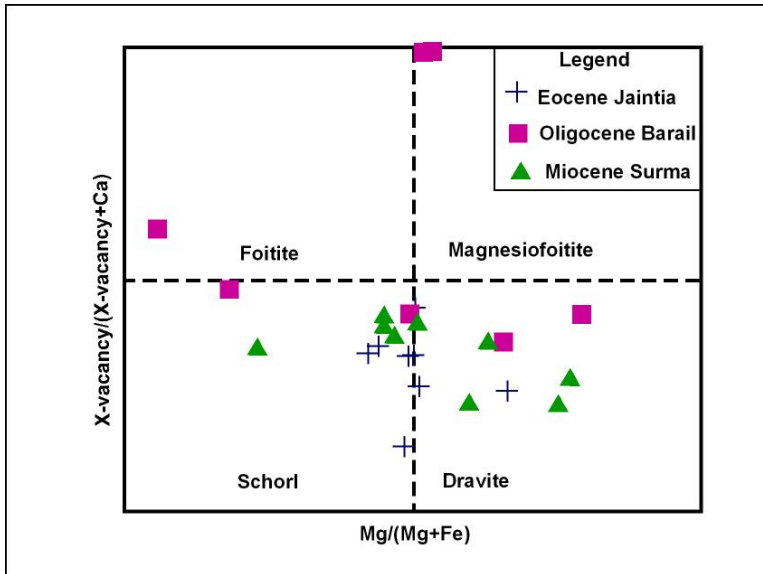
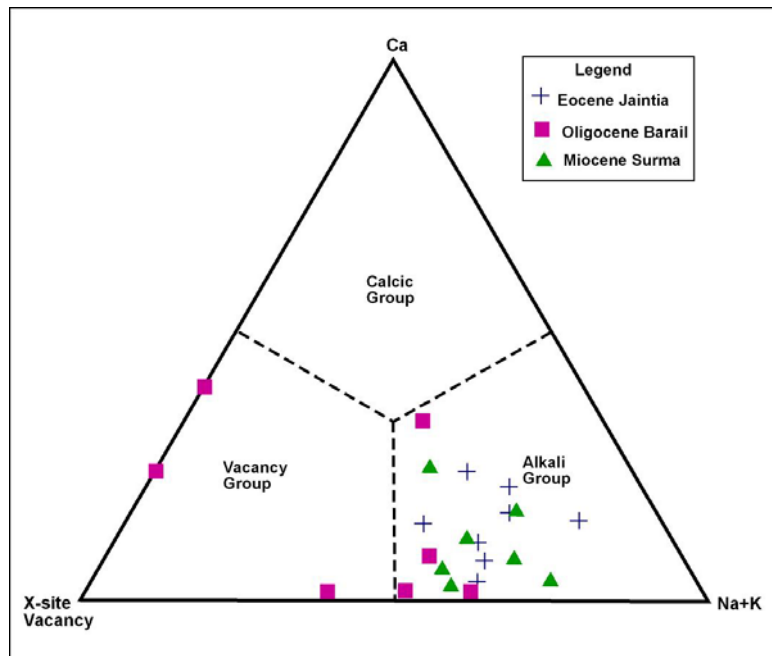


Figure 30. Classification of detrital tourmalines from southeast of Shillong Plateau

Figure 31. Detrital tourmalines plotted on X-site occupancy diagram.



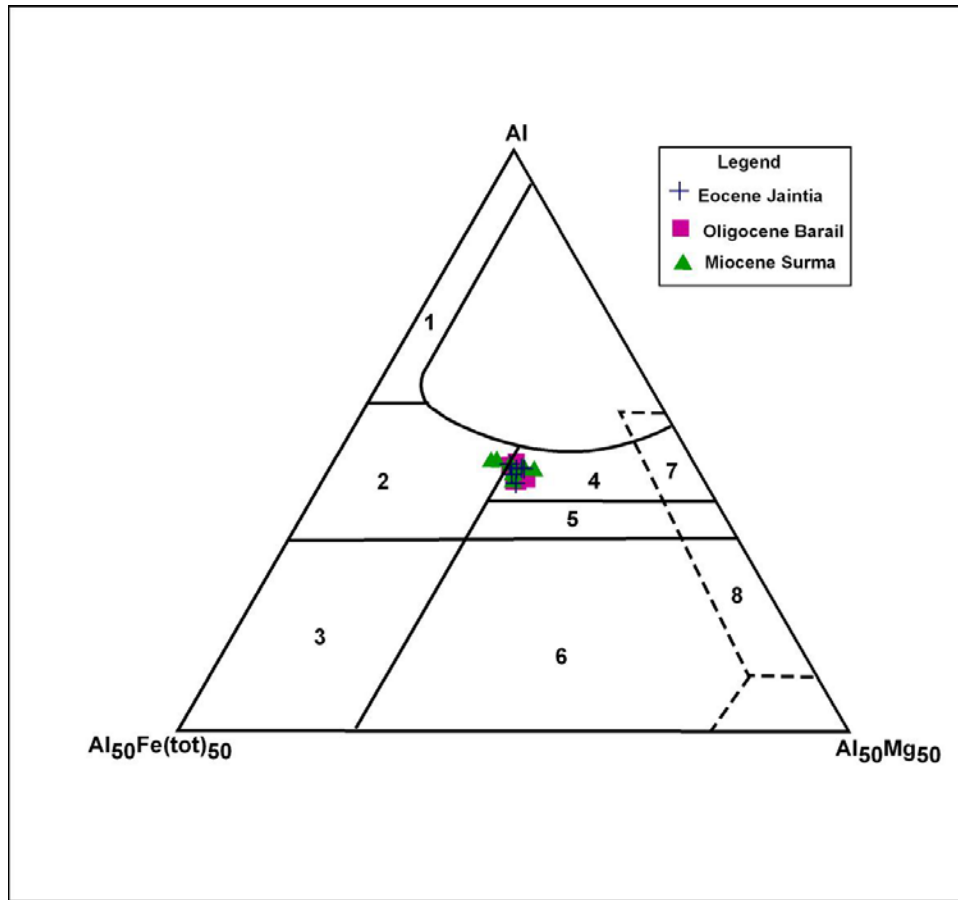


Figure 32. Al-Fe(tot)-Mg plot (in molecular proportion) of tourmalines from southeast of Shillong plateau. Fe(tot) represents the total iron in the tourmaline. Several end members are plotted for reference. Numbered fields correspond to the following rock types: (1) Li-rich granitoid, pegmatites, and aplites, (2) Li-poor granitoids and associated pegmatites and aplites, (3) Fe<sup>3+</sup>-rich quartz-tourmaline rocks (hydrothermally altered granites), (4) Metapelites coexisting with an Al-saturating phase, (5) Metapelites without an Al-saturating phase, (6) Fe<sup>3+</sup>-rich quartz-tourmaline rocks, calc-silicate rocks, and metapelites, (7) Low-Ca meta-ultramafics and Cr and V-rich metasediments, and (8) Metacarbonates and meta-pyroxenites.

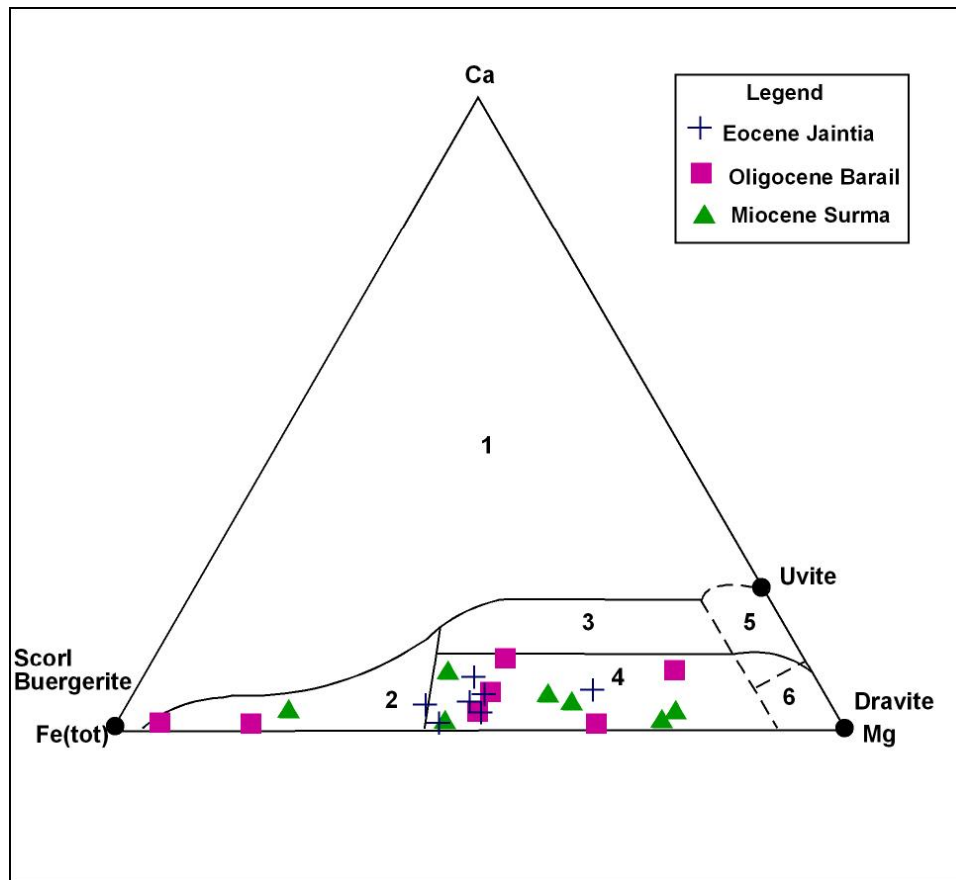


Figure 33. Ca-Fe(tot)-Mg plot (in molecular proportion) for tourmalines from the southeast of Shillong Plateau. Several end members are plotted for reference. The numbered fields correspond to the following rock types: (1) Li-rich granitoid pegmatites and aplites, (2) Li-poor granitoids and associated pegmatites and aplites, (3) Ca-rich metapelites and calc-silicate rocks, (4) Ca-poor metapelites and quartz-tourmaline rocks, (5) Metacarbonates, and (6) Meta-ultramafics.



### 6.4.2 Chrome Spinel

Detrital chrome spinel is useful to determine the tectonic setting of the source, as its unusual chemical stability favors preservation of compositional signature after burial. Chrome spinel is comparatively more durable than other ultramafic minerals, and it may be only mineral unaltered by sub greenschist facies serpentinization common in marine environments (Hekinian, 1985, cited in Cookenboo et al., 1997). The use of chrome spinel in provenance analysis is limited although it is widely used in petrologic study.

A total of 11 detrital chrome-spinel grains were analyzed from Oligocene and Miocene units from the study area. The elemental percent of chromium in these spinels is moderate to high, ranging from 16.9% to 77.8% (average 54%). Other important trivalent cations common in these spinels are  $\text{Al}^{3+}$  and  $\text{Fe}^{3+}$  and divalent  $\text{Mg}^{2+}$  and  $\text{Fe}^{2+}$ .  $\text{Cr}\# \{ \text{Cr}/(\text{Cr}+\text{Al}) \}$  varies from 0.17-0.79, mostly above 0.35.  $\text{Mg}\# (\text{Mg}/\text{Mg}+\text{Fe}^{2+})$  varies from 0.23-0.72, with Mg concentrations generally decreasing with increasing Fe. It is noteworthy that more fractionated mafic-ultramafic rocks are enriched in Fe compared to Mg. The total  $\text{TiO}_2$  weight percent is less than 1% in all samples.

Chrome spinel from a variety of ultramafic sources can be differentiated by plotting major element concentration, i.e. Cr, Al, and Fe content (Irvine, 1974; Basu and McGregor, 1975; Dickey, 1975; Dick and Bullen, 1984). A ternary plot with  $\text{Cr}^{3+}$ ,  $\text{Al}^{3+}$ , and  $\text{Fe}^{3+}$  as end members (Fig. 34) is useful for distinguishing Alpine-type peridotites from Alaskan-type and stratiform peridotite complexes (Dick and Bullen, 1984). In Alpine-type peridotites,  $\text{Cr}^{3+}$  increases with increasing  $\text{Fe}^{3+}$ , but  $\text{Fe}^{3+}$

remains low overall. Both stratiform and Alaskan type complexes have much higher concentrations of  $\text{Fe}^{3+}$  than the Alpine type peridotites.  $\text{Fr}^{3+}/(\text{Fe}^{3+}+\text{Cr}+\text{Al})$  against Mg# plot shows the importance of iron-rich (both  $\text{Fe}^{3+}$  and  $\text{Fe}^{2+}$ ) spinels in ultramafic rocks is formed by the fractional crystallization in the crust (Alaskan-type and stratiform type) is shown in Fig. 35. Except for one grain, all samples fall in the field of Alpine-type peridotite (Irvine, 1974). Hence, contributions from Alaskan-type ophiolite can be ruled out. The field of stratiform peridotite partially overlaps with that for Alpine type peridotites (Fig. 36). Only one sample plots outside the Alpine-type field. However, that grain is rich enough in  $\text{Fe}^{3+}$  to have been derived from a stratiform peridotite. Hence, considering figures 35 and 36 together, it can be concluded that detrital spinel from the study area have affinities to Alpine- type peridotite.

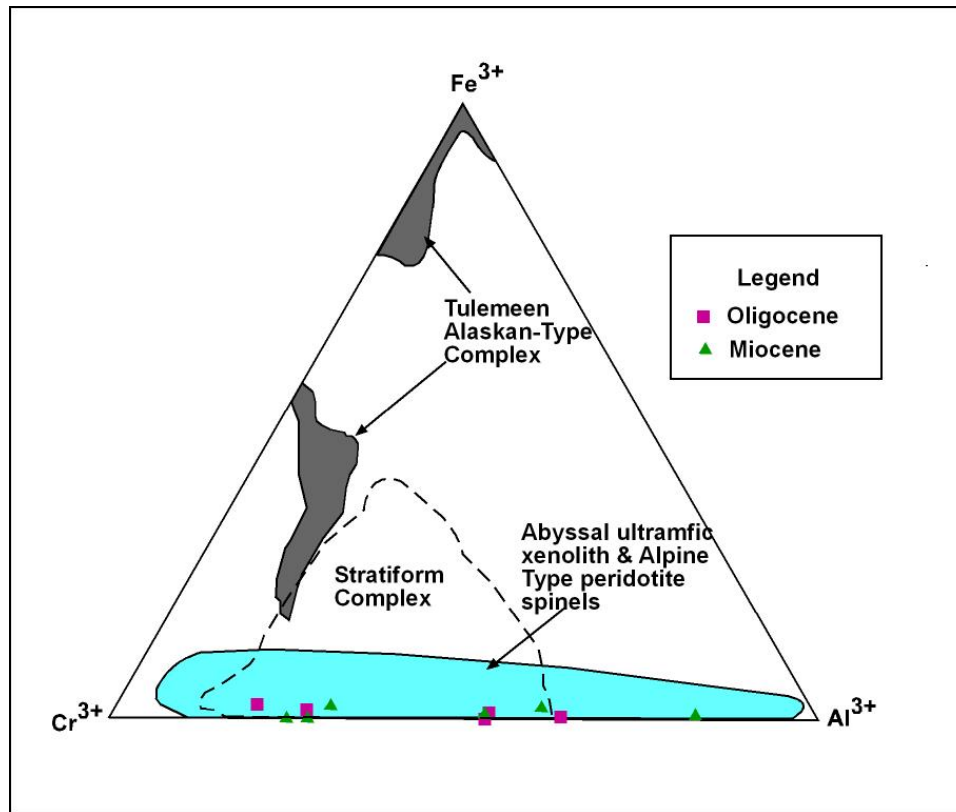


Figure 34. Ternary plot of major trivalent cations in chrome spinel. Three major provenance fields have been drawn to show the data distribution. The colored area denotes the field for chrome spinel of mantle melting origin, including ultramafic xenoliths, abyssal dunites, spinel and plagioclase peridotites, and Alpine-type peridotites (Dick and Bullen, 1984).

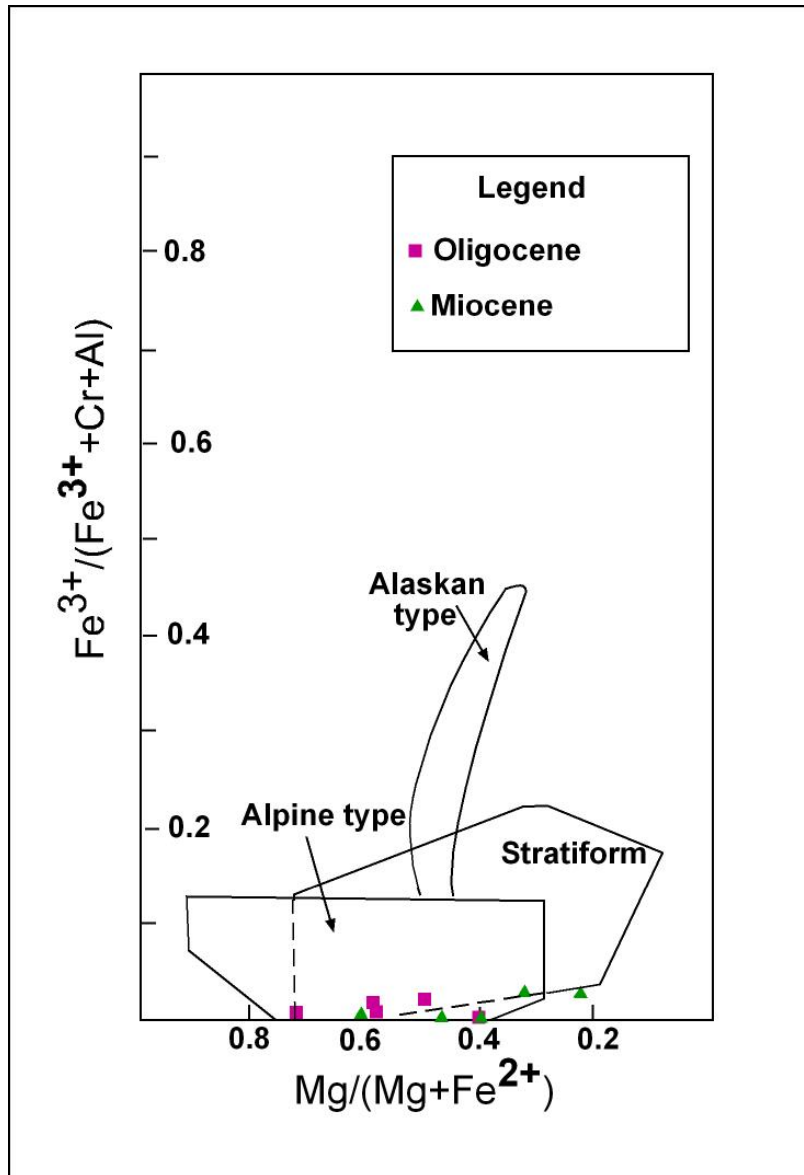


Figure 35. Plot of  $Mg/(Mg+Fe^{2+})$  against the ratio of trivalent cations  $Fe^{3+}/(Fe^{3+}+Al+Cr)$  for detrital spinel showing that Alpine and stratiform types overlap one another (Irvine, 1977).

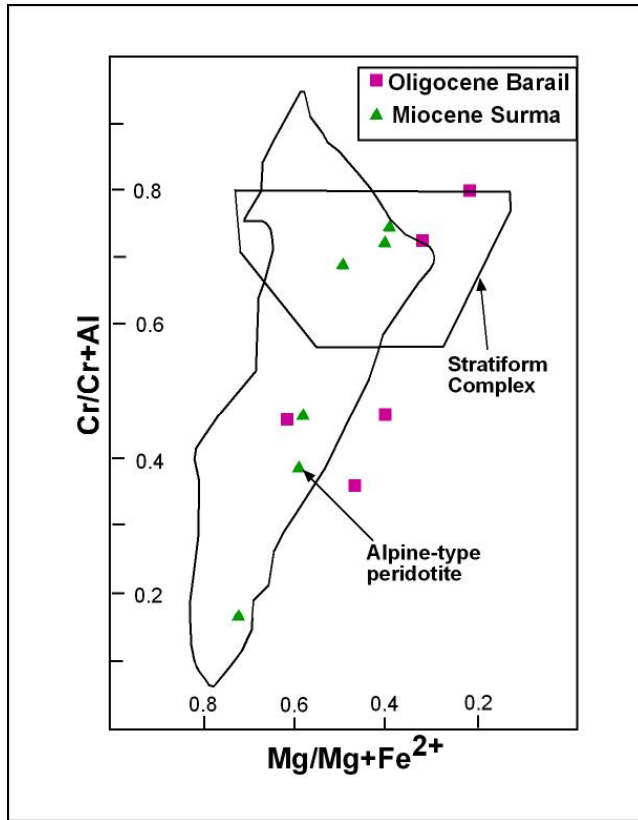


Figure 36.  $Mg/(Mg+Fe^{2+})$  versus  $Cr/(Cr+Al)$  plot for detrital chrome spinel showing the distribution of samples relative to different provenance fields. Note that although some data points fall in the overlap between the stratiform complex field (layers rich in chromite in a layered igneous complex) and Alpine-type peridotite (ophiolites), data generally reflect an Alpine-type peridotite provenance (after Dick and Bullen, 1984).

### 6.4.3 Garnet

Five garnets from Oligocene and Miocene units were analyzed. Garnet is characteristic of metamorphic rocks but it is also found in igneous rocks (Deer et al., 1992). Garnet is widely used as a provenance indicator because it is one of the most abundant detrital heavy minerals found in sandstones and it has a wide range of compositions. Garnet geochemical studies have proved particularly useful in characterizing, distinguishing, and correlating sand bodies on the basis of their provenance (Morton, 1985; Hallsworth and Chisholm, 2000).

Garnet chemistry data are plotted in figures 37-40. In the (Sp+Gro)-Py-Alm plot (Fig. 37), three garnet grains plot by the Py-Alm axis, indicating low

spessartine+grossular contents. However, on the (Py+Alm)-Sp-Gro plot (Fig. 38), these three samples cluster near to the Py+Alm apex. When garnet compositions are plotted on the Sp-Alm-Py ternary diagram (Fig. 39), grains plots in a wide range of fields. One Oligocene and one Miocene garnet fall in granulite facies metamorphic field, one Oligocene sample falls in the amphibolite facies field, and two Oligocene samples fall close to Alm-Sp axis. The Al+Sp-Gr-Py plot shows that three out of five garnets are high in pyrope and low in grossular content, suggesting that they are derived from high-grade metamorphic facies (Fig. 40). Remaining two contain low pyrope content indicating low- to medium-grade metamorphic sources. The range of garnet composition indicates derivation of these garnets from a wide spectrum of metamorphic facies. The source rock composition probably ranges from granulite-charnockite to garnet-mica schist from a proximal source in the Indian Craton and the orogenic belts (Le Fort, 1996; DeCelles, et al., 2001).

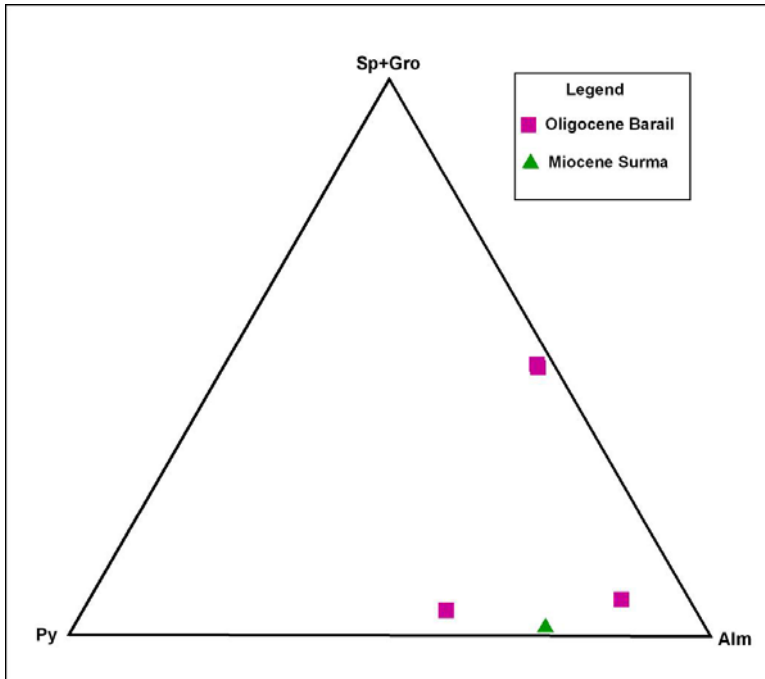
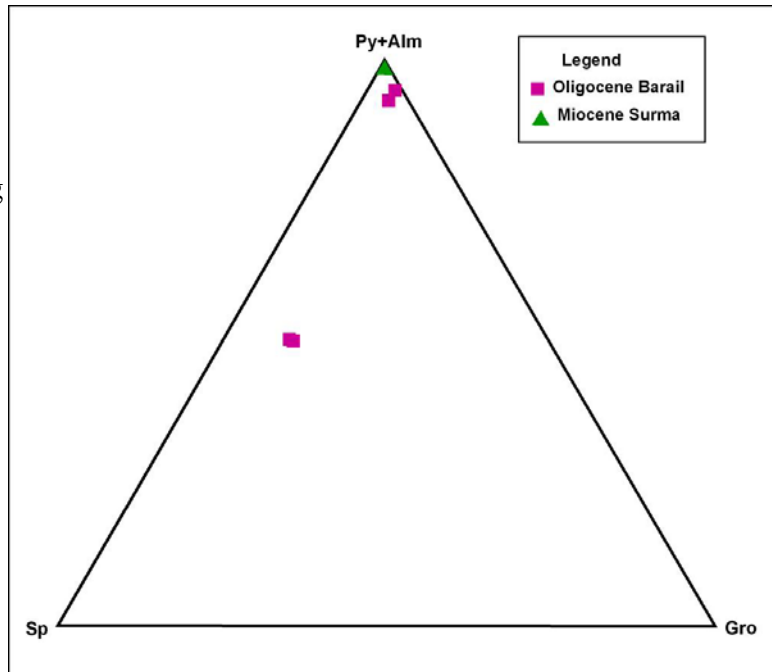


Figure 37. Chemical composition of garnets from southeast of Shillong Plateau plotted on a (Sp+Gro)-Py-Alm diagram. Sp - Spessartine; Gro - Grossular; Alm – Almandine; Py – Pyrope (after Nanayama, 1997).

Figure 38. Chemical composition of garnets from southeast of Shillong Plateau plotted on a (Py+Alm)-Sp-Gro diagram. Sp-Spessartine; Gro-Grossular, Alm-Aalmandine, Py-Pyrope (after Nanayama, 1997)



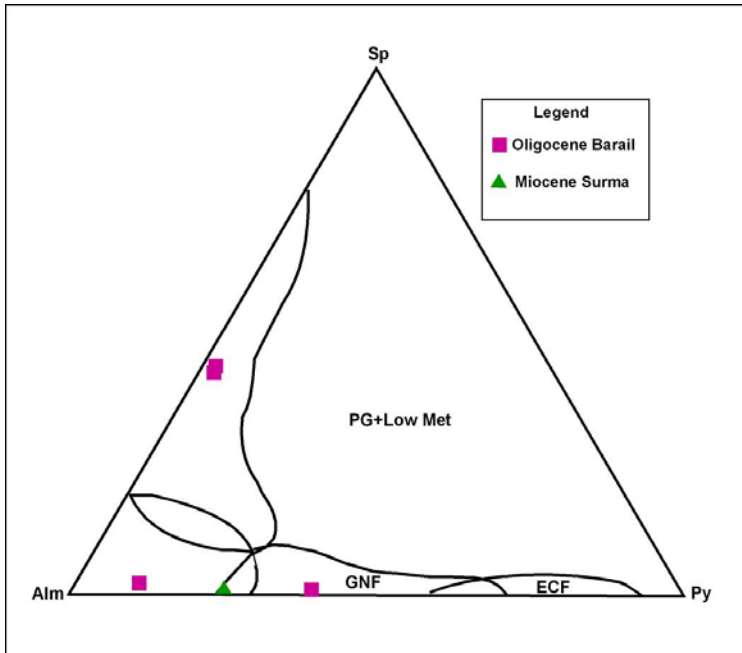
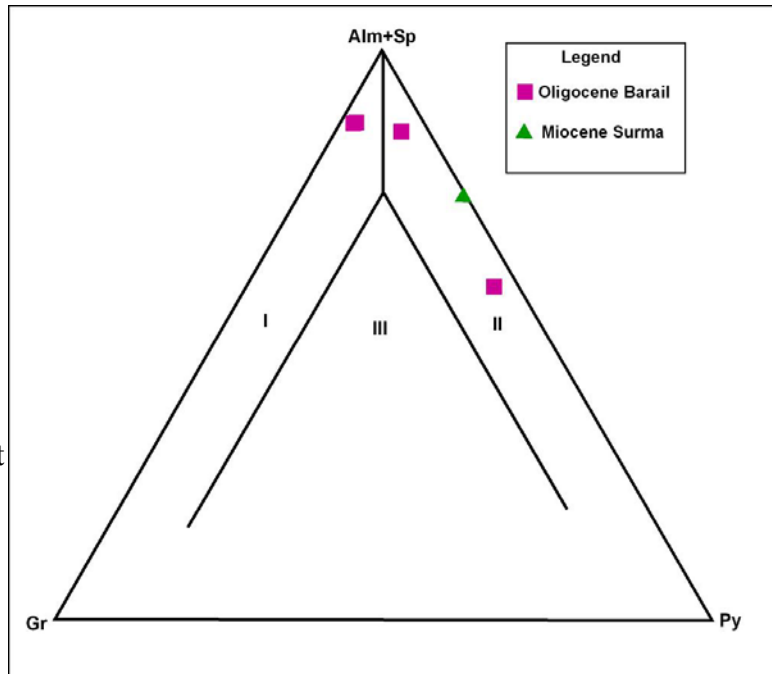


Figure 39. Chemical composition of garnet grains from southeast of Shillong Plateau, plotted on Sp-Alm-Py ternary diagram. Sp - Spessartine; Gro - Grossular; Alm - Almandine; Py - Pyrope, after (Nanayama, 1997).

Figure 40. Chemical composition of garnet grains from southeast of Shillong Plateau, plotted on (Alm+Sp)-Gr-Py ternary diagram. Sp - Spessartine; Gro - Grossular; Alm - Almandine; Py - Pyrope (after Nanayama, 1997). Fields I, II and III are various garnet groups that are discussed in the text.





## **6.5 DISCUSSION**

### **6.5.1 Tourmaline**

Microprobe data show that the vast majority of the detrital tourmalines are schrol and dravite types, probably deriving from metagraywacke and metapelites (Figs. 32 & 33). Detrital tourmalines are rich in Na and low in Ca, belongs to alkali groups (Fig. 31). These tourmalines were likely derived from metapelites, metapsammites, and quartz-tourmaline supracrustal rocks, with a subordinate contribution from Li-poor granitoids and associated pegmatites (Figs. 32 & 33).

### **6.5.2 Chrome Spinel**

The primary source of chrome spinel grains from the study area is interpreted to be Alpine- type peridotites (Figs. 34, 35 & 36). The origin of Alpine-type peridotites can be constrained considering the Cr# and Mg# plotted against modern oceanic rocks (Fig. 36). Chrome spinel from mid-ocean ridge basalts and peridotite have Cr# less than 0.06, and typically have high Mg# (0.7 to 8.5; Dick and Bullen, 1984). In contrast, spinel in back-arc basin basalts usually have lower Mg# for a given Cr#, and associated island-arc spinel show Cr# in excess of 0.60 (Dick and Bullen, 1984). Detrital spinels from the study area have variable Cr#, including values both above and below the abyssal limit of 0.60, suggesting a complex Alpine-peridotite source (Cookenboo et al., 1997). Wide range of Cr# composition in detrital chrome spinel composition exclude abyssal rocks (i.e., MORB and abyssal peridotites) to be as potential source rock (Fig. 41).

Peridotites from ophiolite complexes are classified as Type I, Type II, and III ophiolites based on spinel composition. Spinel compositions in Type I ophiolites are similar in chemical characteristics with spinel from mid-oceanic ridge basalts. In contrast, spinels from Type III populations are largely similar in chemistry to the spinel from arc-settings and oceanic plateaus (Dick and Bullen, 1984). Ophiolites with spinel ranging between Type I and III are called transitional or Type II ophiolites (Dick and Bullen, 1984).

Figure 42 indicates that spinels from the study area may have been derived from a mixture of mid-ocean ridge-derived basalts (type I) and more depleted marginal-basin and island-arc suites (type III). Spinel with high Al (Cr # = 0.10-0.30) and high Mg (Mg # 0.70-0.85) contents are common constituents of abyssal peridotites, dunites, and basalt (Dick and Bullen, 1984). The majority of the chrome spinels from the study area have low Al but high Cr content (Cr# 0.36 to 0.8). Only one Miocene sample (SM 8) has high-Al and high-Mg. Low-Al and high Cr# in of majority of the spinels suggest that they were not derived from mid-oceanic ridge basalts. Considering the geotectonic configuration of the basin, these spinels likely were derived from the Alpine-type ophiolite complex to the east (Naga ophiolite) or from Ti-poor continental flood basalt of the Rajmahal traps on the Indian Craton.

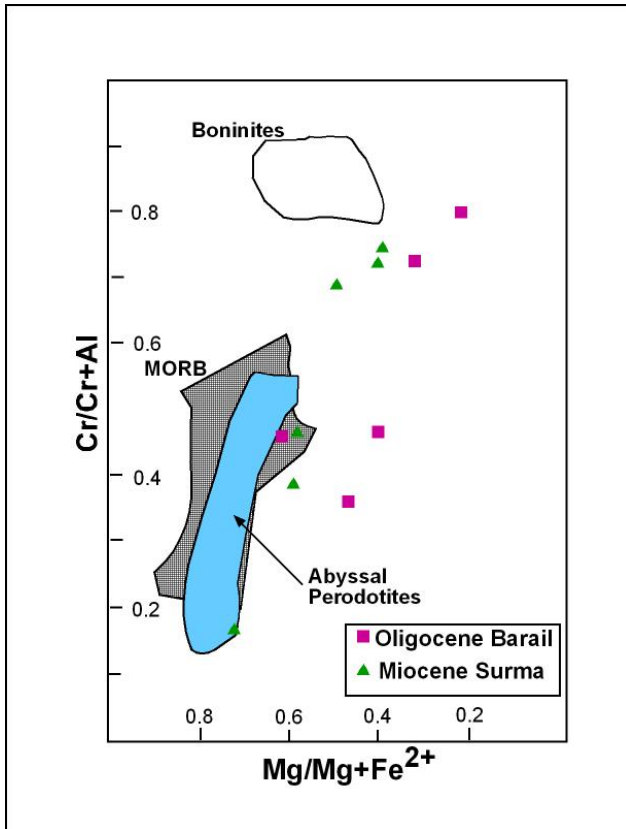


Figure 41.  $Mg/(Mg+Fe^{2+})$  versus  $Cr/(Cr+Al)$  plot is compared with mid-oceanic ridge basalt (MORB) (gray shaded area) derived peridotites (abyssal peridotite, basalts; Dick and Bullen, 1984).

Chrome spinles from this area has wide range of Cr# ( $Cr/(Cr+Al)$ ) than abyssal spinels (including both MORB and abyssal peridotites).

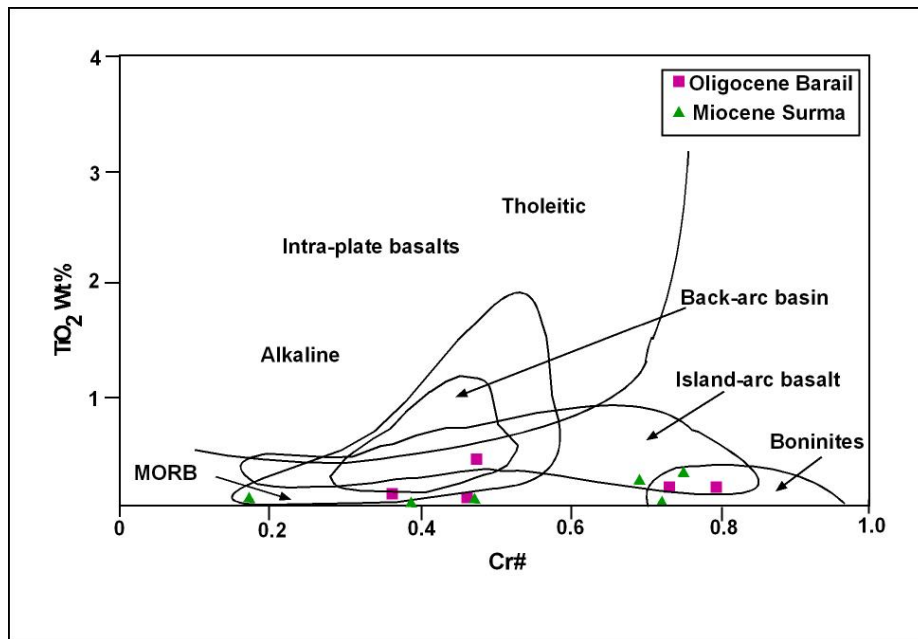


Figure 42. Plot of  $TiO_2$  vs. Cr# of detrital chrome spinel from southeast of Shillong Plateau. All chrome spinels have very low  $TiO_2$ . MORB = Mid-oceanic ridge basalt (after Arai, 1992).

### 6.5.3 Garnet

Garnets from the present area have been classified into three groups (after Morton et al., 1992): (1) type-I garnet reflects a solid solution between almandine and grossular with <10% pyrope; (2) type-II garnets reflect a solid solution between almandine and pyrope with <10% grossular; and (3) type-III garnets are those wherein both pyrope and grossular are >10%. Three out of five garnets of the study area are type-II grains (Fig. 40). The wide range of pyrope and grossular content suggest a wide spectrum of metamorphic facies, ranging from greenschist-amphibolite to granulite facies metamorphism as seen in figure 43.

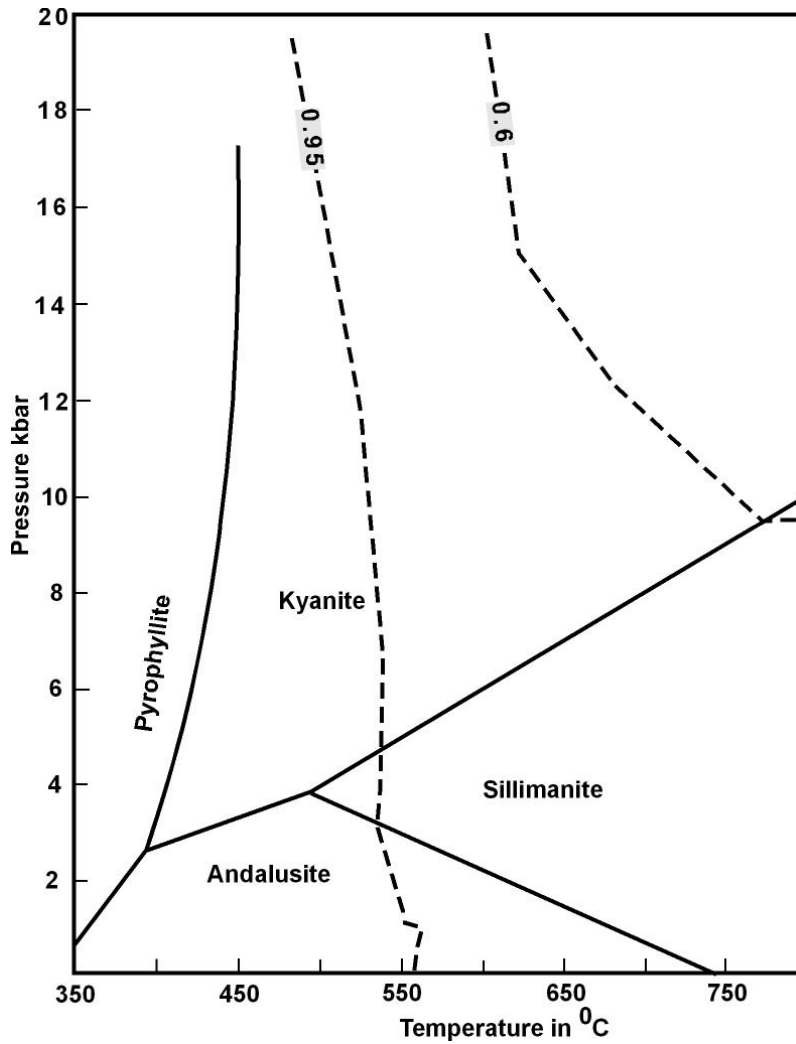


Figure 43. Pressure-temperature diagram for garnet data from southeast of Shillong Plateau, Meghalaya. Dashed lines are garnet Fe/(Fe+Mg) isopleths, constructed for the two garnet compositions observed in this study and assuming that garnet formed in equilibrium with biotite (Spear, 1993). Garnet shows a wide spectrum of metamorphic P-T conditions.

## CHAPTER 7: MUDROCK GEOCHEMISTRY

### 7.1 INTRODUCTION

Mudrock geochemical analyses are important tools to study provenance of terrigenous sedimentary rocks because they can provide information about rock types, tectonic settings, and weathering history of the source rocks. Recent developments in the field of sedimentary geochemistry highlight that chemical composition of the clastic sedimentary rocks is a function of complex interplay of several variables, including the nature of the source rocks, source area weathering and diagenesis (McLennan et al., 1993; McLennan et al., 2003). However, plate tectonic processes impart a distinctive geochemical signature to sediments in two separate ways. First, different tectonic environments have distinctive provenance characteristics and, second, they are characterized by distinctive sedimentary processes. Therefore, clastic sedimentary rocks have been used to determine provenance and identify ancient tectonic settings (Bhatia, 1983; McLennan et al., 1993). Sedimentary basins may be assigned to the following tectonic settings: (1) oceanic island-arcs, (2) continental island-arcs, (3) active continental margins, and (4) passive continental margins (Bhatia and Crook, 1986; Rahman and Faupl, 2003). Roser and Korsch (1988) used discriminant function analysis of major elements ( $\text{TiO}_2$ ,  $\text{Al}_2\text{O}_3$ ,  $\text{Fe}_2\text{O}_3$  tot.,  $\text{MgO}$ ,  $\text{CaO}$ ,  $\text{Na}_2\text{O}$ ) to discriminate four different provenance groups: (1) mafic detritus, (2) intermediate, dominantly andesite detritus, (3) felsic plutonic and volcanic detritus, and (4) recycled-mature polycyclic quartzose detritus from sandstones and argillites.

Major element geochemistry and mineralogy of siliciclastic rocks (Taylor and McLennan, 1985) is strongly affected by chemical weathering (Fedó et al., 1996). Plotting  $\text{Al}_2\text{O}_3$ -( $\text{CaO}+\text{Na}_2\text{O}$ )- $\text{K}_2\text{O}$  relationships in ternary diagrams provides important information about weathering processes, sedimentary sorting, and identifying certain post-depositional processes. The potential influence exerted on sediment geochemistry by weathering, detrital sorting, and diagenesis/metamorphism are reasonably well understood. Trace element ratios of immobile elements normally reflect source-rock composition rather than the sedimentary processes (Taylor and McLennan, 1985).

In the present study, bulk geochemical analysis of mudrocks were performed to constrain possible source terranes, and to understand the weathering conditions prevailed in the detrital system.

## **7.2 METHODS**

Twelve mudrock samples were collected from different lower Cenozoic stratigraphic units in the study area (Fig. 3). Samples were dried in an oven at  $50^\circ\text{C}$  for nearly 24 hours. Approximately 20 gm of dried sediment for each sample was crushed with a mortar and pestle to a grain size of  $<0.63$  mm and homogenized. Afterwards, these samples were sent to the ACME Laboratories Ltd., Vancouver, BC, Canada, for analysis. In the lab, splits of 0.2 g of each sample were analyzed by ICP-emission spectra following lithium metaborate/tetraborate fusion and dilute nitric digestion. Loss of Ignition was calculated by weighing the difference after ignition at  $1000^\circ\text{C}$ . Geochemical analysis included the measurements of 11 oxides ( $\text{SiO}_2$ ,  $\text{Al}_2\text{O}_3$ ,

Fe<sub>2</sub>O<sub>3</sub>, MgO, CaO, Na<sub>2</sub>O, K<sub>2</sub>O, TiO<sub>2</sub>, P<sub>2</sub>O<sub>5</sub>, MnO, and Cr<sub>2</sub>O<sub>3</sub>) and 7 trace elements (Ba, Ni, Sr, Zr, Y, Nb, and Sc).

### **7.3 RESULTS**

The results of mudrock analyses are presented in Table 6.

#### **7.3.1 Major and Trace Elements**

Mudrock samples from the study area exhibits variation in major oxides (e.g., SiO<sub>2</sub>, Al<sub>2</sub>O<sub>3</sub>, Fe<sub>2</sub>O<sub>3</sub>, MgO, and K<sub>2</sub>O) concentration through time. The average major elemental compositions of the mudrock samples from this study area are similar in magnitude to that of the average shale (Wedpohl, 1971; Rahman and Faupl, 2003), with the exception of CaO content. The depletion in CaO contents could possibly be due to overall scarcity of calcic minerals in the mudrock samples analyzed. The lowest SiO<sub>2</sub> content is seen in the mudrocks from lower Kopili Formation of the Jaintia Group, near the contact with the Prang Limestone. The same horizon has the highest Al<sub>2</sub>O<sub>3</sub>. The mudrock samples from the Laisong Formation have the highest SiO<sub>2</sub> and lowest Al<sub>2</sub>O<sub>3</sub> content. (Fig. 44A). The abundance of Al<sub>2</sub>O<sub>3</sub> varies inversely with SiO<sub>2</sub>. Fe<sub>2</sub>O<sub>3</sub> concentration is highest in the lower part of the Kopili Formation of Eocene Jaintia Group. The same formation is also characterized by relatively elevated MgO and CaO (Fig. 44a), although sandstone units from same horizon do not contain any calcite cement. Highest concentrations of MgO and CaO are observed in the Bhuban Formation of lower Miocene Surma Group. K<sub>2</sub>O content increases and TiO<sub>2</sub> decreases in up-section (Fig. 44A).



Major element oxides are compared with the composition of Post Archean Australian Shale (PAAS) composite, regarded as the best representative of the post-Archean upper continental crust (Fig. 44B; Taylor and McLennan, 1985; Condie, 1993; Roddaz et al., 2006). Compared to PAAS, mudrock samples are strongly depleted in CaO, Na<sub>2</sub>O, MnO and slightly depleted in MgO, K<sub>2</sub>O. SiO<sub>2</sub>, Al<sub>2</sub>O<sub>3</sub> contents are similar to PAAS. TiO<sub>2</sub> and Fe<sub>2</sub>O<sub>3</sub> contents are variable with respect to the PAAS; in some formations, they are slightly enriched and in others slightly depleted.

The linear relationship of CaO, MgO, Fe<sub>2</sub>O<sub>3</sub> and Al<sub>2</sub>O<sub>3</sub> with SiO<sub>2</sub> in the mudrock is conspicuous in the Harker variation diagram (Fig. 45). The negative correlation of all these four oxides is due to the fact that most of the silica is sequestered in quartz. TiO<sub>2</sub> concentrations increase with Al<sub>2</sub>O<sub>3</sub> in mudrocks of the Barail and Surma groups. SiO<sub>2</sub>/ Al<sub>2</sub>O<sub>3</sub> values in most of the mudrock samples are  $\leq 5$ , which is typical for an active margin setting (excluding samples SM1 and SM 22). The Al<sub>2</sub>O<sub>3</sub>/TiO<sub>2</sub> weight ratios in the Surma Group samples are between 20-21, comparable to values of most granitic, volcanic and sedimentary rocks (18-31; Hayashi et al., 1997b). The relatively lower value of Al<sub>2</sub>O<sub>3</sub>/TiO<sub>2</sub> in Eocene and Oligocene samples can be explained by the presence of rutile/illmenite (TiO<sub>2</sub> bearing phase) in these horizons. Heavy mineral data also suggest a higher percentage of rutile in older sediments (chapter 5). The ratio of K<sub>2</sub>O and Al<sub>2</sub>O<sub>3</sub> (Fig. 46) can be used as an indicator of the original composition of the mudrock. K<sub>2</sub>O/ Al<sub>2</sub>O<sub>3</sub> ratios are markedly different for clay minerals and mudrocks. K<sub>2</sub>O/Al<sub>2</sub>O<sub>3</sub> ratios for clay

minerals range from 0.0 to 0.3 and those for feldspars range from 0.3 to 0.9 (Cox et al., 1995).

Illite has a  $K_2O/Al_2O_3$  value of 0.28 (Lee, 2000). The  $K_2O/Al_2O_3$  values of mudrocks (0.15 to 0.19) from the study area lie within the ranges of clay minerals.

Trace element data show a gradual increase in Ba contents up-section (Fig. 47 A & B). Trace elements data are normalized with respect to PAAS in Fig. 47B. One mudrock sample (SM 1) shows very strong enrichment of Zr. A strong negative correlation is observed between Zr and Sr. Like  $K_2O$ , Rb is incorporated into clays during chemical weathering, in contrast to divalent Ca and Sr, which along with Na tend to be leached (Asiedu et al., 2000; Kasanzu et al., 2008). CaO,  $Na_2O$  and Sr are strongly depleted with respect to PAAS, where  $K_2O$  is close to the average concentration for PAAS.

Table 6. of whole-rock chemical analysis of mudrock samples from southeast of Shillong Plateau

Sample No	SM10	SM11	SM12	SM15	SM19	SM22	SM24	SM26	SM27	SM30	SM31	SM1
Formation	Bokabil	Bhuban	Bhuban	Jenum	Jenum	Laisong	Laisong	Kopili	Kopili	Kopili	Kopili	Sylhet
Group	Surma			Barail			Jaintia					
SiO <sub>2</sub>	63.82	60.81	59.09	60.22	62.68	71.62	66.26	58.05	67.15	67.49	52.96	63.82
Al <sub>2</sub> O <sub>3</sub>	16.44	17.50	17.23	15.44	16.38	13.20	15.74	16.51	15.09	15.82	20.61	12.55
Fe <sub>2</sub> O <sub>3</sub>	6.54	6.70	6.59	9.59	6.39	4.71	5.41	7.96	5.93	4.93	9.94	10.68
MgO	1.66	2.50	2.83	1.98	1.81	1.17	1.68	1.58	1.21	1.28	2.45	1.04
CaO	0.07	0.72	1.57	0.46	0.32	0.19	0.26	0.14	0.26	0.17	0.80	0.37
Na <sub>2</sub> O	0.63	1.21	1.14	0.92	0.76	0.77	0.65	0.74	0.69	0.74	0.48	0.04
K <sub>2</sub> O	2.96	3.25	3.18	2.63	2.90	2.29	2.97	3.13	2.57	2.40	3.07	2.41
TiO <sub>2</sub>	0.80	0.84	0.82	1.01	1.05	0.87	1.04	1.09	1.19	1.23	1.08	1.55
P <sub>2</sub> O <sub>5</sub>	0.12	0.14	0.13	0.14	0.13	0.11	0.09	0.10	0.16	0.10	0.12	0.07
MnO	0.05	0.06	0.09	0.18	0.08	0.05	0.03	0.03	0.05	0.03	0.04	0.01
Cr <sub>2</sub> O <sub>3</sub>	0.02	0.02	0.02	0.02	0.02	0.01	0.02	0.02	0.02	0.02	0.02	0.04
Ba	527	448	430	393	402	322	386	417	334	260	268	179
Ni	62	86	65	57	59	42	46	49	61	46	64	37
Sr	65	99	109	107	116	80	99	98	94	103	212	61
Zr	216	199	211	300	271	345	414	231	369	455	198	1877
Y	34	32	32	41	35	34	36	38	38	38	34	113
Nb	14	17	14	18	16	17	21	26	19	15	24	31
Sc	15	17	17	17	17	12	16	17	15	17	21	13
LOI	6.70	6.10	7.10	7.20	7.30	4.80	5.70	10.50	5.50	5.60	8.20	7.00
Sum	99.94	99.91	99.90	99.95	99.93	99.95	99.93	99.92	99.95	99.94	99.89	99.87
TOT/C	0.07	0.41	0.79	1.18	0.79	0.37	0.32	1.65	0.40	0.39	0.50	0.59
TOT/S	<0.02	0.17	0.04	0.05	0.15	0.04	0.18	2.77	<0.02	0.06	0.17	0.03
CIA	79.01	71.96	67.83	74.82	76.72	76.34	76.79	77.26	77.47	79.32	78.73	78.94
PIA	91.92	80.91	74.46	84.27	87.85	86.93	89.04	89.91	88.45	89.65	88.51	93.08
SiO <sub>2</sub> /Al <sub>2</sub> O <sub>3</sub>	3.88	3.47	3.43	3.90	3.83	5.43	4.21	3.52	4.45	4.27	2.57	5.09
Al <sub>2</sub> O <sub>3</sub> /TiO <sub>2</sub>	20.55	20.83	21.01	15.29	15.60	15.17	15.13	15.15	12.68	12.86	19.08	8.10
K <sub>2</sub> O/Al <sub>2</sub> O <sub>3</sub>	0.18	0.19	0.18	0.17	0.18	0.17	0.19	0.19	0.17	0.15	0.15	0.19

Cr, Ni and Sc are compatible components in mafic rocks (Camire' et al., 1993). Sc is correlated with  $\text{Al}_2\text{O}_3$ , suggesting Sc may be bounded in clays and concentrated during weathering. Ni shows no correlation with  $\text{Al}_2\text{O}_3$ . Zr, Nb, and Y belong to the high field strength elements group (HFSE), preferentially partitioned into melts during crystallization and anatexis (Feng and Kerrich, 1990). Therefore, these elements are enriched in felsic rocks. Figure 47B shows that these elements are enriched to various levels with respect to PAAS, whereas the large ion lithophile elements (LILE) like Ba and Sr are strongly depleted with respect to PAAS. One mudrock sample shows very high Zr content, which could be either due to higher concentrations of recycled Zr in that particular layer or derivation of more zircon from felsic igneous rocks (Soreghan and Soreghan, 2007).

The major element composition of mudrocks is sensitive to the intensity of pre- and post-depositional weathering. The progressive weathering during erosion and transport tends to increase the abundance of cation-poor clays and oxides of iron and aluminum at the expense of both non-clay and compositionally complex clays (Nesbitt and Young, 1984; Lee, 2002). One sample (SM 31) from the lower part of the Kopili Formation has the highest  $\text{Al}_2\text{O}_3$  content and lowest  $\text{SiO}_2$  content, which is inferred to reflect intense weathering in the source area. The same horizon is also accompanied by increased Mg and Fe contents, which suggest the presence of chlorite/hematite.  $\text{SiO}_2$  content of mudrocks from this area is similar to PAAS; which can be suggested that the abundance of other elements are free of quartz dilution (McLennan, 1989, cited in Kasanzu et al., 2002). CaO and Sr are depleted with respect to PAAS in the mudrocks. Ca and Sr are contained in minerals that weather

more rapidly (e.g., plagioclase feldspar) than those that contain K, Ba (e.g., muscovite; Roddaz et al., 2006). Depletion of Ca and Sr in mudrocks can be attributed to be less plagioclase weathering in the source area and/or low plagioclase content in the source rocks. However, Sr content in mudrock is affected by many factors in low temperature depositional environments.

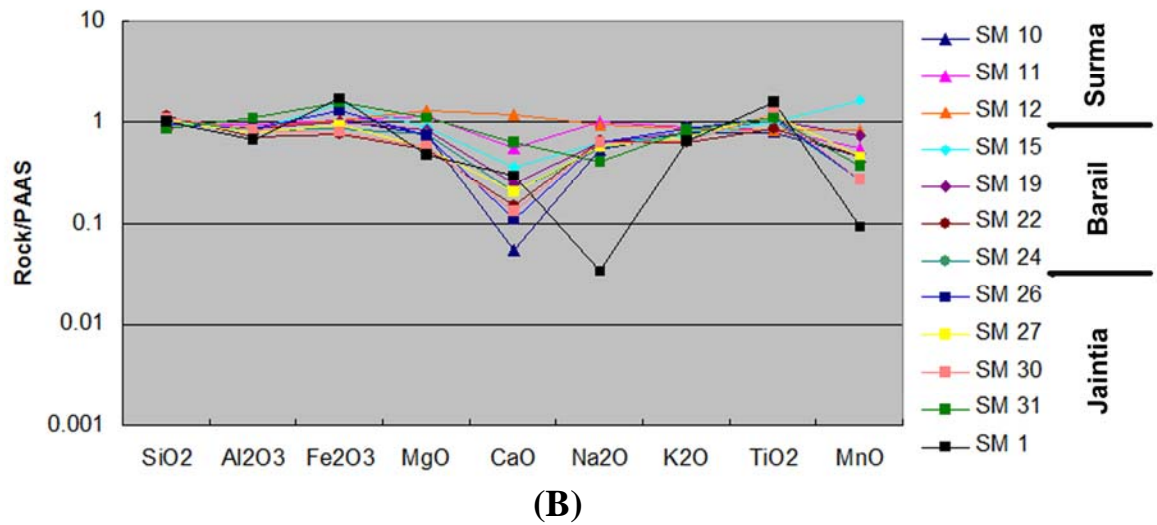
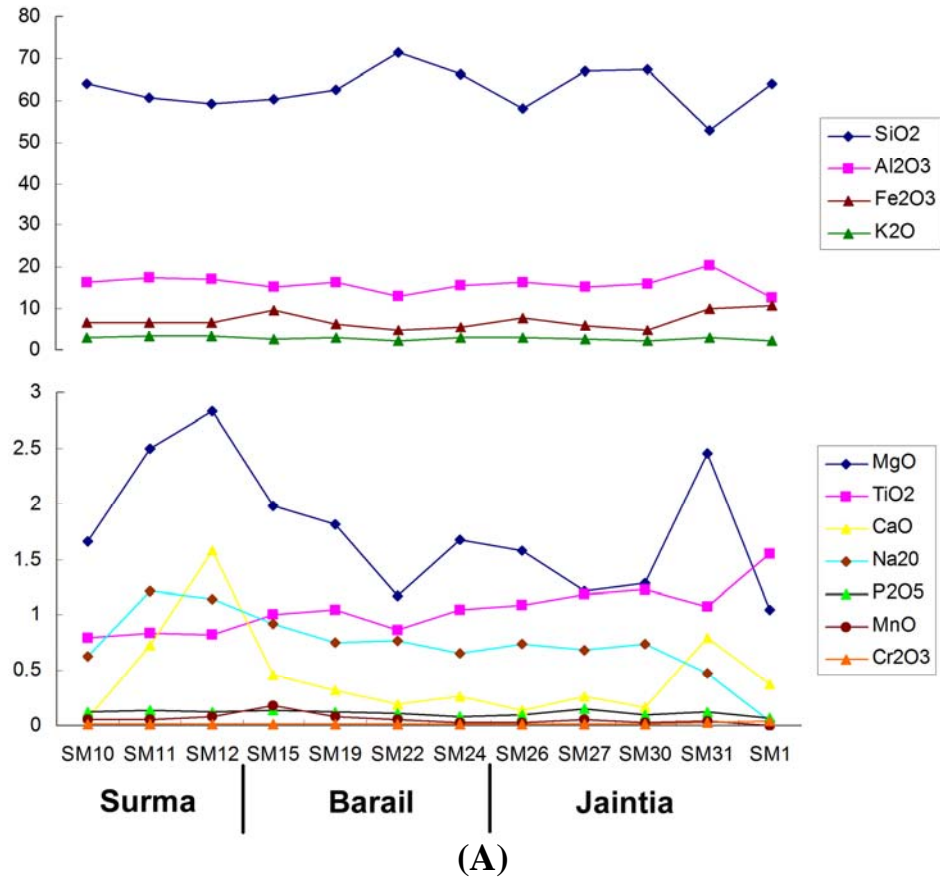


Figure 44. (A) Stratigraphic variation of major element oxide concentrations. Data are recalculated as volatile free. (B) Stratigraphic variation of post-Archean Australian average shale (PAAS; Taylor and McLennan, 1985)-normalized major element composition.

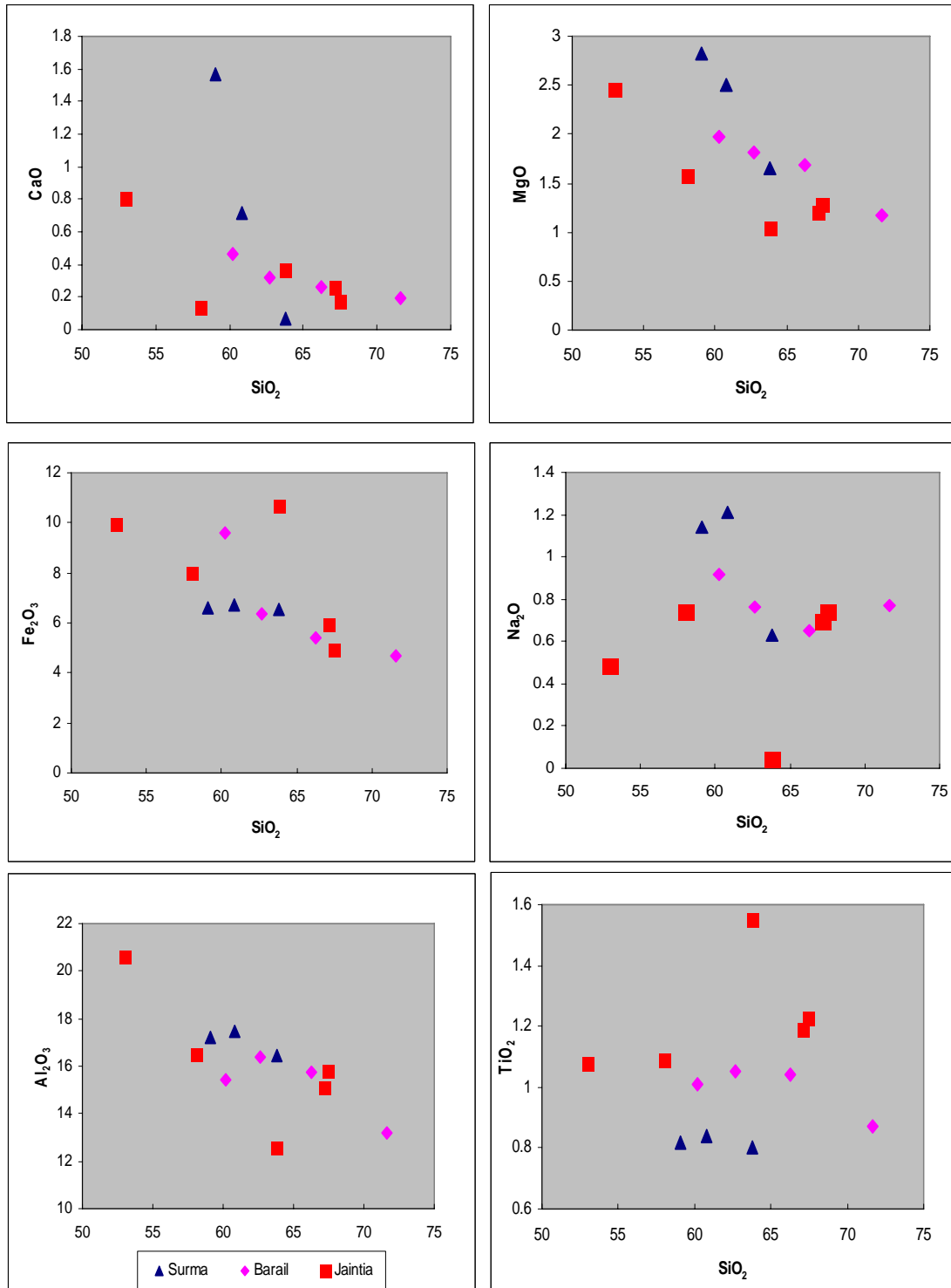


Figure 45. Harker variation diagrams of major elements for mudrocks from the study area.

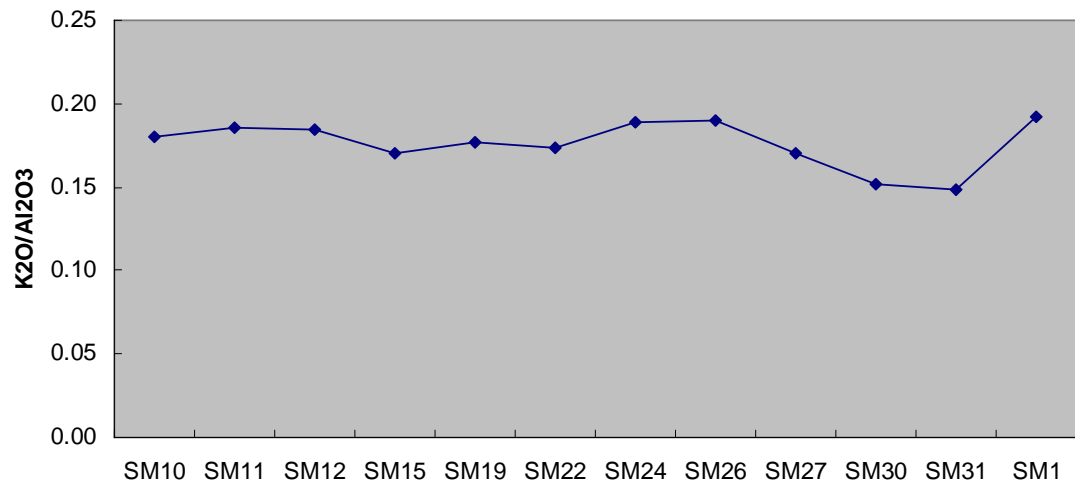
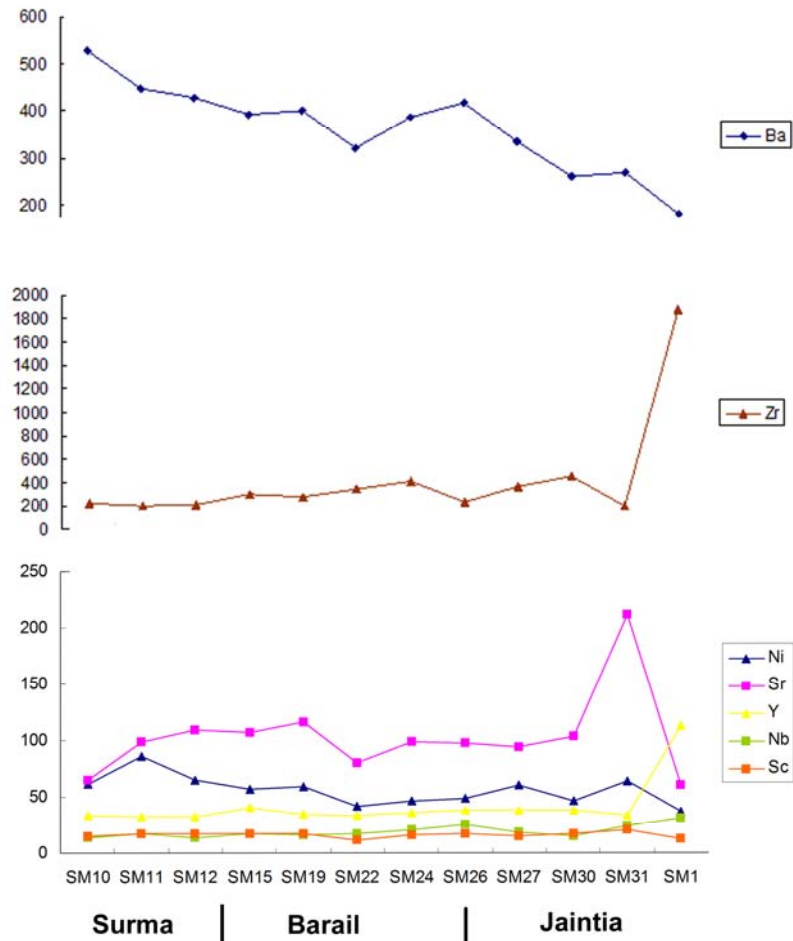
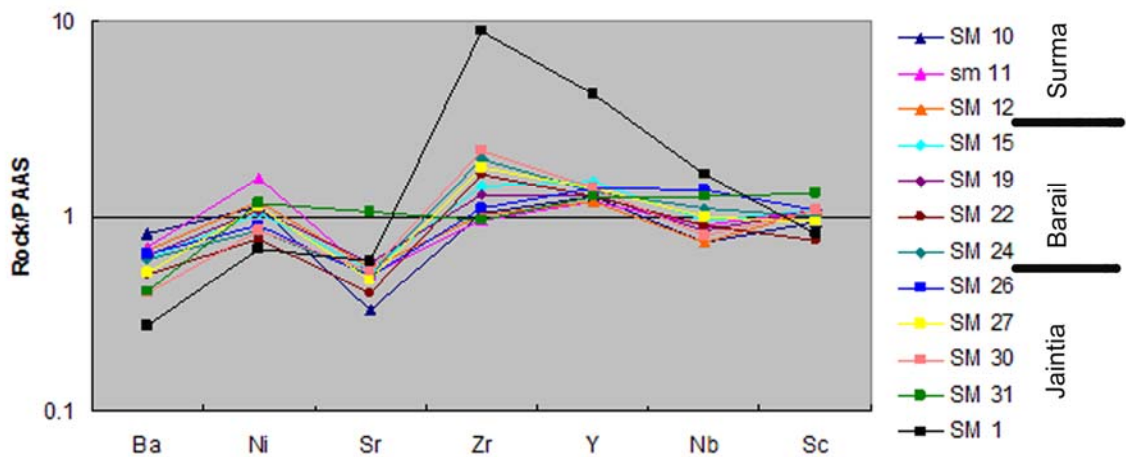


Figure 46. Stratigraphic variation of  $K_2O/Al_2O_3$  ratios for mudrock samples from study area. Stratigraphically older sediments are to the right. All samples are with the clay mineral field.





(A)



(B)

Figure 47. (A) Stratigraphic variation of trace element concentrations. (B) Spider plot of trace element composition of mudrocks from the study area normalized against PAAS.

### 7.3.2 Source Area Weathering and Diagenesis

Several studies reported that the chemical index of alteration (CIA) accurately reflects the intensity of weathering of rocks of varied geological ages. Low CIA values (50% to 60%) indicate relatively unweathered rocks, whereas intermediate (60% to 80%) and higher (80% to 100%) CIA values indicate moderate to extreme weathering conditions (Nesbitt and Young, 1984). This index is calculated using the equation:

$$\text{CIA} = \text{Al}_2\text{O}_3 / (\text{Al}_2\text{O}_3 + \text{CaO}^* + \text{Na}_2\text{O} + \text{K}_2\text{O})$$

In the above equation, CaO\* is defined as CaO in silicates only. However, in the present study there was no objective way to distinguish carbonate CaO from silicate CaO, so total CaO is plotted in figure 48 (Bock et al., 1998; Kasanzu et al., 2008).

This is justified as none of the mudrock samples appeared to be calcareous. CIA values for these mudrock samples (Fig. 48) range from 67%-79%, which indicate moderate weathering in the source area. This is also supported by high values of the plagioclase index of alteration (PIA) of the mudrock samples (Table 5). PIA is calculated (Fedo et al., 1995) using the following equation:

$$\text{PIA} = 100 \times (\text{Al}_2\text{O}_3 - \text{K}_2\text{O}) / (\text{Al}_2\text{O}_3 + \text{CaO}^* + \text{Na}_2\text{O} - \text{K}_2\text{O})$$

The average CIA values for mudrocks in the study area are higher than that for PAAS (69%) (Nesbitt et al., 1997; Kasanzu et al., 2008). Mudrock samples from the study area fall along a linear trend parallel to A-CN line  $\text{Al}_2\text{O}_3 - (\text{CaO}^* + \text{Na}_2\text{O}) - \text{K}_2\text{O}$  (A-CN-K) ternary plots. This A-CN-K diagram is also useful in interpreting post-depositional metasomatic alteration (Fedo et al., 1996). The weathering trend line for mudrock samples from the study area shows an ideal trend for weathering of primary source

rock of granodioritic composition. As none of the samples fall parallel to the A-K axis of A-CN-K diagram or close to illite-muscovite area suggesting post-depositional K-metasomatism likely played an insignificant role in this basin.

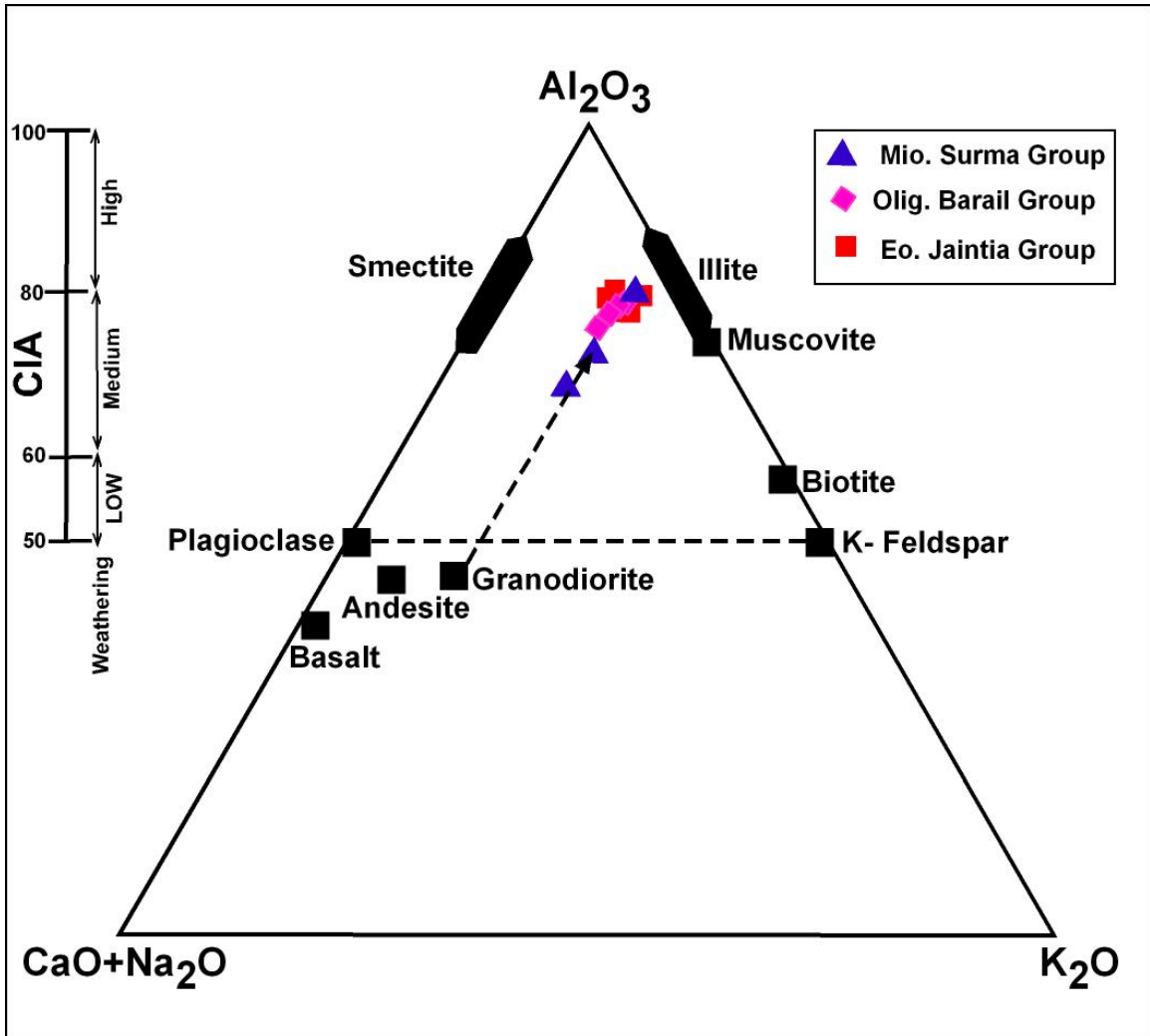


Figure 48.  $Al_2O_3$ - $CaO^*+Na_2O$ - $K_2O$  (Nesbitt and Young, 1984) diagram for mudrock samples from the study area. Black dotted arrow show weathering trend of these samples. Average CIA (chemical index of alteration) values for these are moderate to high (i.e., 80%).

## 7.4 TECTONIC SETTING AND SOURCE ROCKS

Plots of two discriminant functions based on oxides of Ti, Al, Fe, Mg, Ca, Na, and K most effectively differentiate four provenances (P1 – P4) (Roser and Korsch, 1988). Figure 49 shows a discriminant function diagram for mudrock samples from the study area. The majority of samples fall in the P4 field, which represents mature poly-cyclic quartzose detritus. One sample from the Jaintia Group falls within the P1 field, suggesting a mafic to intermediate source. The majority of the mudrocks from the Surma and Barail groups were derived from active continental margin settings (ACM) settings (Fig. 50A), related to recycled quartzose sediments of mature continental sources, possibly deriving from highly weathered granite-gneiss terrains and/or from pre-existing sedimentary wedges. Low concentrations of Na<sub>2</sub>O in Oligocene and Miocene samples shift the provenance to the PM (passive margin) field. The majority of the mudrocks from the Jaintia group represent a “passive margin” setting with slight overlap with “active continental margin.” The Zr versus TiO<sub>2</sub> discriminant diagrams (Fig. 50B) help to differentiate among felsic, intermediate and mafic source rocks. The Zr-TiO<sub>2</sub> diagram (Fig. 50b) shows that the majority of the mudrock samples analyzed for this study fall within the field of felsic to intermediate igneous rocks related to the higher Zr content in these samples. The discriminant diagram (Fig. 49) also shows that the majority of the mudrocks of the Jaintia Group represent quartzose recycled sediment with little influx of mafic to intermediate source rocks. Therefore it can be concluded that this basin started to receive orogenic sediments after deposition of Jaintia units.

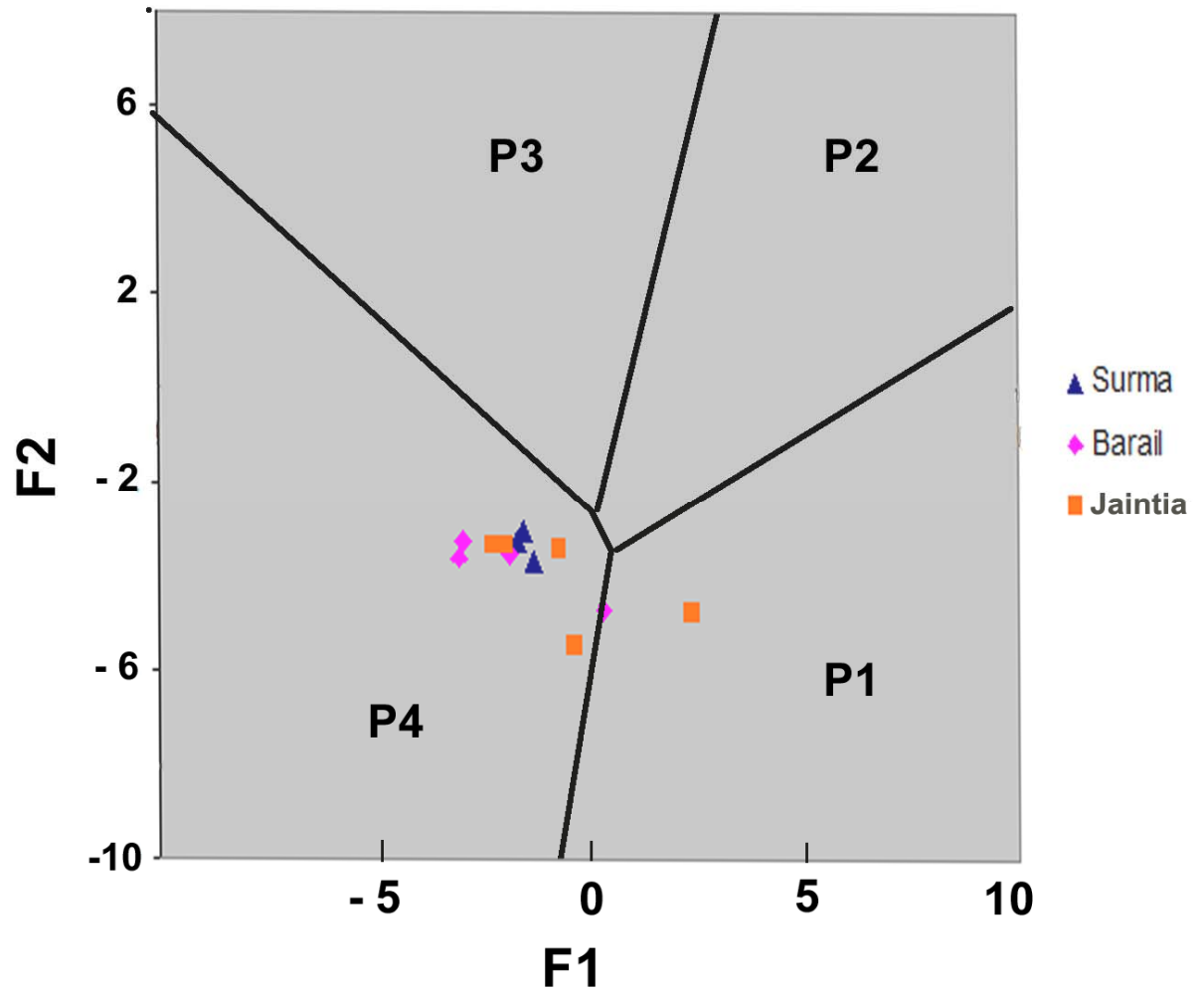
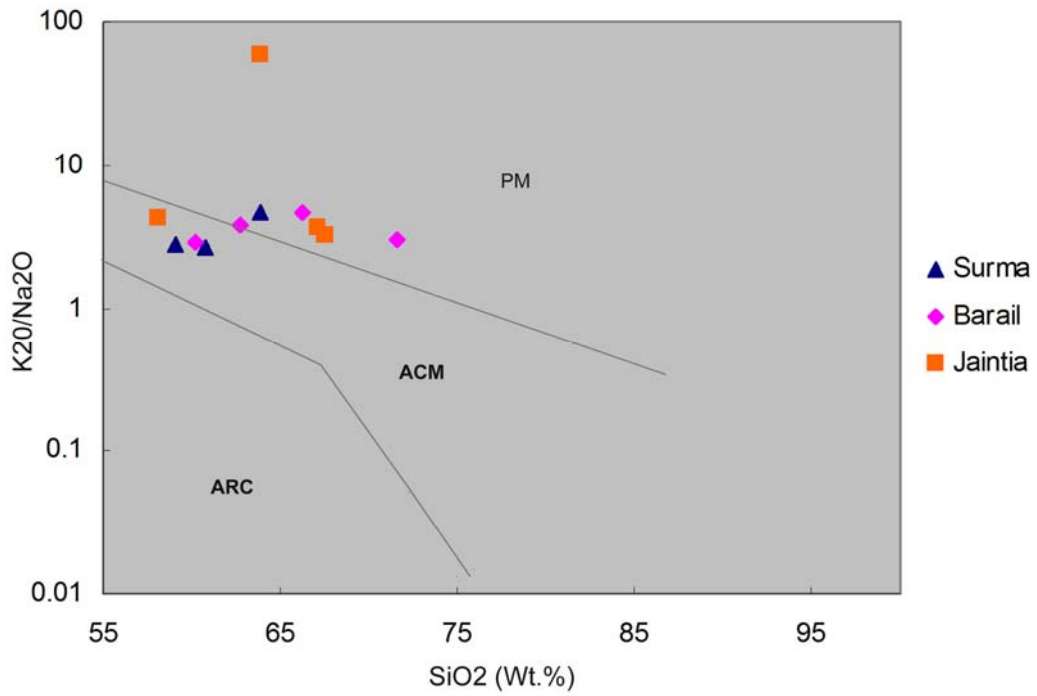
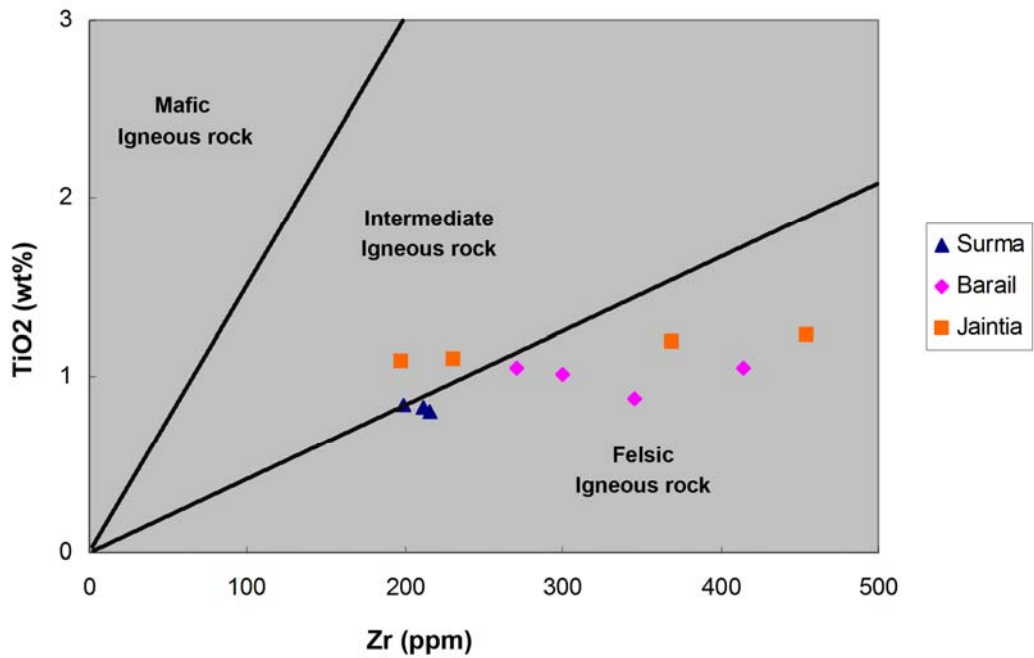


Figure 49. Plot of discrimination functions F1 and F2 for mudrocks from the study area. Provenance fields are after Roser and Korsch (1988). P1 -mafic and intermediate igneous provenances; P2 -intermediate igneous provenances; P3 -felsic igneous provenances; and P4 -recycled-mature polycyclic quartzose detritus.



(A)



(B)

Figure 50. (A) Tectonic discrimination diagram for mudrocks from southeast of Shillong Plateau. Boundaries are after Roser and Korsch (1986). PM – passive margin, ACM – active continental margin, ARC – oceanic island arc margin. (B)  $TiO_2$ -Zr discrimination diagram from southeast of Shillong Plateau (Hayashi et al., 1997a).

## **CHAPTER 8: DISCUSSION**

### **8.1 SYNTHESIS**

Nearly 11 km thick clastic sequences are preserved to the southeast of Shillong Plateau in the study area, junction between the Assam and Bengal basins, of northeast India. Detrital sandstone petrography, heavy mineral analysis, single grain mineral chemistry and mudrock geochemistry helped in understanding the detrital history and paleotectonic settings of the study area.

### **8.2 EOCENE PROVENANCE**

Early Eocene sandstones from Tura and Sylhet formations are fine-to coarse-grained quartzose sandstone (Fig. 16). These sandstones are dominated by monocrystalline quartz over polycrystalline quartz; feldspars and lithic fragments are rare to absent. The abundance of quartz and scarcity of feldspar and lithic fragments suggest that these sediments eroded from a low-relief area under strong chemical weathering. The dominance of monocrystalline quartz and scarcity of metamorphic lithic fragments suggest erosion from a craton, likely the Precambrian Indian Craton to the west of the present study area.

The late Eocene Kopili Formation is quartzolithic sandstone ( $Qt_{73}F_4L_{23}$ ) (Figs. 16 & 17), containing abundant metamorphic rock fragments. The presence of common polycrystalline (both foliated and non-foliated) quartz, feldspar and lithic fragments suggest a change in source-rock composition. Sandstone composition of the Kopili

Formation suggests a recycled orogenic source (Dickinson, 1985). The abundance of medium-grade metamorphic lithic fragments in this formation likely to have derived from the adjacent Shillong Plateau.

The heavy mineral assemblages of Eocene sandstones are dominated by opaque and ultrastable minerals (Figs. 25 & 26). Among the ultrastable minerals, tourmaline is more common than zircon and rutile. High maturity indices of the heavy mineral assemblages suggest long transportation of the detritus from source areas.

In comparison, Eocene sandstone compositions from two adjacent basins (i.e., Assam Basin and Bengal Basin) show variation to that of the present study area (Fig. 51). The Eocene Disang sandstones from the Schuppen Belt of upper Assam Basin are orogenic in nature. They range from quartzolithic to phyllarenitic ( $Qt_{68}F_3L_{29}$ ), and contain abundant sedimentary and metasedimentary lithic fragments suggesting a derivation from proximal orogenic source at the eastern Himalaya (Uddin et al., 2007b). In contrast, Eocene Cherra sandstones from the neighboring Bengal Basin are dominantly quartzose ( $Qt_{90}F_3L_7$  to  $Qt_{99}F_1L_0$ ) (Uddin et al., 2007). Sandstones are composed of predominantly of monocrystalline grains, with very minor polycrystalline quartz grains; polycrystalline grains and lithic fragments, having scarce metamorphic lithic fragments with no volcanic lithic fragments (Uddin and Lundberg, 1998a). As a summary, it is interpreted that in Early Eocene tectonic set up of upper Assam Basin was similar to an active plate margin; whereas in the present study area and Bengal Basin it was more likely to a passive margin setting. In late part of Eocene the study area turned to an active setting, similar to the upper Assam Basin.



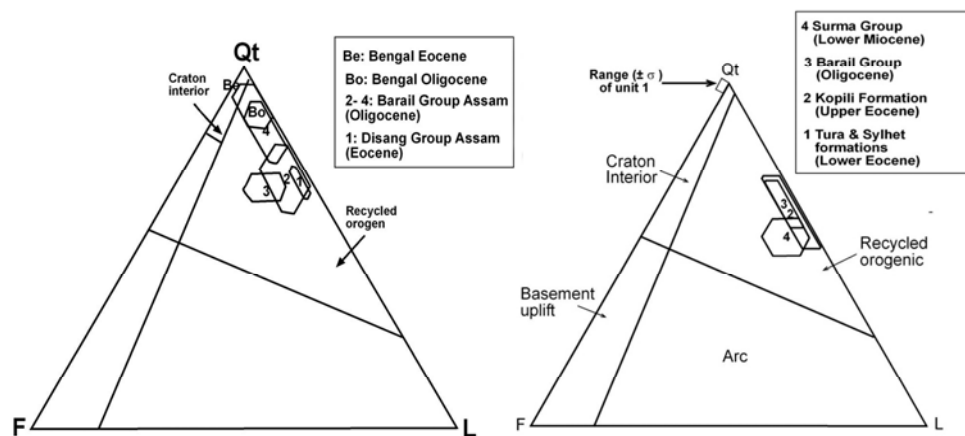


Figure 51. QtFL diagrams showing lower Cenozoic sandstone compositions from Assam Basin, Bengal Basin (Uddin et al., 2007a), and present study area.

### 8.3 OLIGOCENE PROVENANCE

Oligocene Barail sediments in the study area are composed of medium-to fine-grained sandstone and are quartzolithic ( $Qt_{65}F_4L_{31}$ ; Figs. 16 & 21). Lithic grains consist of sedimentary and metamorphic fragments; volcanic fragments are rare. All Oligocene samples from the present study area plot in the “recycled orogenic” provenance fields in QtFL and QmFLt diagrams (Figs. 16 & 17). The higher percentage of unstable lithic fragments, similar to the underlying Kopili Formation, suggests continued supply of sediments from orogenic belts. The heavy mineral maturity indices for Oligocene sandstones are lower than that of the underlying Eocene. Abundance of unstable heavy minerals, which include amphibole, serpentine, chrome-spinel, chlorite-chloritoid, suggest that the Barail sediments were derived from an orogenic belt.

Oligocene sandstone compositions from the adjacent basins (i.e., Assam and Bengal basins) also show changes with that of the present study area (Fig.51). The average compositions of Oligocene sandstones from the Schuppen Belt of upper Assam

Basin are quartzolitic to phyllarenite ( $Qt_{72}F_9L_{19}$ ) (Uddin et al., 2007b). Oligocene sandstones from upper Assam Basin are also interpreted to have been derived from sedimentary and low grade metamorphic units of an orogenic source (Uddin et al., 2007b), similar to that of the present study area. In contrast, Oligocene sandstones from the Bengal Basin are medium- to fine-grained and quartzolitic with low feldspar contents. The dominance of monocrystalline quartz and paucity of metamorphic lithic fragments and feldspars suggest derivation primarily from the Indian Craton (Uddin and Lundberg, 1998a). Minor contributions could have been from ‘recycled orogenic’ sources of the Indo-Burma Ranges (Zahid, 2005). Hence, it is interpreted that an active margin tectonic setting prevailed on the study area as well as on Assam Basin during the Oligocene.

#### **8.4 MIOCENE PROVENANCE**

Early Miocene Surma sandstones are also quartzolitic ( $Qt_{56}F_8L_{36}$ ), points to “recycled orogenic” provenance based on detrital modes (Figs. 16 & 17). Higher chert contents in Surma sandstones suggest possible derivation from the pelagic units of the eastern ophiolite belt of the Indo-Burma Ranges. Higher percentages of potassium feldspar in the Surma sandstones indicate uplift of the adjacent Shillong Plateau during the Miocene. This observation also supports the view of Clark and Bilham (2008) that the Shillong Plateau was uplifted in the Miocene. Heavy mineral maturity indices for Miocene sandstones is lower compared to underlying Barail sandstones indicating a shorter transport history of detritus than that in the Barail sands. The Indo-Burma orogenic front was most likely located close to the study area during the Miocene.

Miocene sandstone composition from the adjacent basins (i.e., Assam and Bengal basins) shows temporal relationship in detrital history in comparison to the study area.

Miocene Surma unit in the Schuppen Belt of upper Assam is not well developed and rests

on the Oligocene-Miocene unconformity. This indicates that at the end of the Oligocene the whole area was exposed. Average compositions of the Miocene sands are quartzolitic in composition (Kumar, 2004; Rahman, 2008) and points to “recycled orogenic” provenance. The younger Miocene units in this area are rich in plagioclase and lithic fragments, suggesting tectonic loading at the hinterland (Kumar, 2004). Sandstone units from Miocene Surma Group of the Bengal Basin have much higher feldspar contents compared to the underlying Barail Group, and are quartzolitic to quartzofeldspathic in composition suggesting derivation from uplifted eastern Himalaya and the Indo-Burma Ranges (Uddin and Lundberg, 1998a; Zahid, 2005). In summary, this can be suggested that an active margin setting existed during early Miocene on the study area and Bengal Basin.

## **8.5 MICROPROBE ANALYSIS**

### **8.5.1 Tourmaline**

Tourmalines are ubiquitous minerals throughout the lower Cenozoic sections in the study area. Detrital tourmaline grains are predominantly alkali groups (Fig. 31) and belongs to schorl-dravite solid solution series. Schorl belongs to the granitic group of rocks, whereas the magnesian tourmalines are usually found in mafic igneous rocks. In Henry and Guidotti's (1985) Al-Fe(tot)-Mg environmental diagram (Figs.32 & 33) suggests probable source of tourmalines in the study area are metapelites, metapsammities, and quartz-tourmaline rocks. A few younger Miocene samples are interpreted to have derived from Li-poor granitoids and associated pegmatites and aplites. Hence it can be concluded that the tourmalines found in the present study area were derived from two distinct sources; recycled sedimentary rocks of the Indo-Burma Ranges and the

Himalayas, and granitoids and associated pegmatite, probably from the adjacent Shillong Plateau.

### **8.5.2 Chrome Spinel**

Chrome spinels are common in Oligocene and Miocene sandstone in the study area. These are generally associated with the mafic and ultramafic suite of rocks. Plot of  $Fr^{3+}/(Fe^{3+}+Cr+Al)$  against Mg# (Fig. 35) shows most of the detrital chrome spinel grains are derived from the Alpine-type or Stratiform peridotites (Irvine, 1974). However, these chrome spinel are not rich enough in  $Fe^{3+}$  to have been derived from a stratiform peridotite complex. Spinel with high Al (Cr # = 0.10-0.30) and high Mg (Mg # 0.70-0.85) contents are common constituents of abyssal peridotites, dunites, and basalt (Dick and Bullen, 1984). The majority of the chrome spinels from this area have low Al but high Cr content (Cr# 0.36 to 0.8) (Fig. 36). Low-Al, low Mg, and high Cr# in majority of the spinel suggest that they were not derived from mid-oceanic ridge basalts. Considering the geotectonic configuration of this basin, it is suggested that spinels were derived from the Alpine-type ophiolite complex (Naga ophiolites) to the east or from Ti-poor continental flood basalt of the Indian Craton. Abundance serpentine grains in heavy mineral fractions of Oligocene and Miocene sandstone also points to ultramafic ophiolite source of the Indo-Burma Ranges.

### **8.5.3 Garnet**

Garnets are not abundant in sandstones in the study area. These are found only in a few Oligocene and Miocene units. Most of the garnets show solid solution between almandine and pyrope with <10% grossular (Fig. 41). The wide range of pyrope and

grossular contents suggest a wide spectrum of metamorphic facies, ranging from greenschist-amphibolite to granulite facies metamorphism (Fig. 43) with a wide range of P-T conditions in the source region. Wide range of metamorphic rocks, reported from Shillong Gneissic Complex (i.e., from Shillong Plateau) to the northwest and from Mogok Schist Belt to the east of study area, could be the probable source for Oligocene and Miocene garnets.

## **8.6 MUDROCK GEOCHEMISTRY**

Discriminant function analysis (Roser and Korsch, 1988) shows that the majority of the samples are recycled mature polycyclic quartzose detritus (Fig. 49). Mudrocks from Jaintia Group suggest a wide source rock composition intermediate to felsic, probably the granitic-granodioritic rock from the eastern Indian Craton. The majority of samples from the area have higher concentrations of Zr compared to the average crust, (PAAS; Fig. 47B). Mudrock data from Miocene Surma Group of rocks fall in the polycyclic quartzose field of Roser and Korsch (1988) diagram, similar to the coeval sediments from the neighboring Bengal Basin (Rahman and Suzuki, 2007; Rahman, 2008). Therefore, the source of Surma sediments in the study area and the Bengal Basin are similar source areas.

Chemical indices of alteration (CIA) for mudrocks from the study area range from 67-79%, indicating medium to high intensity of weathering. No effects of K-metasomatism in the source area have been observed. The moderate to high values of CIA suggest tropical climates prevailing in the source terranes (Nesbitt et al., 1997).

## 8.7 PALEOTECTONIC SETTING

Modal composition of sandstones from the present study area reflects the changes in detrital history and hinterland tectonics. Quartzose composition, paucity of unstable grains (e.g., lithic fragments and feldspar), and high ZTR indices of sandstone from the early Eocene Tura and Sylhet formations of the Jaintia Group suggest proximity to the stable Indian Craton (Fig. 52A). A switch of provenance (i.e., from stable craton to orogenic belts) occurs during late Eocene in the study area, evidenced by quartzolitic sandstone compositions and mudrock chemistry. The upper Assam Basin was receiving sediments from the orogenic belts from early Eocene time. The Himalaya and Indo-Burma Ranges probably supplied sediments in both upper Assam and study area during the late Eocene (52B). In contrast, coeval Eocene strata in the Bengal Basin are highly mature, suggesting sediment derivation from the Indian Craton to the west. So in late Eocene, the Bengal Basin was not in the immediate south of the present area.

During the Oligocene and Miocene, the study area received sediments continuously from orogenic source as revealed from sandstone composition and mudrock chemistry data. The depositional lobe, which formed in upper Assam during the Eocene, prograded south-southwestward over study area and western part of Indo-Burma Ranges (Fig. 52C,D). This lobe followed a northeast-southwest oriented asymmetrical syncline, the shallow western flank of which was in the present study area, and the eastern deeper part was on the western part of Indo-Burma Ranges. Deep marine turbidite beds have been reported from Oligocene sequences from the deeper flank side of the asymmetric syncline (Dasgupta et al., 2005). Due to continuous crustal shortening, the underlying Disang Formation started to deform, and the Barail sediments were deposited on top of

deformed Disang beds in deeper part of the basin. In the present study area, the Barail sediments were deposited on undeformed Janitia units in shallower part of the trough. A similar scenario is reported from upper Assam (Kent et al., 2002). Towards the end of Oligocene, the basin was shallowing up in the upper Assam area. This can be explained by high rate of uplift in the hinterland area located to the north and east; and the sea receded southward prevailing a shallow-water deltaic environment in upper Assam. During this time, the study area witnessed shallow water sedimentation, whereas western part of Indo-Burma Ranges was milieu for deep water sedimentation (Dasgupta and Biswas, 2000). Source of sediments during this time was continued to be orogenic belts, evidenced by the sandstone modal data, chrome-spinel data, and mudrock geochemistry data from the study area. During the Miocene, depositional lobe prograded further south-southwestward over the study area and the Bengal Basin (Fig. 52). Due to continuous crustal shortening, the Indo-Burma Ranges became a structural high towards the end of Oligocene-Miocene and became the source of detritus in the basin near the study area and the Bengal Basin. This is indicated by low ZTR indices, chrome spinel data, abundance of serpentine and chert grains from Miocene sandstones of the study area. Synorogenic sedimentation continued in the Bengal and upper Assam basins, and Tipam and Dupi Tila sandstones were deposited in front of the Indo-Burma Ranges. Toward the east of the present study area post Mio-Pliocene Naga-Haflong thrust brought the Eocene Disang unit against the upper Miocene to Pliocene Dupi Tila sequences. Probably, the current location of the Naga-Haflong thrust delineates the western periphery of the deformation front of the Paleogene accretionary prism of this area.

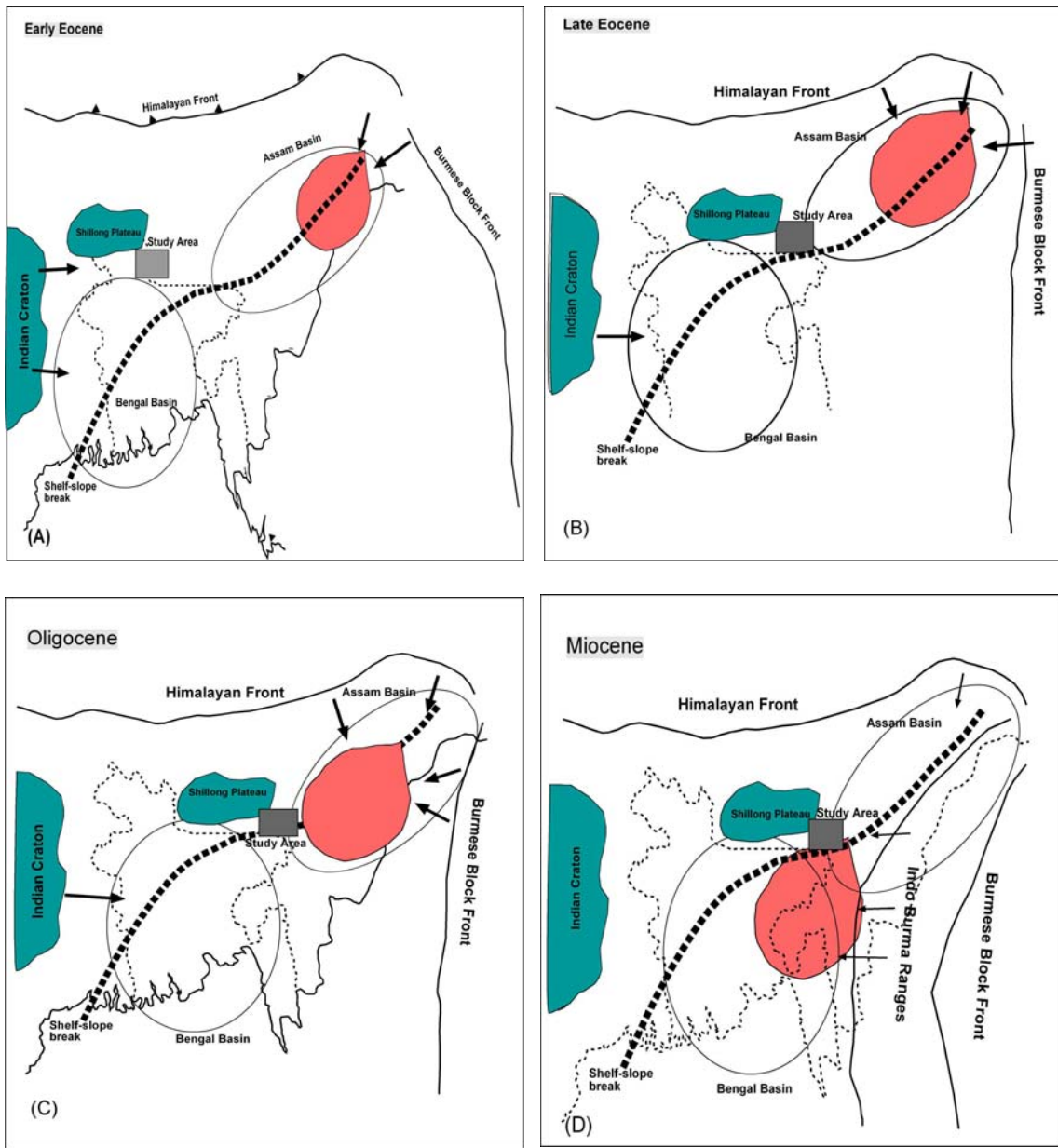


Figure 52. Paleogeographic reconstruction of the present study area (in black box) with reference to Assam and Bengal basin. Red body is the deposition lobe prograding basinward with time and progressive uplift of the hinterland blocks.



## 8.8 CONCLUSIONS

Based on the sandstone modal composition, heavy mineral assemblages, mineral chemistry and mudrock geochemistry, these following inference can be drawn from this study:

1. During the early part of Eocene the present area was receiving detritus from Indian Craton, similar to the Bengal Basin. In the later part of Eocene, Oligocene and Miocene, the study area became a basin of orogenic sedimentation.
2. Large scale depositional lobes migrated south-southwest in the Assam-Bengal system as the orogenic belts were uplifted in the north and east.
3. High chrome #, low Al and Mg contents, and abundance of serpentine and chert grains in the younger sequences suggest derivation from tectonic mélange zones to the eastern part of the Indo-Burma Ranges.
4. Mudrock data support that the orogenic sedimentation started sometime towards the end of Eocene. The chemical index of alteration shows moderate weathering in the source rock terranes.
5. Presences of upper grade metamorphic lithic fragments in several Miocene strata indicate that the Shillong Plateau was uplifted by the Miocene as opposed to the existing view that the uplift has been a Pliocene event.

## REFERENCES

- Acharyya, S. K., 1980, Structural framework and tectonic evolution of the Eastern Himalaya: Geological Survey of India, v. 10, p. 412-439.
- , 1998, Break-up of the greater Indo-Australian continent and accretion of the blocks framing south and East Asia: Journal of Geodynamics, v. 26, p. 149-170.
- , 2007a, Collisional emplacement history of the Naga-Andaman ophiolites and the position of the eastern Indian suture: Journal of Asian Earth Sciences, v. 29, p. 229-242.
- , 2007b, Evolution of the Himalyan Palogene foreland basin, influence of its litho-packet on the formation of the thrust-related domes and windows in the Eastern Himalayas- A overview: Journal of Asian Earth Sciences, v. 31, p. 1-17.
- Acharyya, S. K., and Ray, K. K., 1982, Concealed Mesozoic-Paleogene sediments below the Himalayan nappe, their hydrocarbon possibilities-reappraisal in the light of recent finding: American Association of Petroleum Geologists Bulletin, v. 66, p. 57-70.
- Alam, M., Alam, M. M., Curray, J. R., Chowdhury, M. L. R., and Gani, M. R., 2003, An overview of the sedimentary geology of the Bengal Basin in relation to the regional tectonic framework and basin-fill history: Sedimentary Geology, v. 155, p. 179-208.
- Amano, K., and Taira, A., 1992, Two-phase uplift of Higher Himalayas since 17 Ma: Geology v. 20, p. 391-394.
- Arai, S., 1992, Chemistry of chromian spinel in volcanic rocks as a potential guide to magma chemistry: Mineralogical Magazine, v. 56, p. 173-184.
- Asiedu, D. K., Suzuki, S., Nogami, K., and Shibata, T., 2000, Geochemistry of lower Cretaceous sediments, inner zone of southwest Japan: Constraints on provenance and tectonic environment journal of Geochemistry, v. 34, p. 155-173.
- Barnes, s. J., and Roeder, P., 2001, The range of spinel compositions in terrestrial mafic and ultramafic rocks: Journal of Petrology, v. 42, p. 2279– 2302.

- Bastia, R., 2006, An overview of Indian sedimentary basins with special focus on emerging east coast deepwater frontiers *The Leading Edge*, v. 25, no. 7, p. 818-829.
- Basu, A., 1976, Petrology of Holocene alluvial sand derived from plutonic source rocks; implication to paleoclimate interpretation: *Journal of Sedimentary Petrology*, v. 4, p. 694-709.
- , 2003, A Perspective on quantitative provenance analysis.: In: Valloni, R., Basu, A. (Eds.), *Quantitative Provenance Studies in Italy, Memorie Descrittive della Carta Geologica dell'Italia*, v. 61, p. 11-22.
- Basu, A., and Molinaroli, E., 1991, Reliability and application of detrital opaque Fe-Ti oxide minerals in provenance determination. In Morton, A.C., Todd, S.P., Haughton, P.D., Eds., *Developments in sedimentary provenance studies*. British Geological Society Special Publications, v. 57, p. 55-65.
- Basu, A., Young, S. W., Suttner, L. J., James, W. C., and Mach, G. H., 1975, Re-evaluation of the use of undulatory extinction and polycrystallinity in detrital quartz for provenance interpretation: *Journal of Sedimentary Petrology*, v. 45, p. 873-882.
- Basu, A.R., and Macgregor, I.D., 1975, Chromite spinels from ultramafic xenoliths: *Geochimica et Cosmochimica Acta*, v.39, p. 937-945.
- Bhandari, L. L., Fuloria, R. C., and Sastri, V. V., 1973 Stratigraphy of Assam Valley: *American Association of Petroleum Geologists Bulletin*, v. 57, p. 642-657.
- Bhatia, M., 1983, Plate tectonics and geochemical composition of sandstones: *Journal of Geology*, v. 91, p. 611-627.
- Bhatia, M. R., and Crook, K. A. W., 1986, Trace element characteristics of graywacke and tectonic setting discrimination of sedimentary basins: *Contributions to Mineralogy and Petrology*, v. 92, p. 181-193.
- Bhattacharyya, C. C., 1991, The ophiolites of northeast India - a subduction zone ophiolite complex of the Indo-Burma orogenic belt: *Tectonophysics*, v. 191, p. 213-222.
- Bhattacharyya, P. M., and Kayal, J. R., 2002, Fractal dimension and b-value mapping of in the northeast India: *Current Science*, v. 82, p. 1486-1491.
- Bock, B., McLennan, S. M., and Hanson, G. N., 1998, Geochemistry and provenance of the middle Ordovician Austin Glen member (Normanskill Formation) and the Taconian orogeny in New England: *Journal of Sedimentology*, v. 45, p. 635-655.

- Brunnschweiler, R. O., 1966, On the Geology of the Indo-Burma Ranges: *Journal Geological Society of Australia*, v. 13, no. 1, p. 137-194.
- Burbank, D. W., Beck, R. A., and Mulder, T., 1996, The Himalayan Foreland Basin: In: Yin, A., Harrison T.M., eds., *The Tectonic evolution of Asia*: Cambridge University Press, p. 149-188.
- Camire', G. E., Lafleche, M. R., and Ludden, J. n., 1993, Archean metasedimentary rocks from the northwestern Pontiac superprovince of the Canadian Shield: Chemical characterization, weathering and modeling of the source areas: *Precambrian Research*, v. 62, no. 285-305.
- Cervený, P. F., 1986, Uplift and erosion of the Himalaya over the past 18 Million years: Evidence from fission track dating of detrital zircon and heavy mineral analysis [Unpublished M.S. thesis]: Dartmouth College, 198 p.
- Chandra, D., Mazumdar, K., and Basumallick, S., 1983, Distribution of Sulphur in the Tertiary Coals of Meghalaya, India: *International Journal of Coal Geology*, v. 3, p. 63--75.
- Chatterjee, N., Mazumder, A. C., Bhattacharya, A., and Saikia, R. R., 2007, Mesoproterozoic granulites of the Shillong-Meghalaya Plateau, Evidence of westward continuation of the Prydz Bay Pan-African suture into northeastern India: *Precambrian Research*, v. 152, p. 1-26.
- Chattopadhyay, B., Venkataramana, P., Roy., D.K., Ghosh, S., and Bhattacharyee, S., 1983, *Geology of Naga Hills ophiolites*: Bangalore, Geological Survey of India, 112 p.
- Clark, M. K., and Bilham, R., 2008, Miocene rise of the Shillong Plateau and the beginning of the end for the Eastern Himalaya: *Earth and Planetary Science Letters*, v. 269, p. 337-351.
- Condie, K. C., 1993, Chemical composition and evolution of the upper continental crust: Contrasting results from surface samples and shale: *Chemical Geology*, v. 104, p. 1-37.
- Cookinboo, H. O., Bustin, R. M., and Wilks, K. R., 1997, Detrital chromian Spinel composition used to reconstruct the tectonic setting of the Provenance: Implication for orogeny in the Canadian cordillera: *Journal of sedimentary research*, v. 67, no. 1, p. 116-123.
- Cox, R., Lowe, D. R., and Cullers, R. L., 1995, The influence of sediment recycling and basement composition on evolution of mudrock chemistry in the southwestern United States: *Geochimica et Cosmochimica Acta*, v. 59, no. 4, p. 2919-2940.

- Curry, J. R., Moore, D. G., Lawver, L. A., Emmel, F. J., Taitt, R. W., Henry, M., and Kieckhefer, R., 1979, Tectonics of the Andaman Sea and Burma, in Watkins, J.S., Montadert, L., and Dickinson, P., eds., Geological and geophysical investigations of continental margins: American Association of Petroleum Geologists, Memoir 29, p. 189-198.
- Dasgupta, A. B., 1977, Geology of Assam and Arakan region: Quaternary Journal of Geology, Mineralogical, Metallurgical Society of India, v. 49, p. 1-54.
- Dasgupta, A. B., and Biswas, A. K., 2000, Geology of Assam: Geological Society of India, Bangalore, 169 p.
- Dasgupta, P.K., Mukherjee, R., and Biswas, A., 2005, Evolution of the Assam-Arakan orogen: Basinal configuration and sedimentation: Himalaya (Geological Aspects), v. 1, Saklani, P.S, eds., Satish Serial Publishing Home, Delhi, p. 465-493.
- Daurah, R., Saikia, M. M., and Bhattacharya, C. C., 1983, Occurrence of radiolarian cherts in flysch-ophiolite succession of Indo-Burma orogen: Geological Magazine, v. 120, p. 178-182.
- DeCelles, P.G., Gehrels, G.E., Quade, J., Ojha, T.P., Kapp, P.A., and Upreti, B.N., 1998, Neogene foreland basin deposits, erosional unroofing, and the kinematic history of the Himalayan fold-thrust belt, western Nepal: Geological Society of America Bulletin, v. 110, p. 2-21.
- DeCelles, P.G., Robinson, D.M., Quade, J., Ojha, T.P., Garzzone, C.N., Copeland, P., and Upreti, B.N., 2001, Stratigraphy, structure, and tectonic evolution of the Himalayan fold-thrust belt in western Nepal: Tectonics, v. 20, p. 487-509.
- DeCelles, P. G., Gehrels, G. E., Najman, Y., Martin, A. J., and Garzanti, E., 2004, Detrital geochronology and geochemistry of Cretaceous-early Miocene strata of Nepal: Implication for timing and diachroneity of initial Himalaya orogenesis: Earth and Planetary Science Letters, v. 227, p. 313-330.
- Deer, W. A., Howie, R. A., and Zussman, J., 1992, An introduction to the rock-forming minerals: Harlow, United Kingdom, Longman Scientific Technical, 696 p.
- Dick, H. J. B., and Bullen, T., 1984, Chromian spinel as a petrogenetic indicator in abyssal and alpine-type peridotites and spatially associated lavas: Contributions to Mineralogy and Petrology, v. 86, p. 54-76.
- Dickinson, W. R., 1970, Interpreting detrital modes of greywacke and arkose: Journal of Sedimentary Petrology, v. 40 p. 695-707.

- , 1985, Interpreting provenance relations from detrital modes of sandstones, *in* Zuffa, G.G., ed., *Reading Provenance from Arenites*: Dordrecht, The Netherlands, Riedel, p. 333-361.
- Dickinson, W. R., Ingersoll, R. V., Cowan, D. S., Helmo, K. P., and Suczek, C. A., 1982, Provenance of Franciscan graywackes in coastal California: *Geological Society of America Bulletin*, v. 93, p. 95-107.
- Dickinson, W. R., and Suczek, C., 1979, Plate Tectonics and Sandstone compositions: *American Association of Petroleum Geologists Bulletin*, v. 63, p. 2164-2182.
- Dorsey, R. J., 1988, Provenance evolution and unroofing history of a modern arc-continent collision: Evidence from petrography of Plio-Pleistocene sandstones, eastern Taiwan: *Journal of Sedimentary Petrology*, v. 58, p. 208-218.
- Evans, P., 1964, The tectonic framework of Assam: *Journal of Geological Society of India*, v. 5, p. 80-96.
- Falvey, D. A., 1974, The development of the continental margins in plate tectonic theory: *Journal of Australian Petroleum Exploration Association*, v. 14, p. 95-106.
- Fedo, C. M., Eriksson, K. A., and Krogstad, E. J., 1996, Geochemistry of Shales from the Archean (~3.0 Ga) Buhwa Greenstone Belt, Zimbabwe: Implications for Provenance and source-area weathering: *Geochimica et Cosmochimica Acta*, v. 60, p. 1751-1763.
- Fedo, C. M., Nesbitt, H. W., and Young, G. M., 1995, Unraveling the effects of metasomatism in sedimentary rocks and paleosols, with implications for paleoweathering conditions and provenance: *Geology*, v. 23, p. 921-924.
- Feng, R., and Kerrich, R., 1990, Geochemistry of fine grained clastic sediments in the Archean Abitibi Greenstone Belt, Canada: Implication for provenance and tectonic setting: *Geochimica et Cosmochimica Acta*, v. 54, p. 1061-1081.
- Fleet, W.F., 1926, Petrological notes on the Old Red Sandstones of the West Midlands: *Geological Magazine*, v. 63, p. 505-516.
- Ganju, J. L., Khar, B. M., and Chaturvedi, J. G., 1986, Geology and hydrocarbon prospects of Naga Hill, south of 27 degree latitude: *Bulletin Oil and Natural Gas Commissions of India*, v. 86, p. 129-145.
- Ghosh, S., Fallick, A. E., Paul, D. K., and Potts, P. J., 2005, Geochemistry and origin of Neoproterozoic granitoids of Meghalaya, northeast India: Implication for linkage with amalgamation of Gondwana supercontinent: *Gondwana Research*, v. 8, p. 421-432.

- Ghosh, S., S.Chakrabarty, Paul, D. K., Bhalla, J. K., Bishui, P. K., and Gupta, S. N., 1994, New Rb-Sr isotopic ages and geochemistry of granitoids from Meghalaya and their significance in middle to late Proterozoic crustal evolution: *Indian Minerals*, v. 48, p. 33-44.
- Graham, S. A., Ingersoll, R. V., and Dickinson, W. R., 1976, Common provenance for lithic grains in Carboniferous sandstones from Ouachita Mountains and Black Warrior Basin: *Journal of Sedimentary Petrology*, v. 46, p. 620-632.
- Gururajan, N. S., and Choudhuri, B. K., 2003, Geology and tectonic history of the Lohit Valley, Eastern Arunachal Pradesh, India *Journal of Asian Earth Sciences*, v. 21, p. 731-743.
- Hallsworth, C. R., and Chisholm, J. I., 2000, Stratigraphic evolution of provenance characteristics in Westphalian sandstones of the Yorkshire coalfield: *Proceedings of the Yorkshire Geological Society*, v. 53, p. 43–72.
- Hawthorne, F. C., MacDonald, D. J., and Burns, P. C., 1993, Reassignment of cation site occupancies in tourmaline: Al-Mg disorder in the crystal structure of dravite: *American Mineralogist*, v. 78, p. 265-270.
- Hayashi, K.-I., Fujisawa, H., Holland, H. D., and Ohmoto, H., 1997a, Geochemistry of 1.9 Ga sedimentary rocks from northeastern Labrador, Canada: *Geochimica et Cosmochimica Acta*, v. 61, p. 4115-4137.
- Hayashi, K. I., H.Fujisawa, Holland, H. D., and H.Ohmoto, 1997b, Geochemistry of 1.9 Ga sedimentary rocks from northeastern Labrador, Canada: *Geochimica et Cosmochimica Acta*, v. 61, p. 4115–4137.
- Hekinian, R., 1985, *Petrology of the ocean floor*: Amsterdam, Elsevier, 407 p.
- Henry, D. J., and Dutrow, B. L., 1992, Tourmaline in a low grade clastic metasedimentary rocks: an example of the petrogenetic potential of tourmaline: *Contributions to Mineralogy and Petrology*, v. 112, p. 203-218.
- Henry, D. J., and Guidotti, C. V., 1985, Tourmaline in the staurolite grade metapelites of NW Maine: a petrogenetic indicator mineral: *American Mineralogist*, v. 70, p. 1-15.
- Hisada, K., Arai, S., and Lee, Y. I., 1999, Tectonic implication of lower Cretaceous chromian spinel-bearing sandstones in Japan and Korea: *The Island Arc*, v. 8, p. 336-348.
- Hodges, K. V., 2000, Tectonics of the Himalaya and southern Tibet from two perspectives: *Geological Society of America Bulletin*, v. 112, p. 324-350.

- Ingersoll, R. V., 1978, Petrofacies and petrologic evolution of the Late Cretaceous fore-arc basin, northern and central California: *Journal of Geology*, v. 86, p. 335-352.
- Ingersoll, R. V., Bullard, T. F., Ford, R. L., Grimm, J. P., Pickle, J. D., and Sares, S. W., 1984, The effect of grain size on detrital modes: A test of the Gazzi-Dickenson point-counting method: *Journal of Sedimentary Petrology*, v. 54, p. 103-116.
- Irvine, T. N., 1977, Origin of chromitite layers in the Muskox Intrusion and other stratiform intrusions; a new interpretation: *Geology*, v. 5 p. 273-277.
- Irvine, T.N., 1974, Petrology of the Duke Island ultramafic complex, southern Alaska: *Geological Society of America Bulletin*, v. 138, p. 240.
- Jauhri, A. K., and Agarwal, K. K., 2001, Early Palaeogene in the south Shillong Plateau, NE India: local biostratigraphic signals of global tectonic and oceanic changes: *Palaeogeography, Palaeoclimatology, Palaeoecology*, v. 168, p. 187-203.
- Johnson, M. J., 1993, The system controlling the composition of clastic sediments. : In: Johnson M.J., Basu A, eds., *Processes controlling the composition of clastic sediments*. Boulder, Geological Society of America, p. 1-19.
- Johnson, S. Y., and Alam, A. M. N., 1991, Sedimentation and tectonics of the Sylhet trough, Bangladesh: *Geological Society of America Bulletin*, v. 103, p. 1513-1527.
- Kasanzu, C., Maboko, M. A. H., and S. Many, 2008, Geochemistry of the fine-grained clastic sedimentary rocks of the Neoproterozoic Ikorongo Group, NE Tanzania: Implication for provenance and source rock weathering: *Precambrian Research*, v. 164, p. 201-213.
- Kent, W. N., and Dasgupta, U., 2004, Structural evolution in response to fold and thrust belt tectonics in northern Assam. A key to hydrocarbon exploration in the Jaipur anticline area: *Marine and Petroleum Geology* v. 21, p. 785-803.
- Kent, W. N., Hickman, R. G., and Dasgupta, U., 2002, Application of ramp/flat model to interpretation of the Naga thrust and possible implication for petroleum exploration along the Naga thrust front: *American Association of Petroleum Geologists Bulletin*, v. 86, p. 2023-2045.
- Kumar, D., Mamallan, R., and Dwivedy, K. K., 1996, Carbonatite magmatism in northeast India: *Journal of Southeast Asian Earth Sciences*, v. 13, p. 145-158.
- Kumar, P., 2004, Provenance history of Cenozoic sediments near Digboi-Margherita area, eastern syntaxis of the Himalayas, Assam, northeast India [Unpublished M.S. Thesis]: Auburn University, 131 p.



- Lee, T. T., and Lawver, L. A., 1995, Cenozoic plate reconstruction of Southeast Asia: *Tectonophysics*, v. 251, p. 85-138.
- Lee, Y. I., 2002, Provenance derived from the geochemistry of the Paleozoic-early Mesozoic mudrocks of the Pyeongan Supergroup, Korea: *Sedimentary Geology*, v. 149, p. 219-235.
- Mack, G.H., 1984, Exceptions to the relationship between Plate Tectonics and sandstone composition: *Journal of Sedimentary Research*, v. 54, p. 54-65.
- Le Fort, P., 1996, Evolution of the Himalaya, in Yin, A., and Harrison, M., eds., *The tectonic evolution of Asia: New York, Cambridge University Press, World and Regional Geology Series*, p. 95-109.
- Lihou, J. C., and Mange-Rajetzky, M. A., 1996, Provenance of the Sardona Flysch, eastern Swiss Alps: example of high-resolution heavy mineral analysis applied to an ultrastable assemblage: *Sedimentary Geology*, v. 105, p. 141-157.
- Mamallan, R., Kumar, D., and Bajpai, R.K., 1994, Jasra ultramafic-mafic-alkaline complex: a new find in the Shillong Plateau, Northeastern India: *Current Science*, v.66, p.64-65.
- Mange, M. A., and Maurer, H. F. W., 1992, *Heavy minerals in color*: London, Chapman & Hall, London, 147 p.
- Mathur, N., Raju, S. V., and Kulkarni, T. G., 2001, Improved identification of pay zones through integration of geochemical and log data: A case study from upper Assam basin: *American Association of Petroleum Geologists Bulletin*, v. 85, p. 309-323.
- Mazumdar, S. K., 1976, A summary of the Precambrian geology of the Khasi Hills, Meghalaya: *Miscellaneous publication, Geological Survey of India*, v. 23, p. 311-334.
- McLennan, S. M., 1989, Rare earth elements in the sedimentary rocks: influence of provenance and sedimentary processes: *Reviews in Mineralogy and Geochemistry*, v. 21, p. 169-200.
- McLennan, S. M., Barbara, B., Hemming, S. R., Hurowitz., J. A., lev, S. M., and McDaniel, D. K., 2003, The role of provenance and sedimentary processes in the geochemistry of sedimentary rocks. In *Geochemistry of sediments and sedimentary rocks: Evolutionary considerations to mineral deposit-forming environments*, Geological Association of Canada, v.4, p. 7-38.
- McLennan, S. M., Hemming, S., McDaniel, D. K., and Hanson, G. N., 1993, Geochemical approaches to sedimentation, provenance and tectonics. In Johnson, M. J., Basu, A., eds, *processes controlling the composition of the clastic*

- sediments: Geological Society of America., Boulder, Colorado, Special Paper, v. 284, p. 21-40.
- Misra, B. K., 1992, Optical properties of some Tertiary coals from northeastern India: their depositional environment and hydrocarbon potential: *International journal of Coal Geology*, v. 20, p. 115-144.
- Mitra, S., and Mitra, C., 2001, Tectonics setting of the Precambrian of the northeastern India, Meghalaya Plateau, and age of the Shillong group of rocks: *Geological Survey of India Special publication*, v. 64, p. 653-658.
- Morton, A., Hallsworth, C., and Chalton, B., 2004, Garnet compositions in Scottish and Norwegian basement terrains: a framework for interpretation of North Sea sandstone provenance: *Marine and Petroleum Geology*, v. 21, p. 393-410.
- Morton, A. C., 1985, A new approach to provenance studies: electron microprobe analysis of detrital garnets from Middle Jurassic sandstones of the northern North Sea: *Sedimentology*, v. 32, p. 553-566.
- , 1991, Geochemical studies of heavy minerals and their application to provenance research. In: Morton, A.C., Todd, S.P., Haughton, P.D.W, eds., *Development in sedimentary provenance studies*, Geological Society of London Special Publication, v. 57, p. 31-45.
- Morton, A. C., and Hallsworth, C. R., 2007, Stability of detrital heavy mineral during burial diagenesis. In: Mange, M. A., Wright, D.T. eds., *Heavy Mineral in Use, Development in Sedimentology*, p. 215-246.
- Morton, A. C., and Hallsworth, H. C., 1994, Identifying provenance-specific features of detrital heavy mineral assemblages in sandstones: *Sedimentary Geology*, v. 90, p. 241-256.
- Morton, A. C., and Taylor, P. N., 1991, Geochemical and isotopic constraints on the nature and age of basement rocks from Rockall bank, NE Atlantic: *Journal of the Geological Society, London*, v. 148, p. 630-634.
- Naik, G. C., Kumar, R., and Soren, M. N., 2004, Tectonic setting and petroleum system of pre-Tertiary sediments, Assam Basin, northeast India: 5<sup>th</sup> Conference & Exposition on Petroleum Geophysics, Hyderabad, India, p. 365-371.
- Najman, Y., Bickle, M., BouDagher-Fadel, M., Carter, A., Garzanti, E., Paul, M., Wijbrans, J., Willett, E., Oliver, G., Parrish, R., Akhter, S. H., Allen, R., Ando, S., Chisty, E., Reisberg, L., and e, G. V., 2008, The Paleogene record of Himalayan erosion: Bengal Basin, Bangladesh: *Earth and Planetary Science Letters*, v. 273, p. 1-14.

- Nanayama, F., 1997, An electron microprobe study of the Amazon Fan: Proceedings of the Ocean Drilling Program, Scientific Results, v. 155, p. 147-168.
- Nandy, D. R., 2001, Geodynamics of Northeastern India and the adjoining region: Kolkata, ACB Publication, 209 p.
- Nesbitt, H. W., Fedo, C. M., and Young, G. M., 1997, Quartz and feldspar stability steady and non-steady state weathering, and petrogenesis of siliciclastic sands and muds: *Journal of Geology*, v. 105, p. 173-191.
- Nesbitt, H. W., and Young, G. M., 1984, Prediction of some weathering trend of plutonic and volcanic rocks based on thermodynamic and kinetic considerations: *Journal of Geology*, v. 48, p. 1523-1534.
- Pandey, J., 1990, Cretaceous/Tertiary boundary, iridium anomaly and foraminiferal breaks in the Um Sohryngkew river section, Meghalaya: *Current Science*, v. 59, p. 570-575.
- Pettijohn, F. J., Potter, P. E., and Siever, R., 1987, *Sand and Sandstone*: Berlin, Springer-Verlag, 553 p.
- Rahman, M. J. J., and Faulp, P., 2003, The composition of the subsurface Neogene shales of the Surma group from the Sylhet Trough, Bengal Basin, Bangladesh: *Sedimentary Geology*, v. 155, p. 407-417.
- Rahman, M. J. J., and Suzuki, S., 2007, Geochemistry of sandstones from the Miocene Surma Group, Bengal Basin, Bangladesh: Implications for Provenance, tectonic setting and weathering: *Geochemical Journal*, v. 41, p. 415-428.
- Rahman, M. W., 2008, Sedimentation and Tectonic Evolution of Cenozoic Sequences from Bengal and Assam Foreland Basins, Eastern Himalayas [Unpublished M.S. Thesis]: Auburn University, 180 p.
- Rajasekhar, R. P., and Mishra, D. C., 2008, Crustal structure of Bengal Basin and Shillong Plateau: extension of Eastern Ghat and Satpura Mobile Belts to Himalayan fronts and seismotectonics: *Gondwana Research*, v. 14, p. 523-534.
- Rangarao, A., 1983, Geology and Hydrocarbon Potential of a part of Assam-Arakan Basin and its adjacent area: *Petroleum Asia Journal*, p. 127-158.
- Roddaz, M., J.Viers, S.Bruset, Baby, P., Boucayrand, C., and Herail, G., 2006, Controls on weathering and provenance in the Amazonian foreland basin: insight from major and trace element geochemistry of Neogene Amazonian sediments: *Chemical Geology*, v. 226, p. 31-65.

- Roser, B. P., and Korsch, R. J., 1988, Provenance signatures of sandstone-mudstone suites determined using discriminant function analysis of major-element data *Chemical Geology*, v. 67, p. 119-139.
- Sabeena, H. M., Ramanujama, N., and Morton, A. C., 2002, The provenance of garnet: constraints provided by studies of coastal sediments from southern India *Sedimentary Geology*, v. 152, no. 3-4, p. 279-287.
- Saha, T., Chowdhury, B.K., Chakraborty, D., Prusty, S.K., Khatri, B. L., and Reddy, G.V., 2006, Understanding structural configuration on the basis of 3D seismic attributes in Dhansiri Valley, Assam: *Geohorizon*, January, p. 28-31.
- Saikia, M. M., 1999, Indo-Burma orogenic belt, its plate tectonic evolution, in *Geological studies in Eastern Himalayas: Delhi, Pilgrims Book (Pvt.) Ltd.* p. 19-39
- Samanta, B. K., and Raychoudhury, A. K., 1983, A revised lithostratigraphic classification of the Cretaceous-Lower Tertiary shelf sediments of eastern Khasi and Jaintia Hills, Meghalaya: *Quaternary Journal of Geology, Mineralogical, Metallurgical Society of India* v. 55, p. 101-129.
- Sengupta, S., Ray, K. K., Acharyya, S. K., and Smith, J. B. D., 1990, Nature of ophiolite occurrence along the eastern margin of the Indian plate and their tectonic significance: *Geology*, v. 18, p. 439-442.
- Singh, M. P., 1989, On the origin of fusain in the Tertiary coals of Meghalaya: *Journal of Geological Society of India*, v. 33, p. 99-103.
- Singh, M. P., and Singh, A. K., 2000, Petrographic characteristics and depositional conditions of Eocene coals of platform basins, Meghalaya, India: *International Journal of Coal Geology*, v. 42, p. 315-356.
- Sinha, R. N., and Sastri, V. V., 1973, Correlation of the Tertiary geosynclinal sediments of the Surma valley, Assam, and Tripura state (India): *Sedimentary Geology*, v. 10, p.107-134.
- Soreghan, M. J., and Soreghan, G. S. L., 2007, Whole-rock geochemistry of upper Paleozoic loessite, western Pangaea: Implication for paleo-atmospheric circulation: *Earth and Planetary Science Letters*, v. 255, p. 117-132.
- Spear, F. S., 1993, *Metamorphic phase equilibria and pressure-temperature-time paths*, Mineralogical Society of America: Washington, DC, 799p.
- Srivastava, R. K., and Sinha, A. K., 2005, Geochemistry of Early Cretaceous alkaline ultramafic-mafic complex from Jasra, Karbi Anglong, Shillong Plateau, Northeastern India: *Gondwana Research*, v. 7, no. 2, p. 549-561.

- Suttner, L. J., 1974, Sedimentary petrographic provinces: An evaluation: In: Ross C. A eds., Paleogeographic provinces and provinciality, SEPM Special Publication, v. 21, p. 75-84.
- Talukdar, S.C., and Nandy, D.R., 1976, A Petrological framework of the Lohit Himalayas: Abstract Proceedings Symposium on geology and mineral resources of the Northeastern Himalayas, Shillong: Geological Survey of India, p. 42-43.
- Taylor, S. R., and McLennan, S. M., 1985, The continental crust: Its composition and evolution: Oxford, Blackwell Scientific Publication, p.
- Tucker, M., 1988, Techniques in sedimentology: London, Blackwell Scientific Publications., 395 p.
- Uddin, A., Kumar, P., Sarma, J. N., and Akhter, S. H., 2007a, Heavy-mineral constraints on provenance of Cenozoic sediments from the foreland basins of Assam, India and Bangladesh: Erosional history of the eastern Himalayas and the Indo-Burma ranges, in Mange, M.A., and Wright, D.T., eds., : Heavy minerals in use: Developments in Sedimentology, v. 58, p. 823-847.
- Uddin, A., Kumar, P., and Sharma, J. N., 2007b, Early orogenic history of the eastern Himalayas: compositional studies of Paleogene sandstones from Assam, northeast India: International Geology Review, v. 49, p. 798-810.
- , 2004, Miocene sedimentation and subsidence during continent–continent collision, Bengal Basin, Bangladesh: Sedimentary Geology, v. 164, p. 131-146.
- Uddin, A., and Lundberg, N., 1998a, Cenozoic history of the Himalayan-Bengal system: Sand composition in the Bengal basin, Bangladesh: Geological Society of America Bulletin, v. 110, p. 497-511.
- , 1998b, Unroofing of the eastern Himalaya and the Indo-Burma ranges: Heavy-minerals study of Cenozoic sediments from the Bengal basin, Bangladesh: Journal of Sedimentary Research, v. 68, p. 465-472.
- , 1999, A paleo Brahmaputra? Subsurface lithofacies analysis of the Miocene Deltaic sediments in the Himalayan-Bengal system, Bangladesh: Sedimentary Geology, v. 123, p. 239-254.
- Vance, D., and Harris, N., 1999, Timing of prograde metamorphism in the Zaskar Himalaya: Geology, v. 27, p. 395-398.
- Viator, D. B., 2003, Detrital tourmaline as an indicator of provenance: A chemical and sedimentological study of modern sands from Black Hills, South Dakota [Unpublished M.S. Thesis]: Louisiana State University, Baton Rouge, 86 p.

- Yokoyama, K., A. Taira, A., and Saito, Y., 1990, Mineralogy of silts from the Bengal Fan: Proceedings of Ocean Drilling Programs: Scientific Results, v. 116, p. 59-73.
- Zahid, K. M., 2005, Provenance and basin tectonics of Oligocene-Miocene sequences of the Bengal basin, Bangladesh [Unpublished M.S. Thesis]: Auburn University, 142 p.

## APPENDICES

### Appendix-A

Detrital tourmaline data in sandstones from the study area.

Sample No.	Standard	Sylhet & Tura formations				Kopili Formation		
		SM 6 trm1	SM 6 trm2	SM6 trm3	SM 6 trm4	SM 29 trm1	SM 29 trm2	SM 29 trm3
SiO <sub>2</sub>	40.27	34.54	35.94	35.99	35.79	34.21	39.04	35.97
TiO <sub>2</sub>	4.87	0.75	0.73	0.73	0.43	0.87	0.34	1.02
Al <sub>2</sub> O <sub>3</sub>	14.60	34.49	30.51	30.67	31.57	34.45	33.49	33.50
MgO	12.89	4.91	5.86	6.32	8.10	4.14	4.72	5.05
FeO	10.53	9.09	11.09	10.78	7.36	10.10	8.27	9.01
CaO	10.23	1.35	0.86	0.94	1.21	0.63	0.82	0.44
MnO	0.05	0.11	0.04	0.04	0.22	0.00	0.00	0.00
K <sub>2</sub> O	1.84	0.02	0.00	0.00	0.05	0.01	0.03	0.03
Na <sub>2</sub> O	2.47	1.52	2.24	1.87	1.77	1.77	1.47	1.86
Cr <sub>2</sub> O <sub>3</sub>	0.00	0.00	0.01	0.07	0.09	0.00	0.01	0.05
F	0.00	0.00	0.00	0.00	0.00	0.00	0.00	0.00
Cl	0.00	0.00	0.00	0.00	0.05	0.03	0.01	0.02
Total	97.75	86.79	87.27	87.41	86.63	86.20	88.19	86.94
Si	-	5.79	6.00	6.00	5.93	5.79	6.47	6.02
Ti	-	0.09	0.09	0.09	0.05	0.11	0.04	0.13
Al	-	6.82	6.00	6.03	6.16	6.87	6.54	6.61
Mg	-	1.23	1.46	1.57	2.00	1.04	1.17	1.26
Fe	-	1.27	1.55	1.50	1.02	1.43	1.15	1.26
Ca	-	0.24	0.15	0.17	0.21	0.11	0.15	0.08
Mn	-	0.02	0.01	0.01	0.03	0.00	0.00	0.00
K	-	0.00	0.00	0.00	0.01	0.00	0.01	0.01
Na	-	0.50	0.72	0.60	0.57	0.58	0.47	0.60
B	-	3.04	3.02	3.02	3.00	3.07	3.00	3.03
Cr	-	0.00	0.00	0.01	0.01	0.00	0.00	0.01
Total	-	19.00	19.00	19.00	19.00	19.00	19.00	19.00
Ca	-	8.85	4.84	5.19	6.63	4.39	5.93	3.04
Mg	-	44.71	46.16	48.45	61.85	40.36	47.44	48.46
Fe (tot)	-	46.44	49.00	46.36	31.52	55.24	46.63	48.50
Total	-	100.00	100.00	100.00	100.00	100.00	100.00	100.00

Contd...

Sample No.	Standard	Kopili Fm.	Barail Group						
		SM 29 trm4	SM 23 trm1	SM 18 trm1	SM 18 trm2	SM 16 trm1	SM 16 trm2	SM 16 trm3	SM 16 trm4
SiO2	40.27	35.74	33.95	35.08	37.25	35.43	36.28	35.48	34.87
TiO2	4.87	0.72	1.04	0.60	0.63	0.75	0.62	0.11	1.02
Al2O3	14.60	33.95	29.84	34.87	33.01	34.35	32.07	34.63	26.97
MgO	12.89	4.32	6.44	1.63	6.93	4.69	9.64	0.52	7.23
FeO	10.53	9.72	9.84	12.51	6.43	8.28	4.53	14.18	12.05
CaO	10.23	0.23	2.14	0.11	0.09	0.49	1.90	0.10	1.29
MnO	0.05	0.09	0.01	0.12	0.02	0.05	0.00	0.23	0.00
K2O	1.84	0.04		0.03	0.00	0.01	0.01	0.06	
Na2O	2.47	1.86		1.52	1.93	1.57	1.19	1.12	
Cr2O3	0.00	0.00	0.07	0.05	0.00	0.00	0.03	0.06	0.09
F	0.00	0.00		0.00	0.00	0.00	0.00	0.00	
Cl	0.00	0.00		0.01	0.01	0.00	0.02	0.00	
Total	97.75	86.68	83.34	86.54	86.29	85.63	86.27	86.49	83.53
Si	-	6.01	5.96	6.01	6.19	6.00	5.98	6.14	6.14
Ti	-	0.09	0.14	0.08	0.08	0.10	0.08	0.01	0.14
Al	-	6.73	6.17	7.04	6.47	6.86	6.23	7.07	5.60
Mg	-	1.08	1.69	0.42	1.72	1.18	2.37	0.13	1.90
Fe	-	1.37	1.44	1.79	0.89	1.17	0.62	2.05	1.78
Ca	-	0.04	0.40	0.02	0.02	0.09	0.34	0.02	0.24
Mn	-	0.01	0.00	0.02	0.00	0.01	0.00	0.03	0.00
K	-	0.01	0.00	0.01	0.00	0.00	0.00	0.01	0.00
Na	-	0.61	0.00	0.51	0.62	0.52	0.38	0.38	0.00
B	-	3.05	3.18	3.10	3.01	3.07	2.99	3.14	3.19
Cr	-	0.00	0.01	0.01	0.00	0.00	0.00	0.01	0.01
Total	-	19.00	19.00	19.00	19.00	19.00	19.00	19.00	19.00
Ca	-	1.63	11.42	0.92	0.63	3.64	10.08	0.86	6.22
Mg	-	43.48	47.70	18.71	65.36	48.42	71.16	6.06	48.46
Fe (tot)	-	54.89	40.88	80.36	34.02	47.95	18.76	93.08	45.31
Total	-	100.00	100.00	100.00	100.00	100.00	100.00	100.00	100.00
Al	-	45.83	44.38	46.36	45.42	46.04	44.64	46.41	42.95
Al50Fe(tot)50	-	27.57	27.38	29.08	25.85	26.96	24.56	29.95	28.29
Al50Mg50	-	26.60	28.24	24.56	28.74	27.00	30.81	23.64	28.76
Total	-	100.00	100.00	100.00	100.00	100.00	100.00	100.00	100.00



Contd...

		Surma Group							
Sample No.	Standard	SM 14 trm1	SM 14 trm2	SM 8 trm1	SM 8 trm2	SM 8 trm3	SM 9 trm1	SM 9 trm2	SM9 trm3
SiO2	40.27	36.25	37.38	34.62	34.21	36.72	35.93	36.36	35.81
TiO2	4.87	1.05	0.41	0.70	0.89	0.73	0.96	0.74	0.41
Al2O3	14.60	34.50	31.83	33.76	34.11	32.80	31.78	34.49	34.22
MgO	12.89	6.22	8.66	2.23	4.50	8.30	6.66	4.96	4.30
FeO	10.53	6.51	5.13	13.22	9.70	4.33	8.00	8.51	9.35
CaO	10.23	0.66	0.23	0.42	1.39	0.43	0.92	0.33	0.16
MnO	0.05	0.07	0.00	0.16	0.00	0.00	0.02	0.00	0.08
K2O	1.84	0.06	0.01	0.08	0.07	0.03	0.00	0.01	0.03
Na2O	2.47	1.71	2.29	1.77	1.28	2.03	1.96	1.71	1.75
Cr2O3	0.00	0.00	0.00	0.07	0.06	0.01	0.00	0.04	0.00
F	0.00	0.00	0.00	0.00	0.00	0.00	0.00	0.00	0.00
Cl	0.00	0.01	0.00	0.00	0.01	0.00	0.00	0.00	0.00
Total	97.75	87.04	85.94	87.05	86.23	85.38	86.24	87.14	86.12
Si	-	6.00	6.16	5.89	5.80	6.09	6.01	6.07	6.05
Ti	-	0.13	0.05	0.09	0.11	0.09	0.12	0.09	0.05
Al	-	6.73	6.19	6.77	6.81	6.42	6.26	6.78	6.81
Mg	-	1.54	2.13	0.57	1.14	2.05	1.66	1.23	1.08
Fe	-	0.90	0.71	1.88	1.37	0.60	1.12	1.19	1.32
Ca	-	0.12	0.04	0.08	0.25	0.08	0.16	0.06	0.03
Mn	-	0.01	0.00	0.02	0.00	0.00	0.00	0.00	0.01
K	-	0.01	0.00	0.02	0.02	0.01	0.00	0.00	0.01
Na	-	0.55	0.73	0.58	0.42	0.65	0.64	0.55	0.57
B	-	3.00	2.99	3.08	3.07	3.01	3.03	3.02	3.06
Cr	-	0.00	0.00	0.01	0.01	0.00	0.00	0.00	0.00
Total	-	19.00	19.00	19.00	19.00	19.00	19.00	19.00	19.00
Ca	-	4.58	1.42	3.04	9.12	2.80	5.60	2.39	1.20
Mg	-	60.12	73.99	22.45	41.14	75.19	56.40	49.74	44.51
Fe (tot)	-	35.30	24.59	74.51	49.75	22.01	38.00	47.87	54.29
Total	-	100.00	100.00	100.00	100.00	100.00	100.00	100.00	100.00
Al	-	45.85	44.86	45.85	45.78	45.31	45.01	45.90	45.95
Al50Fe(tot)50	-	26.00	24.99	29.30	27.51	24.78	26.52	26.97	27.43
Al50Mg50	-	28.15	30.15	24.85	26.71	29.91	28.47	27.13	26.63
Total	-	100.00	100.00	100.00	100.00	100.00	100.00	100.00	100.00

Appendix-B

Detrital chrome-spinel data in sandstones from the present study area.

Sample No.	Standard	Barail Group										Surma Group			
		SM 23 crsp1	SM 23 crsp2	SM16 crsp1	SM16 crsp2	SM16 crsp3	SM9 crsp 1	SM9 crsp 2	SM9 crsp 3	SM8 crsp1	SM9 crsp 1	SM9 crsp 2	SM9 crsp 3	SM8 crsp1	
SiO2	0.04	0.01	0.02	0.03	0.01	0.57	0.03	0.01	0.16	0.16	0.03	0.02	0.00	0.01	
TiO2	0.13	0.11	0.07	0.41	0.16	0.16	0.41	0.16	0.16	0.16	0.23	0.27	0.00	0.06	
Al2O3	23.68	32.58	30.04	28.08	9.13	12.44	28.08	9.13	12.44	15.02	15.02	12.69	34.02	29.38	
MgO	16.63	12.98	13.89	8.52	4.59	6.84	8.52	4.59	6.84	10.61	10.61	8.08	13.82	13.18	
FeO	12.35	25.48	15.73	21.44	28.37	26.44	21.44	28.37	26.44	20.10	20.10	21.11	17.74	17.22	
CaO	0.00	0.00	0.00	0.00	0.05	0.00	0.00	0.05	0.00	0.03	0.03	0.01	0.02	0.01	
MnO	0.17	0.28	0.20	0.22	0.65	0.49	0.22	0.65	0.49	0.14	0.14	0.19	0.25	0.12	
Cr2O3	47.23	27.52	38.62	37.13	54.04	49.22	37.13	54.04	49.22	50.28	50.28	56.35	32.26	38.66	
NiO	0.28	0.21	0.21	0.17	0.04	0.00	0.17	0.04	0.00	0.05	0.05	0.00	0.14	0.02	
Total	100.51	99.18	98.78	96.00	97.04	96.16	96.00	97.04	96.16	96.50	96.50	98.72	98.25	98.64	
Si		0.00	0.00	0.00	0.00	0.03	0.00	0.00	0.03	0.00	0.00	0.00	0.00	0.00	
Ti		0.00	0.00	0.02	0.01	0.01	0.02	0.01	0.01	0.01	0.01	0.01	0.00	0.00	
Al		2.27	2.12	2.12	0.76	1.01	2.12	0.76	1.01	1.17	1.17	1.00	2.37	2.09	
Mg		1.14	1.24	0.81	0.48	0.70	0.81	0.48	0.70	1.05	1.05	0.81	1.22	1.19	
Fe(3)		0.00	0.02	0.00	0.10	0.10	0.00	0.10	0.10	0.08	0.08	0.00	0.06	0.03	
Fe(2)		1.26	0.77	1.15	1.58	1.42	1.15	1.58	1.42	1.03	1.03	1.18	0.82	0.84	
Ca		0.00	0.00	0.00	0.00	0.00	0.00	0.00	0.00	0.00	0.00	0.00	0.00	0.00	
Mn		0.01	0.01	0.01	0.04	0.03	0.01	0.04	0.03	0.01	0.01	0.01	0.01	0.01	
Cr(3)		1.29	1.83	1.88	3.02	2.69	1.88	3.02	2.69	2.64	2.64	2.98	1.51	1.84	
Ni		0.02	0.02	0.02	0.00	0.00	0.02	0.00	0.00	0.01	0.01	0.00	0.01	0.00	
Total		3.00	3.00	3.00	3.00	3.00	3.00	3.00	3.00	3.00	3.00	3.00	3.00	3.00	
Al3+		63.83	53.45	52.99	19.61	26.61	52.99	19.61	26.61	30.17	30.17	25.13	60.24	52.72	
Cr3+		36.17	46.10	47.01	77.86	70.63	47.01	77.86	70.63	67.76	67.76	74.87	38.32	46.54	
Fe3+		0.00	0.46	0.00	2.53	2.76	0.00	2.53	2.76	2.07	2.07	0.00	1.44	0.74	
Total		100.00	100.00	100.00	100.00	100.00	100.00	100.00	100.00	100.00	100.00	100.00	100.00	100.00	
Fe3+/Fe3++Cr+Al		0.00	0.00	0.00	0.03	0.03	0.00	0.03	0.03	0.02	0.02	0.00	0.01	0.01	
Mg#(Mg/Mg+Fe2+)		0.48	0.62	0.41	0.23	0.33	0.41	0.23	0.33	0.50	0.50	0.41	0.60	0.59	
Cr#(Cr/Cr+Al)		0.36	0.46	0.47	0.80	0.73	0.47	0.80	0.73	0.69	0.69	0.75	0.39	0.47	
TiO2 (wt%)		0.11	0.07	0.41	0.16	0.16	0.41	0.16	0.16	0.23	0.23	0.27	0.00	0.06	

### Appendix-C

Detrital garnet data in sandstones from the study area.

Sample No.	Standard	Barail Group				Surma Group
		SM23 gt1	SM23 gt2	SM23 gt3	SM23 gt4	SM8 gt1
SiO <sub>2</sub>	38.71	33.49	36.14	36.64	33.59	35.37
TiO <sub>2</sub>	0.17	0.01	0.09	0.87	0.06	2.87
Al <sub>2</sub> O <sub>3</sub>	22.23	21.46	21.09	22.39	21.09	19.65
MgO	10.23	2.42	0.49	9.78	0.50	4.53
FeO	21.00	36.56	21.42	26.24	21.05	24.11
CaO	7.29	1.40	3.61	1.37	3.68	0.02
MnO	0.57	1.29	16.95	0.64	16.44	0.29
Cr <sub>2</sub> O <sub>3</sub>	0.10	0.03	0.00	0.12	0.01	0.00
Total	100.97	96.68	99.78	98.06	96.42	86.84
SiO <sub>2</sub>	-	5.61	5.90	5.73	5.67	6.44
TiO <sub>2</sub>	-	0.00	0.01	0.10	0.01	0.39
Al <sub>2</sub> O <sub>3</sub>	-	4.23	4.06	4.13	4.20	4.22
MgO	-	0.60	0.12	2.28	0.12	1.23
FeO	-	5.12	2.93	3.43	2.97	3.67
CaO	-	0.25	0.63	0.23	0.67	0.00
MnO	-	0.18	2.35	0.08	2.35	0.04
Cr <sub>2</sub> O <sub>3</sub>	-	0.00	0.00	0.01	0.00	0.00
Total	-	8.00	8.00	8.00	8.00	8.00
Pyrope	-	9.82	1.99	37.83	2.04	24.85
Almandine	-	83.13	48.58	56.94	48.62	74.19
Grossular	-	4.09	10.49	3.82	10.89	0.06
Spessartine	-	2.97	38.94	1.41	38.45	0.90
Total	-	100.00	100.00	100.00	100.00	100.00
Fe/(Fe+Mg)	-	0.89	0.96	0.60	0.96	0.75